VISUAL AND OCULOMOTOR INTEGRATION: REPRESENTATIONS AND TEMPORAL MECHANISMS

DEVIN HEINZE KEHOE

A THESIS SUBMITTED TO
THE FACULTY OF GRADUTE STUDIES
IN PARTIAL FULFILLMENT OF THE REQUIREMENTS
FOR THE DEGREE OF
MASTER OF ARTS

GRADUATE PROGRAM IN PSYCHOLOGY
YORK UNIVERSITY
TORONTO, ONTARIO

OCTOBER 2016

Abstract

The visual system recruits the oculomotor system to enhance processing at a particular location of interest with the use of saccadic eye movements. This involves the transfer of visual information from the visual system to the oculomotor system so that the correct location or object may be fixated at the expense of all others—a process called target selection. However, the relative extent of visual processing between the visual and oculomotor systems to facilitate this process is disputed. Here, this question is examined by specifically investigating the extent of oculomotor processing prior to a saccade. First, the nature of object representations in the ventral stream of the visual system is examined to gain insight into how complex visual representations are encoded. Next, target selection was examined in a visual context requiring extremely complex visual computations in order to select the correct stimulus. Last, the temporal factors that affect oculomotor target selection were examined.

This research demonstrated that objects of considerable complexity elicit similar perceptual behaviours as do simple visual features. This elucidates that there are very robust modes of encoding object representations, which generalize to objects of varying complexity and familiarity. Furthermore, when these same complex visual representations were utilized on a target selection task (visual search), there was evidence of oculomotor competition between them. Given the complexity of these stimuli and the limitations of oculomotor visual processing, it was reasoned that the visual system performed these computations, as observed in the previous experiment, and the results of this computation were output to the oculomotor system. Finally, an analysis of the target selection time course suggested that the oculomotor competition observed previously is likely due to cortical top-down input, further elucidating the role of the visual system in mediating oculomotor target selection.

Acknowledgements and Dedication

I first and foremost need to thank my supervisor, mentor, and friend, Dr. Mazyar Fallah, as this thesis would certainly have not been possible without him. Your diligence, sheer brilliance, equanimity, and appreciativeness has made the last two years some of the most productive, exciting, enjoyable, and fulfilling of my life. And I'm thrilled I get to stick around for five more productive years of science! Fingers crossed—as Maz would say.

I would also like to extend a very warm thank you to my research assistant, colleague, and friend Selvi, as she helped me tremendously by collecting most of the data that appears in this thesis, and did so with considerable adeptness and diligence. I wouldn't have been nearly as productive during my tenure as a master's student without your help. Thanks again, and best of luck in your future endeavours! You'll be awesome at anything you try.

Naturally, I need to thank my colleagues in the Visual Perception and Attention Laboratory for their mentorship, encouragement, and most importantly, their friendship. Grad school is not something you can go alone, and I honestly couldn't have asked for a better group. Best of luck to all of you, and I'm sure we'll get up to some shenanigans again in the future!

Also, what would be a thesis acknowledgement section without a shout-out to family and friends? I'll start with a special shout-out to Kate: Thanks for putting up with impromptu lectures on cognitive neuroscience or statistics and any complaining I *may* have done when I was stressed. You're always very positive and encouraging and bring out the best in me, so thank you. Mom, dad, Erin, friends: thank you so much to all of you. I have received a steady flow of encouragement and compliments from you, and it would not have been possible without them.

Lastly, I would like to dedicate this thesis to my mom. Mom: now I, too, am a Master of Psychology! Muahaha!

Table of Contents

List of Tables

List of Figures

Chapter 1. Overview of the Oculomotor and Visual Systems

1.1 Introduction

Humans rely heavily on their sense of vision to navigate and interact with the environment. This reliance is reflected by the fact that perhaps as much as 50% of the human cortex contributes to visual processing in at least some capacity (DeYoe & van Essen, 1988; van Essen, Felleman, DeYoe, Olavarria, & Knierim, 1990). Critically, it is an active process by which we construct a visual representation of the environment, as our visual system selectively prioritizes a subset of the incoming visual information for preferential processing in the following two ways: (1) Visual attention—a covert, cognitive mechanism with diverse anatomical substrates (Bisley, 2011; Moore, Armstrong, & Fallah, 2003)—enhances processing at selected locations in the environment (Carrasco, 2011; Posner & Petersen, 1990). (2) Overt saccadic eye movements—rapid ballistic movements of the eyes (Becker, 1989)—place the fovea centralis on selected locations in the environment, which enhances processing at this location because the density of photoreceptor cells on the retina is greatest at the fovea and rapidly decreases at greater eccentricities away from the fovea (Curcio, Sloan, Kalina, & Hendrickson, 1990). Saccadic eye movements are planned and executed by the oculomotor system (Becker, 1989). Although there is a great deal of anatomical overlap with the visual system (Awh, Armstrong, & Moore, 2006; Corbetta et al., 1998), there is a meaningful functional distinction between the visual and oculomotor systems: the visual system processes visual information and constructs a representation of the environment. On the other hand, the oculomotor system outputs behaviour (e.g., saccades). However, it also processes visual information to some extent, but the extent of this processing remains contentious. The current thesis examines the universality of object representations in the visual system, the extent of

visual processing by the oculomotor system, and the temporal factors pertaining to the flow of visual information from the visual system into the oculomotor system. In the next section is a brief functional and anatomical overview of the visual system followed after by a more detailed functional and anatomical overview of oculomotor system in section 3.

1.2 The Visual System

The following section contains a very brief overview of the major nodes in the visual processing network with an emphasis on the hierarchical transitions from the early to late stages of visual processing as well as the two streams of visual processing and their associated features. Figure 1.1 provides the reader with a visual depiction of the anatomical substrates with added functional notations of the two visual processing streams from the early stages of processing through to the cortical stages of processing.

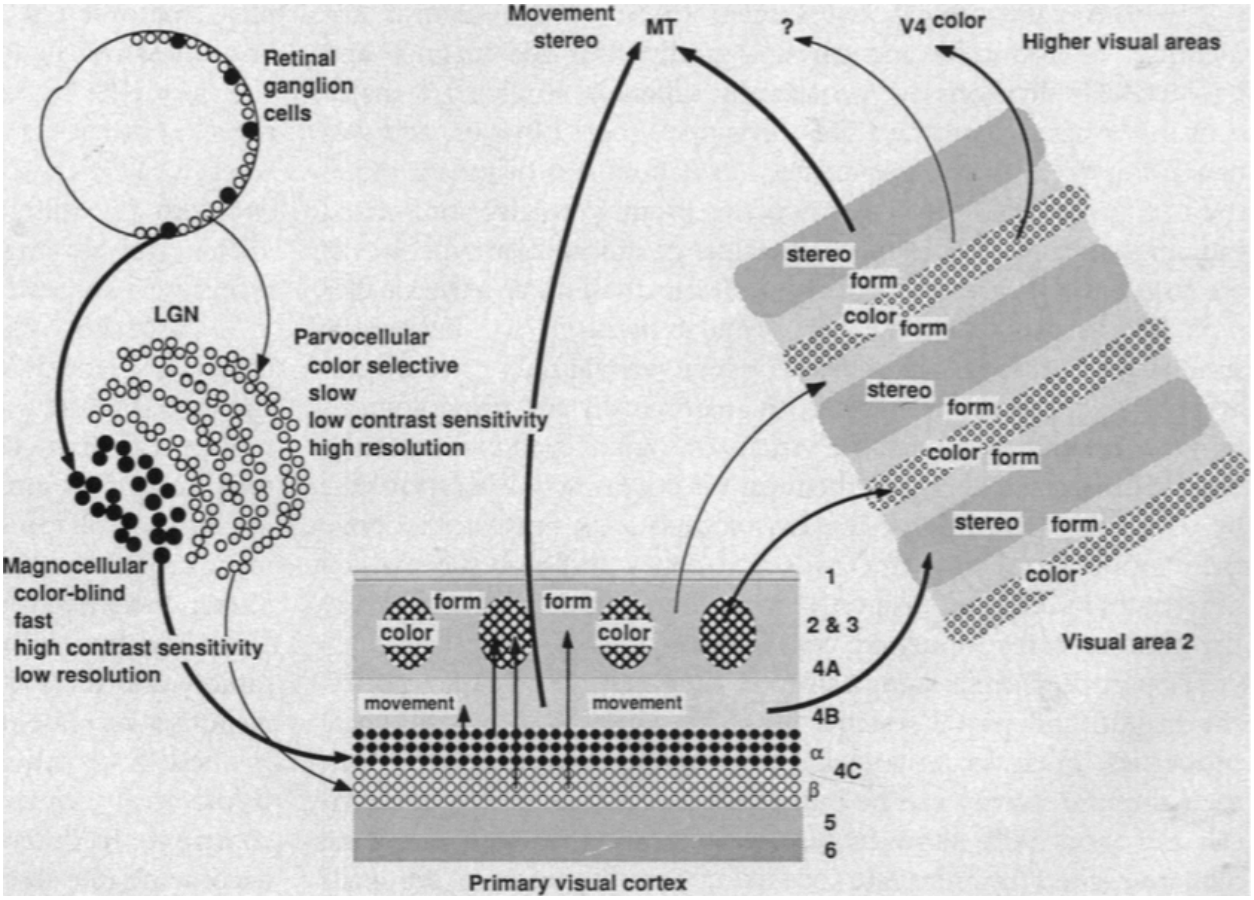

Figure 1.1: Anatomical substrates with associated feature representations for the visual processing hierarchy. Depicted are magno cells (black circles); parvo cells (white circles); the laminar cytoarchitecture of the LGN, V1, and V2; anatomical connections between structures; and visual feature representations associated with the layers in each structure. Note: this figure does not include the medial superior temporal lobe or the inferior temporal lobe, which are discussed in the text. Reprinted from Livingstone, M. & Hubel, D. H. (1988). Segregation of form, color, movement, and depth: Anatomy, physiology, and perception. *Science*, *240*, 740–749.

1.2.1 Early Visual Processing

Visual processing begins in the retina, where specialized cells called photoreceptors transduce visual stimulation into electrochemical signals in the form of graded potentials (Wald, 1968). There are two types of photoreceptors that have different functions and whose names are based on their morphology: cones cells, which are active under photopic conditions; and rod cells, which are active under scotopic conditions (Rodieck, 1998); therefore further discussion on rod cells will be omitted. Cone cells project encoded visual information to other specialized cells called retinal ganglion cells (RGCs) (Polyak, 1957). Beginning with RGCs, is the introduction of action potentials (Rodieck, 1998) and separate visual processing streams, as they project to the lateral geniculate nucleus (LGN) of the thalamus where they selectively terminate in either the magnocellular layers (1-2) or parvocellular layers (3-6), which are anatomically and physiologically distinct (van Essen, Anderson, & Felleman, 1992; Zeki, 1993). LGN magno cells have fast responses with high contrast sensitivity, but are colourblind and demonstrate poor acuity; conversely, parvo cells have slow(er) responses with low contrast sensitivity, but are colour sensitive and demonstrate high acuity (Livingstone & Hubel, 1988). This functional

distinction is preserved throughout higher levels of visual processing. Optic radiations are projected from LGN into the primary visual cortex (V1) where magnocelluar radiations terminate in layer 4Cα and parvocellular radiations terminate in layer 4Cβ (Livingstone & Hubel, 1988). This projection from LGN to V1 is referred to as the geniculostriate pathway. From each specialized layer in V1, this information is projected forward along two specialized, hierarchical visual processing streams (Ungerleider & Mishkin, 1982).

1.2.2 The Ventral Stream

The ventral processing stream is mainly allocated for the perception and recognition of objects that vary in complexity, and is therefore often referred to as the "what" pathway (Goodale & Milner, 1992; Ungerleider & Mishkin, 1982). According to Livingstone and Wiesel, (1988), feedforward projections in the ventral stream start in the 4Cβ layer of V1 and project to the blob and interblob layers 2, 3, and 4A of V1, which encode colour and form information respectively. Colour and form information is then projected to the thin stripes and pale interstripes in visual area 2 (V2) respectively. From V2, colour and form information are projected forward into visual area 4 (V4) where more complex representations emerge, such as perceived colour (Schein & Desimone, 1999) and shape primitives like curvatures and angles, (Pasupathy & Connor, 1999; Yau et al., 2012). V4 projects forward to the interior temporal cortex (IT), which is often divided into posterior and anterior portions (PIT and AIT respectively) (Felleman & van Essen, 1991) since the complexity of visual representations increases from posterior to anterior portions (Logothetis & Sheinberg, 1996). Neurons in the AIT are selective for visual representations at the highest levels of complexity, such as complex shapes and even faces (Desimone, Albright, Gross, & Bruce, 1984; Gross, Rocha-Miranada, & Bender, 1972). Furthermore, these complex selectivities can develop over time with practice

(Baylis & Rolls, 1987; Fahy, Riches, & Brown, 1993; Riches, Wilson, & Brown, 1991), implicating the role of the temporal lobe in memory formation. These complex representations emerge as the concatenation of the underlying constituent visual features represented posteriorly (Brincat & Connor, 2004, 2006). Cognitive psychologists refer to the concatenation of visual features as "feature binding" (Treisman, 1996).

1.2.3 The Dorsal Stream

Dorsal stream processing is mainly allocated for processing motion and other object attributes that help guide motor behaviours such as manual reaches or pursuit eye movements (Goodale & Milner, 1992; Ungerleider & Mishkin, 1982). Given these functional properties, this processing stream is often referred to as the "how" pathway (Goodale & Milner, 1992). As summarized by Livingstone and Hubel (1988), feedforward projections in the dorsal stream start in layer 4Cα of V1 and project to layer 4B in V1, encoding movement and binocular-disparity related information, which is then projected to the thick striped layer in V2. This information is then projected to the middle temporal visual area (MT), which is specialized for motion and stereoscopic depth processing. From MT, visual information is sent to the medial superior temporal area (MST), which performs complex motion processing, such as optic flow and self-motion (Duffy & Wurtz, 1997, 1991a, 1991b). Interestingly, although discussed in terms of anatomically and functionally distinct processing streams here, there is growing evidence that feature representations in the ventral stream is integrated with visual processing performed in the dorsal stream (reviewed by Perry & Fallah, 2014).

Critically, the orderly structure of visual processing from simple to complex representations observed in both cortical visual processing streams is often referred to as the visual hierarchy (thoroughly documented by Felleman & van Essen, 1991). However, visual

processing is not exclusively feedforward as most connections between cortical visual areas are reciprocal (van Essen & Maunsell, 1983). In fact, recurrent feedback projections are necessary for higher cognitive functions such as attention (Connor, Gallant, Preddie, & van Essen, 1996; Reynolds & Chelazzi, 2004) and conscious perception (Lamme & Roelfsema, 2000; Tononi & Koch, 2008).

1.3 The Oculomotor System

The next section contains a detailed overview of the anatomy, physiology, and functionality of two critical nodes in the oculomotor network that have been thoroughly investigated: the superior colliculus (SC) and the frontal eye fields (FEF). Furthermore, this overview specifically highlights the target selection behaviour of neurons in these structures. Although these two structures are the focus of this overview, the oculomotor system contains many important nodes—many of which are mentioned given their connections to SC and FEF. Figure 1.2 has been provided to graphically depict this complicated set of connections. Finally, this section ends with a review of behavioural data linked to competitive oculomotor processing during target selection.

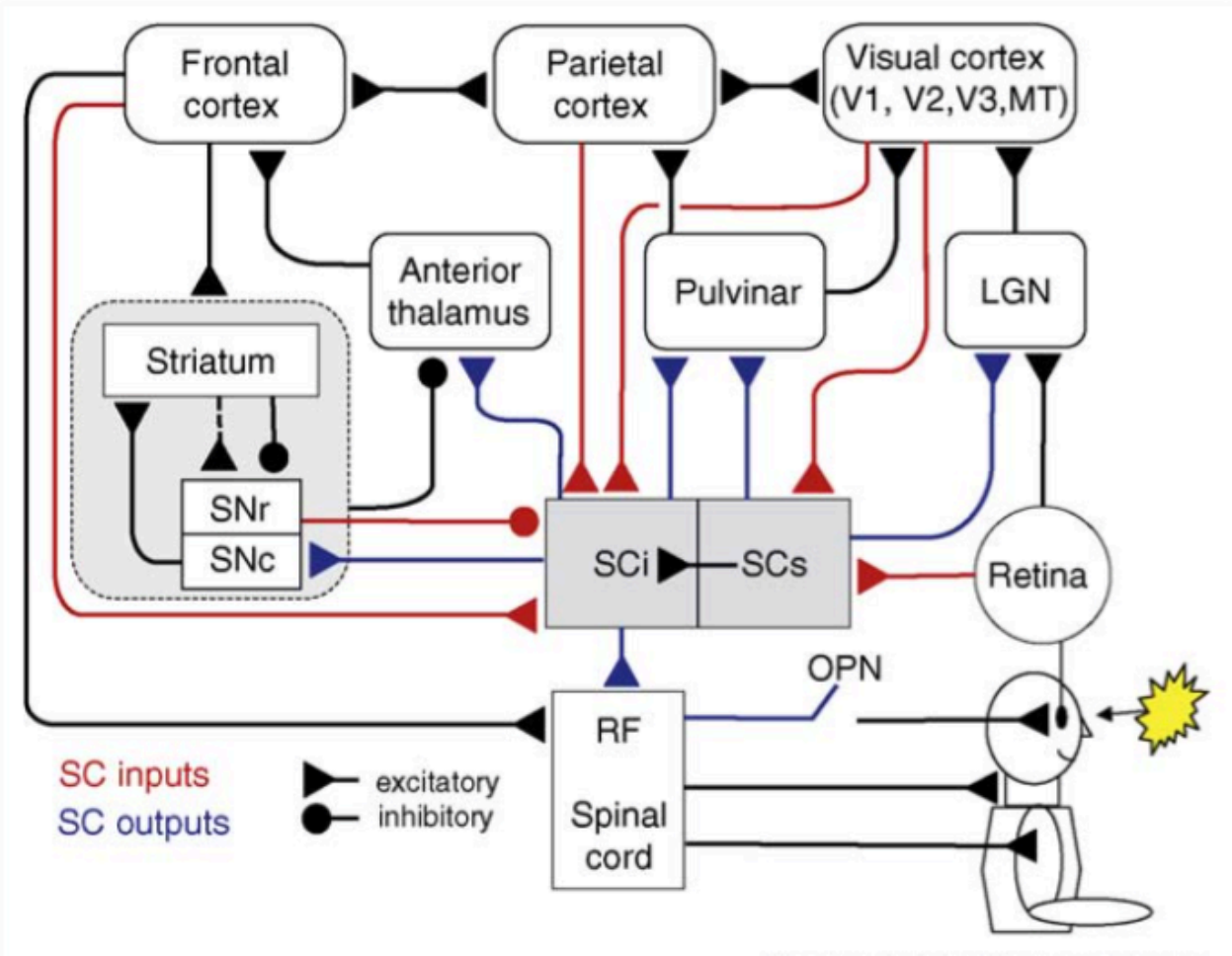

Figure 1.2: The major nodes in the oculomotor system. The role of the SC in this circuit is emphasized as SC inputs are depicted as red lines and SC outputs are depicted as blue lines. Also, excitatory connections are depicted as triangles, while inhibitory connections are depicted with circles. This circuit diagram is not anatomically to scale. Furthermore, the text refers to the PFC, LIP, and MD, which are located respectively in the structures frontal cortex, parietal cortex, and anterior thalamus represented in this diagram. Acronyms not defined in text: OPN: omni-pause neurons (i.e., neurons in the brainstem that suppress saccades and ensure fixation); RF: reticular formation (i.e., the location of the saccadic pulse generators discussed in text). Reprinted from Boehnke, S. E., & Munoz, D. P. (2008). On the importance of the transient visual response in the superior colliculus. *Current Opinion in Neurobiology*, *18*(6), 544–551.

1.3.1 The Superior Colliculus

The superior colliculus is a deep, midbrain structure bilaterally occupying the tectum (Afifi & Bergman, 2005). It consists of 7 anatomically distinct layers, which are divided into two functional groups: the superficial layers (SCs) and the intermediate layers (SCi) (Edwards, 1980). The SCs is topographically organized with a retinotopic visual map (Goldberg & Wurtz, 1972; Schiller & Koerner, 1971), while the SCi is topographically organized with a retinotopic motor map (Robinson, 1972; Wurtz & Goldberg, 1971, 1972). Critically, these maps are highly correlated (Marino, Rodgers, Levy, Munoz, 2008). SCs receives direct excitatory visual input from the retina (i.e., the retinotectal pathway) (Cowey & Perry, 1980; Hubel, LeVay, & Wiesel, 1975; Perry & Cowey, 1984; Schiller & Malpeli, 1977) and visual cortex (Cynader & Berman, 1972; Harting, Updyke, Van Lieshout, 1992; Schiller, Stryker, Cynader, & Berman, 1974), and it projects indirectly back to the visual cortex through the magnocellular layer of the LGN (Harting, Casagrande, & Weber, 1978) and directly to SCi (Isa, 2002; Isa & Saito, 2001). SCi receives direct excitatory inputs from a variety of cortical sources such as the frontal eye fields (FEF) (Künzle & Akert, 1977; Künzle, Akert, & Wurtz, 1976; Stanton, Bruce, & Goldberg, 1995; Stanton, Goldberg, & Bruce, 1988b), lateral intraparietal area (LIP) (Lynch, Graybiel, & Lobeck, 1985), and the dorsolateral prefrontal cortex (DFPFC) (Goldman & Nauta, 1976), and receives inhibitory input from the substantia nigra pars recticulata (SNr) nucleus of the basal ganglia (Hikosaka & Wurtz, 1983, 1985; Hikosaka, Takikawa, & Kawagoe, 2000). There is also evidence for local, lateral inhibitory circuits in SCi (McPeek & Keller, 2002; Munoz & Istvan, 1998).

The SCi is a critical oculomotor substrate because it projects directly to the brainstem saccadic pulse generators for horizontal and vertical saccades in the paramedian potine reticular

formation (PPRF) and the rostral interstitial medial longitudinal fasciculus (riMLF) respectively (Moschovakis, Karabelas, & Highstein, 1988). SCi visual and visuo-movement (VM) neurons elicit a visual transient onset burst ~55 after the onset of a visual stimulus (Basso & Wurtz, 1998; Boehnke & Munoz, 2008; Mays & Sparks, 1980; McPeek & Keller, 2002), while SCi movement and VM neurons elicit a perisaccadic burst of activity ~20 ms prior to the initiation of a saccade (Glimcher & Sparks, 1992; McPeek & Keller, 2002; McPeek, Han, & Keller, 2003; Munoz & Wurtz, 1995; Port & Wurtz, 2003; Wurtz & Goldberg, 1971, 1972). However, both visual transient onset bursts and perisaccadic bursts may be sufficient to elicit a saccade (Boehnke & Munoz, 2008; Dorris, Paré, & Munoz, 1997; Edelman & Keller, 1996; Sparks, Rohrer, & Zhang, 2000), as a saccade is elicited simply when SCi activity reaches a threshold (Robinson, 1972). The control signal for the perisaccadic burst of activity, and thus for saccade initiation, is contentious but it may be received via excitatory projections from FEF as this structure can indirectly elicit saccades via SCi (Dassonville, Schlag, & Schlag-Rey, 1992; Everling & Munoz, 2000; Schlag-Rey, Schlag, & Dassonville, 1992; Segraves & Goldberg, 1987) or via disinhibition of the tonic GABAnergic inhibition imposed on SCi by the SNr, as SNr activity pauses prior to saccade initiation (Hikosaka et al., 2000; Hikosaka & Wurtz, 1983, 1985). An important feature of the SCi motormap is spatial-averaging, as activity is averaged across the motormap prior to saccade initiation (Aizawa & Wurtz, 1998; Glimcher & Sparks, 1993; Lee, Rohrer, & Sparks, 1988; McPeek et al., 2003; Ottes, Van Gisbergen, & Eggermont, 1986; Port & Wutz, 2003; Robinson, 1972; Van Gisbergen, Van Opstal, & Tax, 1987; Van Opstal & Gisbergen, 1990), which can elicit a saccade that is the vector average of two potential saccade goals encoded by the SCi weighted by the neuronal activity at each locus (Port & Wutz, 2003; Van Gisbergen et al., 1987).

The SCi has been heavily implicated in saccadic target selection, the process by which a target is discriminated from a distractor(s) (Basso & Wurtz, 1997, 1998; Carello & Krauzlis, 2004; Horwitz & Newsome, 1999, 2001; Kim & Basso, 2008; Li & Basso, 2005; McPeek & Keller, 2002, 2004; Shen & Paré, 2007, 2014), suggesting that potential saccade goal representations in SCi are competitive. Some authors have argued that SCi functionally contributes to the visual processing required for target selection (Basso & Wurtz, 1997, 1998; Horwitz & Newsome, 1999, 2001; McPeek & Keller, 2004), however it is unclear whether SCi passively receives target and distractor information or functionally contributes to this processing (e.g., McPeek & Keller, 2002).

1.3.2 The Frontal Eye Fields

The frontal eye fields (FEF) are bilaterally located in the anterior bank of the arcuate sulcus of the frontal lobes (Bruce & Goldberg, 1985; Bruce, Goldberg, & Bushnell, & Stanton, 1985). FEF has reciprocal connections with a distributed network of cortical visual and oculomotor areas associated with high-level cognitive functions, encoding complex visual representations, and attentional/spatial visual processing: the prefrontal cortex, superior temporal sulcus (STS), and the lateral bank of the intraparietal sulcus (LIP) respectively (Felleman & Van Essen 1991; Huerta, Brubitzer, & Kaas, 1987; Künzle & Akert, 1977; Stanton et al., 1995; Schall, Morel, King, & Bullier, 1995). FEF also has a rich set of subcortical connections: FEF has reciprocal connections with the SC, receives input from the mediodorsal nucleus of the thalamus (MD) and substantia nigra pars compacta (SNc), and projects directly to the brainstem (Huerta, Krubitzer, & Kaas, 1986; Künzle & Akert, 1977; Künzle et al., 1976; Lynch, Hoover, & Strick, 1994; Lynch & Tian, 2006; Moschovakis & Highstein, 1994; Sommers & Wurtz, 1998, 2004a; Stanton et al., 1988a, 1988b; Tian & Lynch, 1997).

Like SCi, FEF has highly ordered, overlapping retinotopic visual and movement maps (Bruce & Goldberg, 1984, 1985; Bruce et al., 1985; Mohler, Goldberg, & Wurtz, 1973; Robinson & Fuchs, 1969; Schall, 1991; Thompson, Hanes, Bichot, & Schall, 1996; Wurtz & Mohler, 1976) and there is evidence that activity on the FEF motor map is also spatially averaged (McPeek, 2006; Robinson & Fuchs, 1969). FEF contains different proportions of visual, movement, and VM neurons, which discharge after a visual onset and prior to saccades with a similar temporal profile as neurons in SCi (Bruce & Goldberg, 1985; Bruce et al., 1985; Schall, 1991). Additionally, FEF contains neurons that reach peak activity post-saccade and encode the sensory consequences of a saccade by subtracting the saccade vector from the target position (Goldberg & Bruce, 1990). This computation is facilitated by a corollary discharge signal received from SCi indirectly via MD before an impending saccade (Sommer & Wurtz, 2004b, 2006, 2008). Furthermore, there is evidence that FEF controls the initiation of voluntary saccades as on an anti-saccade task, neuronal motor activity increases towards a elicitation threshold, but then decreases after the onset of a countermanding stimulus (Hanes & Schall, 1996; Hanes, Patterson, & Schall, 1998). Finally, there is strong evidence for target selection behaviour in FEF neurons (Bichot & Schall, 1999; Bichot, Schall, & Thompson, 1996; Sato & Schall, 2003; Sato, Watanabe, Thompson, & Schall, 2003; Thompson et al., 1996; Wurtz & Mohler, 1976). The available evidence demonstrates that higher-cognitive processing is integrated with visual information in FEF to guide the control of voluntary saccades.

1.3.3 Target Selection and Behavioural Metrics

Due to the spatial averaging principle observed on oculomotor maps (Aizawa & Wurtz, 1998; Glimcher & Sparks, 1993; Lee et al., 1988; McPeek, 2006; McPeek et al., 2003; Ottes et al., 1986; Port & Wutz, 2003; Robinson, 1972; Robinson & Fuchs, 1969; Van Gisbergen et al.,

1987; Van Opstal & Gisbergen, 1990), target selection on oculomotor maps is reflected behaviourally by the global effect and distractor modulation of saccade curvatures. The global effect is characterized by saccade endpoints landing at the so-called "center of gravity", which is the geometric center between a target and one or more irrelevant distractors (Coren & Hoenig, 1972). On a saccade task, the global effect is typically observed when targets and distractors are within a specific range of angular separation, which has been estimated between 20° (Walker, Deubel, Schneider, & Findlay, 1997) and 45° (Van der Stigchel & Nijboer, 2013). However, previous experiments have also demonstrated that the center of gravity is not exclusively determined by the spatial arrangement of display elements, but by a combination of bottom-up and top-down factors: the center of gravity can be biased towards stimuli with the greatest size (Findlay, 1982), luminance (Deubel, Wolf, & Hauske, 1984), or target probability (He & Kowler, 1989). Furthermore, the global effect can be eliminated by top-down control (Findlay & Blythe, 2009; Findlay & Kapoula, 1992; Heeman, Theeuwes, & Van der Stigchel, 2014). Similar to the global effect, it has been observed on visual search tasks with multiple distractors separated by 90° that saccades often land between the target and a single distractor (Godijn & Theeuwes, 2002; McPeek et al., 2003; McPeek & Keller, 2001; McPeek, Skavenski, & Nakayama, 2000).

Saccade curvature is characterized by any deviation from a straight line between the start- and endpoint of a saccade (see Ludwig & Gilchrist, 2002 for a review). Although saccade trajectories are normally idiosyncratically curved (Bahill & Stark, 1975), several researchers report greater saccade curvatures when a distractor is present than when it is absent in both humans (Doyle & Walker, 2001; Ludwig & Gilchrist, 2003; McSorley et al., 2004) and monkeys (McPeek & Keller, 2001). Similarly, saccades that are erroneously directed towards a distractor

sometimes curve towards the target (McPeek & Keller, 2001). As with the global effect, many visual and cognitive factors modulate saccade curvatures, which is typically examined using a saccade task and manipulating the distractor characteristics. These types of experiments have demonstrated that saccades curve away from irrelevant distractors (Doyle & Walker, 2001), previous distractor locations (Belopolsky & van der Stigchel, 2013), and the locus of visuospatial attention (Sheliga, Riggio, & Rizzolatti, 1994, 1995). Furthermore, saccade curvatures are modulated by distance (McSorley et al., 2009; van der Stigchel et al., 2007), salience (van Zoest, Donk, & van der Stigchel, 2012), colour contingent capture (Ludwig & Gilchrist, 2003; Mulckhuyse, van der Stigchel, & Theeuwes, 2009), target probability (Walker et al., 2006), semantic meaning (Weaver, Lauwereyns, & Theeuwes, 2011), emotional valance (Schmidt, Belopolsky, & Theewues, 2012), and social relevance (Laidlaw, Badiudeen, Zhu, & Kingstone, 2015). The available behavioural evidence suggests that the oculomotor system encodes multiple competing saccade vectors in parallel and computes a weighted average of these vectors (see Godjin & Theeuwes, 2002; Findlay & Walker, 1999). Furthermore, a combination of bottom-up and top-down factors modulates the vector weights used in this computation.

1.4 The Current Research

The purpose of the current research was to answer 3 main questions: Are objects represented with a universal perceptual code? Is the SC capable of highly complex visual processing? And how do temporal factors contribute to competitive processing in the oculomotor system?

There are very robust perceptual effects observed for objects at the lowest and highest ends of the visual hierarchy (e.g., oriented lines and faces respectively) suggesting that these classes of objects are perceptually encoded in a similar manner. However, these effects have not

yet been demonstrated for complex, novel objects. As all three of these object classes are encoded in a similar manner neurologically and since our perceptions of objects and object features arise from the underlying neurophysiology of the visual system, we hypothesized that complex, novel objects should demonstrate similar perceptual effects as other object classes and examined this hypothesis in Chapter 2.

There is extensive evidence that the SC is involved in competitive target selection processing. However, as areas such as FEF are also involved in this process and can impose saccade goals on SC, it is possible that SC simply encodes saccade vectors and does not process visual information at all. In either case, it is unlikely that visual processing in SC is capable of the same complex visual-cognitive computations that occur at the highest levels in the ventral stream, such as computing the visual similarity between highly complex, novel visual representations. Therefore, saccade curvature modulation by these factors would suggest that SC simply represents potential saccade vectors and does not functionally contribute to visual processing. We examined this possibility in Chapter 3.

It is unclear whether curved saccades are always elicited from the same temporal profile of competitive processing between potential targets. The temporal mechanism for eliciting saccades towards a distractor is well understood, while the temporal mechanism for eliciting saccades away from a distractor is disputed. If the temporal profile of competitive interactions does generalize to these different types of saccades, this would predict that by modeling the competitive processes over time for these different types of saccades, the functions should be the same. In Chapter 4, we examined whether the same temporal mechanism elicits saccade curvature across these two competitive processing contexts.

Chapter 2: Nonlinear perceptual similarity encoding of complex, novel objects in object space (Manuscript 1)

This manuscript has been submitted to the ***Journal of Experimental Psychology: Human Perception and Performance***. The co-author of this manuscript is Dr. Mazyar Fallah. Devin Heinze Kehoe and Dr. Mazyar Fallah designed the experiment. Devin Heinze Kehoe implemented the experiment and analyzed the data. Our research assistant, Selvi Aybulut, collected the data. Devin Heinze Kehoe wrote the manuscript with feedback from Dr. Fallah.

Keywords

object perception, feature space, visual similarity, perceptual repulsion, psychometric function

2.1 Summary

Extensive evidence suggests that complex objects are encoded along a series of their underlying feature dimensions that situates them at some location in *N*-dimensional feature space. Consequently, the perceptual similarity between two objects corresponds to the inverse of the distance between their respective locations. This object property predicts that the similarity between objects is an emergent property of the discriminability of their constituent features, although this prediction has not yet been examined. Here, we constructed complex, novel objects by intersecting 6 or 7 line subunits together at right angles (characters; Experiment 1) or embedding them along the medial axes of a circle (wagon wheels; Experiment 2) and systematically varied the similarity between stimuli by adding or removing a line. Our data indicated that the stimuli constructed with smaller orientations are indeed inherently more similar, but that a common similarity computation was utilized for both object classes. By estimating the perceptual distance between our stimuli, we observed perceptual saturation after a sufficient distance in feature space, consistent with nonlinear neuronal response functions. Interestingly, we also observed perceptual repulsion between our character stimuli, which is consistent with other psychophysical effects elicited from complex objects like face adaption.

2.2 Introduction

Examinations of perceptual similarity have provided insights into how the visual system encodes object representations. One influential model of perceptual similarity is the contrast model proposed by Tversky (1977). This model conceptualized perceptual similarity processing as a weighted comparison between the distinctive and shared features between objects. Tversky reported a significant linear relationship between the model and subjective self-reports of perceptual similarity. However, the features input into the model were verbal descriptors of

visual stimuli that varied in concreteness. Therefore, despite the contrast model being quite successful at predicting perceptual data, it does not disentangle the likely separate contributions of visual/structural similarity (Biederman, 1987; Humphreys, Riddoch, & Quinlan, 1988; Palmer, 1977, 1978), conceptual similarity/categorization (Goldstone, 1994; Laws & Gale, 2002; Smith & Heise, 1992), and relational similarity (Gentner, 1983; Goldstone, Medin, & Gentner, 1991; Medin, Goldstone, & Gentner, 1990). For these reasons, it is not very informative about how perceptual similarity relates to the fundamental properties of the human visual system or how it is subserved by the nervous system. To overcome this limitation, other researchers have specifically examined visual/structural similarity by objectively defining features as the geometric subunits of visual stimuli (e.g., Palmer, 1977, 1978).

Extensive research and theorizing has focused specifically on how the individual geometric subunits and structural aspects of objects influence the perceptual similarity between respective objects (Biederman, 1987; Biederman & Cooper, 1991; Biederman & Ju, 1988; Marr & Nishihara, 1978; Palmer 1977; 1978). This work has lead several researchers to argue that object representations that subserve recognition and perception are formed by first detecting the basic geometric constituents of an object (Biederman, 1987; Biederman & Cooper, 1991; Marr & Nishihara, 1978; c.f. Palmer, 1977, 1978). These so-called "structural description" theories (reviewed by Hummel, 2000) were likely influenced by the seminal discovery of orientation and edge selective neurons in early visual cortical areas several decades earlier (Hubel & Wiesel, 1962, 1968) and contour and shape selective neurons in the inferior temporal gyrus (IT) (Desimone et al., 1984). Furthermore, structural description theories necessitate feature binding as these simple geometric visual features will need to be coherently bound together into an object in order for observers to perceive a holistic and unified object rather than disjoint visual features

in isolation (Treisman, 1996; Treisman & Gelade, 1980). Decades of research have demonstrated that feature representations are distributed throughout the primate cortical visual system (reviewed by Perry & Fallah, 2014) and that these feature representations are anatomically organized into a hierarchy of feature complexity from posterior to anterior structures (Felleman & Van Essen, 1991).

An alternative to the contrast model conceptualization of perceptual similarity is multidimensional scaling (MDS), first proposed by Shepard (1962a, 1962b). MDS models assign object representations a location in geometric space with *N* dimensions where each dimension corresponds to a specific visual attribute (e.g., colour, orientation, etc.) and an object's location along that dimension is determined by quantifying the corresponding feature for that visual attribute (e.g., red, vertical, etc.). Therefore, MDS space is often succinctly referred to as "feature space". The utility of MDS is that the perceptual similarity between objects corresponds to the inverse of the *N*-dimensional distance between objects in feature space. The MDS model does not treat attribute dimensions hierarchically *per se*, but it does treat objects as the concatenated whole of their individual features. Since these features can vary in complexity, this does not preclude them from existing in their respective location in the visual hierarchy upon being entered into the MDS model. Furthermore, MDS more closely resembles neurological encoding of simple visual features along each respective dimension in feature space as it treats featural differences as continuous as supposed to categorical like the contrast model.

Conceptualizing objects as existing in multidimensional feature space is useful because it can be used to objectively quantify the similarity between complex objects with multiple feature dimensions. Perhaps the best-studied class of complex objects using this conceptualization is faces. Decades of research examining feature space for faces (called "face space", Valentine,

1991) have validated that face space is encoded by the visual system both perceptually (Anderson & Wilson, 2005; Bruce, Burton, & Dench, 1994; Bruce, Doyle, Dench, Burton, 1991; Johnston, Milne, Williams, & Hosie, 1997; Wilson, Loffler, Wilkinson, 2002) and neurologically (Freiwald, Tsao, & Livingstone, 2009; Leopold, Bondar, & Giese, 2006; Leopold, O'Toole, Vetter, & Blanz, 2001; Loffler, Yourganov, Wilkinson, & Wilson, 2005). For example, on an incidental memory task, humans reported recognizing a prototypical face (i.e., the centroid in face space) despite having never been shown that exact face; interestingly, this prototype learning was strongest for faces but occurred for other complex objects such as houses (Bruce et al., 1991). Furthermore, perceived distinctiveness ratings positively correlate with distances from the centroid in face space constructed using both objective physical measurements of facial features (Bruce et al., 1994) and subjective similarity reports (Johnston et al., 1997).

There is also compelling experimental evidence that face space is represented neurologically. Leopold et al. (2001) elegantly demonstrated that observers adapted to a face after viewing it for several seconds, as psychometric identity functions (i.e., proportion of correct face identifications as a function of distance away from the average face) for faces located on the same axis in face space were skewed towards the adapted face. These facial aftereffects are similar to aftereffects observed for simple visual features represented in early cortical visual areas (Leopold, Rhodes, Müller, & Jeffery, 2005) such as the tilt aftereffect for orientations (Gibson & Radner, 1937). Given that perceptual aftereffects for simple visual features are due to a repulsive shift in neuronal population tunings for the adapted feature (reviewed by Kohn, 2007), these results therefore suggest neuronal tunings for facial prototypes. Furthermore, such neurons would therefore be predicted to exhibit monotonically decreasing firing rates as a face moves away from the preferred prototype in face space. Interestingly, neurophysiological

experiments have validated these predictions: Neurons in IT (Desimone et al., 1984) and the superior temporal sulcus (STS) specifically (Baylis, Rolls, & Leonard, 1985, 1987) are selective for faces, can discriminate between faces, and can discriminate between whole faces and facial features. Critically, more recent neurophysiological investigations have directly observed face space tuning curves: Leopold et al. (2006) observed that the firing rates of IT neurons increased as a face moved away from an average face towards a specific identity. A similar investigation found that the firing rates for face selective neurons in the middle face patch were tuned to a specific subset of face space feature dimensions (Freiwald et al., 2009), therefore also strengthening the notion that simple visual features encoded by posterior neurons are projected forward and concatenated into complex representations encoded by anterior neurons.

Experiments examining face space have provided evidence that faces and simple visual features may be neurally represented in a similar manner. Such similarity between neural encoding of faces and feature singletons is remarkable given the considerable differences in visual complexity between these stimuli. However, one commonality between faces and feature singletons is that they are both very well practiced visual objects with which observers have extensive experience. Interestingly, there are IT neurons selective for complex, novel objects (Desimone et al., 1984; Fujita, Tanaka, Ito, & Cheng, 1992; Kobatake & Tanaka, 1994; Logothetis, Pauls, Poggio, 1995), which have been differentiated from acquired selectivities for complex objects (Baylis & Rolls, 1987; Fahy, Riches, & Brown, 1993; Riches, Wilson, & Brown, 1991). As with faces, neurophysiological investigations have also measured IT neurons tuning curves for specific geometric feature dimensions in feature space for complex, novel objects (Brincat & Connor, 2004, 2006; Kayaert, Biederman, Op de Beeck, & Vogels, 2005). This research therefore suggests that tuning curves are a general property for encoding visual

objects in the primate visual system.

If anterior cortical neurons are tuned to complex visual representations as posterior cortical neurons tuned to simple visual features, then the tuning curve for neurons encoding complex representations should be comparable to those encoding simple features. One property of neuronal tuning curves for certain simple visual features, such as contrast (Albrecht & Geisler, 1991; Albrecht & Hamilton, 1982) and orientation (Hubel & Wiesel, 1968), is saturation: there is a linear relationship between neuronal firing rates and feature values within a certain range of the represented feature; however, firing rates saturate outside of this range. Single cell neuronal tuning curves for face identities (Leopold et al., 2006) or individual feature dimensions in face space (Freiwald et al., 2009) are typically linear (no apparent saturation) with few nonlinear exceptions (apparent saturation). However, using fMRI, Loffler et al. (2005) observed that tuning curves at the population level are clearly sigmoidal. Similarly, single cell tuning curves for complex, novel objects can be linear or nonlinear (Brincat & Connor, 2004, 2006; Kayaert et al., 2005), while at the population level tuning curves for complex, novel objects also appear sigmoidal (Brincat & Connor, 2004; Fujita et al., 1992; Logothetis et al., 1995; Panis, Vangeneugden, Op de Beeck, Wagemans, 2008). A question that arises is what factors determine the saturation point of tuning curves for complex objects.

Here, we examined these factors by computing the perceptual distances between complex, novel, meaningless objects to determine when the perceptual similarity between these objects saturate. We utilized a perceptual judgment task where participants were asked to report which of two test stimuli are perceptually most similar to a referent stimulus (target) (see Sloutsky, Lo, & Fisher, 2001). In two experiments, objective similarity was manipulated by systematically varying the number of line subunits shared between the test stimuli and the target

(Richards, Tombu, Stolz, & Jolicoeur, 2004; Smilek, Eastwood, & Merikle, 2000). We assumed that this manipulation would modulate the perceptual similarity between stimuli and followed up on this assumption by investigating the relationship between objective similarity manipulations and perceptual similarity reporting. Secondly, the differences in objective similarity between the target and each test stimulus were used to construct objective similarity distances in 1-dimensional objective similarity space. We then used the perceptual data to extrapolate the objective similarity distance at which perceptual reporting would become certain (100% responding for the objectively most similar stimulus). By fitting a line through the estimated point of theoretical, perceptual certainty and the point of theoretical perceptual chance (i.e., mathematical origin), we estimated the point of perfect linearity between objective and perceptual similarity. Finally, we then estimated perceptual distances by linearly transforming each objective similarity distance to this line.

2.3 Experiment 1: Character Stimuli

For experiment 1, we constructed novel, complex, and meaningless character stimuli by conjoining individual line subunits together at right angles, similar to those utilized by Palmer (1977, 1978). We utilized stimuli that were both novel and meaningless to minimize or eliminate the influences of conceptual similarity/categorization (Goldstone, 1994; Laws & Gale, 2002; Smith & Heise, 1992) on perceptual judgments of similarity, as participants likely had no prior experience with these stimuli. Furthermore, as we were interested in examining the perceptual distance at which perceptual similarity saturates, we utilized certain task parameters to maximize the likelihood that participants generated a holistic visual perceptual representation of the stimuli (Palmer, 1977; Tanaka & Farah, 1993) when making similarity judgments rather than employ a simple comparative strategy in which every individual line subunit in the test stimuli is

sequentially compared to every line subunit in the target stimulus (we elaborate more on this topic in the General Discussion). We examined whether observers utilized a sequential, comparative process by analyzing response times (RT) as a function of objective similarity (OS) distance since increasing the objective similarity distance would increase the number of line segment comparisons required for this process and since RT should increase linearly as a function of task set size for a sequential process (Neisser, 1967).

2.3.1 Methods

2.3.1.1 Participants

10 York University undergraduate students (18-20 years old, 4 male) participated in the experiment for course credit. Participants had normal or corrected-to-normal vision and were naïve to the purpose and design of the experiment. Written consent was obtained prior to participation. All research was approved by York University's Human Participants Review Committee.

2.3.1.2 Stimuli

2 sets of character stimuli that do not resemble meaningful alphanumerical characters to an English speaker were constructed offline using custom algorithms in MATLAB (MathWorks, Natick, MA) (see Figure 1). We intersected 6 or 7 vertical and horizontal line segments (1°× 0.08°) together at right angles, which occupied 1 of 12 possible locations that were embedded in an imaginary box (2°× 2°). All line segments intersected with at least one other line segment. By adding and/or removing one line segment at a time, we created 6 stimuli that were linearly related in objective similarity (OS). The stimuli were grouped into an exhaustive list (n = 120) of stimulus triplets in which every stimulus was unique and was from the same stimulus set. In every stimulus triplet, one stimulus was assigned as the target, and the remaining two stimuli

were assigned as the left and right test stimuli. We then calculated the relative OS (OS_R) for each triplet. OS_R was defined as the absolute OS between the target stimulus and the left test stimulus (OS_{Left}) subtracted by the absolute OS between the target stimulus and the right test (OS_{Right}) stimulus, such that $OS_R = | OS_{Left} | - | OS_{Right} |$. The magnitude of OS_R therefore indicates how much more objectively similar the most similar stimulus is to the target than the least similar stimulus. For each experimental run, we randomly sampled 56 stimulus triplets without replacement, while constraining the selection so that there were 8 stimulus triplets selected for all relative OS values in the range of −3 to +3. As we were interested in perceptual similarity as a function of objective similarity distances, we analyzed perceptual similarity as a function of the absolute OS_R, which we subsequently refer to as OS distance.

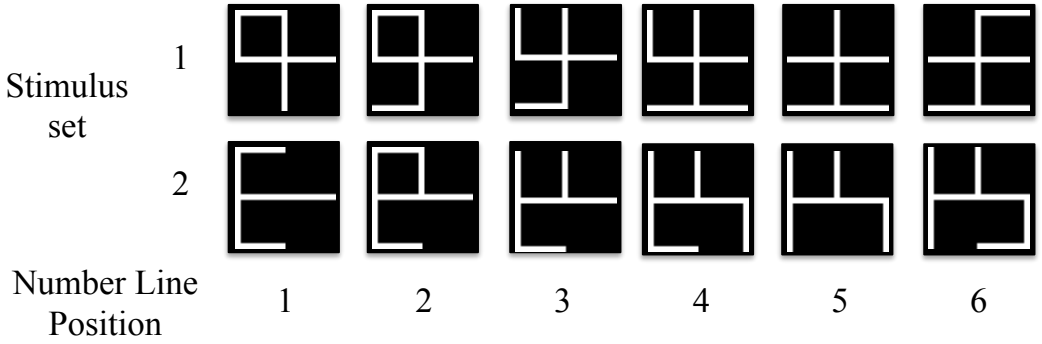

Figure 3.1: Stimulus sets utilized in experiment 1. Stimuli are placed on a conceptual number line on which the absolute difference between number line positions corresponds to the number of line segment dissimilarities (distance).

The stimuli were white ($x = 119.90$, $y = 126.02$) and were displayed against a black background ($x = 0.23$, $y = 0.20$) on a 21-inch CRT monitor (60 Hz, 1024 × 768). Participants viewed stimuli in a dimly lit room from a viewing distance of 57 cm with a headrest stabilizing their head position.

2.3.1.3 Apparatus and measurement

Stimulus presentation was controlled using a computer running Presentation software (www.neurobs.com) and a serial response box (Cedrus, San Pedro, CA). Eye position was recorded using infrared eye tracking (500 Hz, EyeLink II, SR Research, Ontario, Canada). The eye tracker was calibrated at the beginning and halfway point of each experimental session, and as needed.

2.3.1.4 Task procedure

Trials were initiated by pressing the center button on the serial response box (see Figure 2). After maintaining fixation (within a 1.89° square window) to a white, central fixation cross (0.4°× 0.4°) for 200 ms, the fixation cross was replaced with the target stimulus flanked by two grey (x = 28.43, y = 29.98) placeholders subtending 2°× 2° and located 7.5° away from the target along the horizontal meridian. After 500 ms, the target then reverted back to the fixation cross and the placeholders were replaced by the two test stimuli. Participants were instructed to discriminate whether the left or right test stimulus was the most perceptually similar to the target by pushing the left or right button on the serial response box respectively. Participants were required to maintain fixation throughout the trial. The trial ended when a response was made or fixation was broken. Participants heard an error tone when fixation was broken and these trials were randomly replaced back into the block.

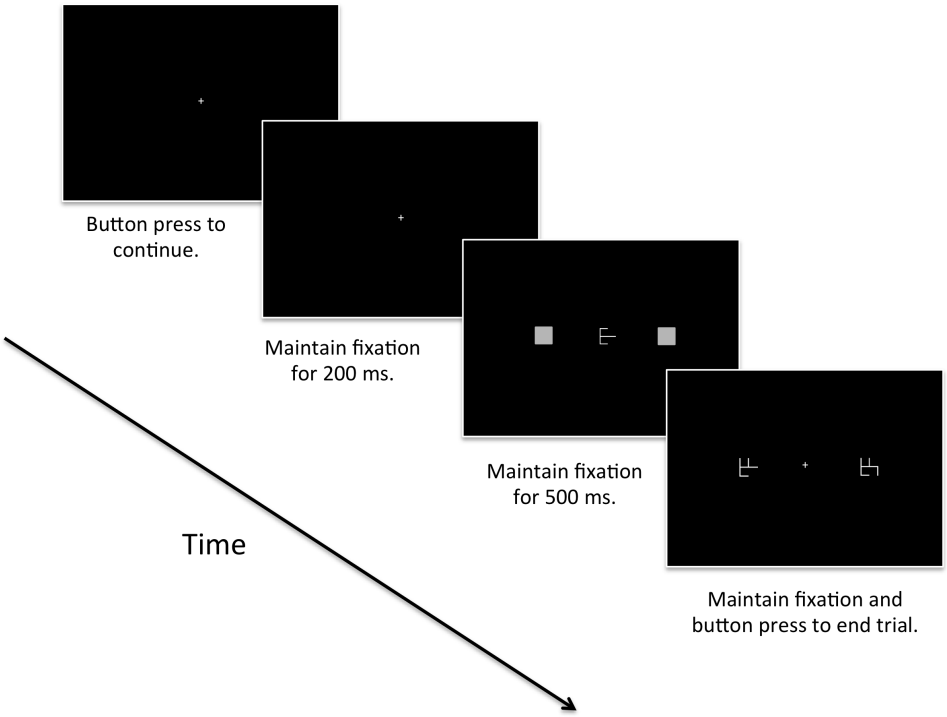

Figure 3.2: Example trial sequence.

Participants completed 1 session with 8 blocks of 56 trials for a total of 448 trials. On the first block, the counterclockwise (CCW)/clockwise (CW) ordering of the test stimuli was randomized. This ordering was reversed after each subsequent block.

2.3.2 Results

For continuous data, repeated-measures ANOVA and paired-samples Student's *t*-tests were used to analyze repeated-measures mean differences if a Shapiro-Wilks test provided evidence for normally distributed data ($p > .05$). Otherwise, non-parametric Friedman tests and Wilcoxon Signed-Rank tests were used. If Mauchley's test of sphericity provided insufficient evidence for the assumption of sphericity, Greenhouse-Geisser ($\boldsymbol{\varepsilon} \leq 0.7$) or Huynh-Feldt ($\boldsymbol{\varepsilon} > 0.7$) corrections were utilized for ANOVAs. Frequency data were analyzed using *Chi*-squared tests. Bonferroni multiplicity α corrections were utilized for all multiple comparisons.

For every trial, we calculated (1) the OS between the selected test stimulus and the target (*selected*) and (2) the OS between the unselected test stimulus and the target (*unselected*). OS was utilized as a manipulation of perceptual distance along 1-dimensional perceptual similarity space. These OS distances were subsequently analyzed both as a continuous and categorical variable.

2.3.2.1 OS distances between target and selected and unselected test stimuli

First, OS distance was treated as a continuous variable. As such, a paired-samples *t*-test between mean selected and unselected test stimulus OS distances to the target demonstrated that the OS distance of the selected stimulus ($M = 1.99$) was reliably lower than the OS distance of the unselected stimulus ($M = 2.93$), $t(9) = -7.66$, $p < .001$, $d = 2.42$.

Second, OS distance was treated as a categorical variable. After removing trials with equal OS distances between the target and both test stimuli (OS distance = 0), we calculated the observed and expected frequencies for every categorical selected and unselected OS distance (min = 1, max = 5) (see Figure 3). Observed frequencies were calculated as the proportion of selected and unselected trials in each OS distance category. Expected frequencies were calculated by dividing the total number of trials in each OS distance category by 2 as participants were forced to choose one stimulus on every trial. A *Chi*-squared analysis demonstrated that the observed frequencies were not randomly distributed across OS distance, $\chi^2(4, N = 3840) = 549.99$, $p < 0.001$, Cramer's $\varphi = 0.19$.

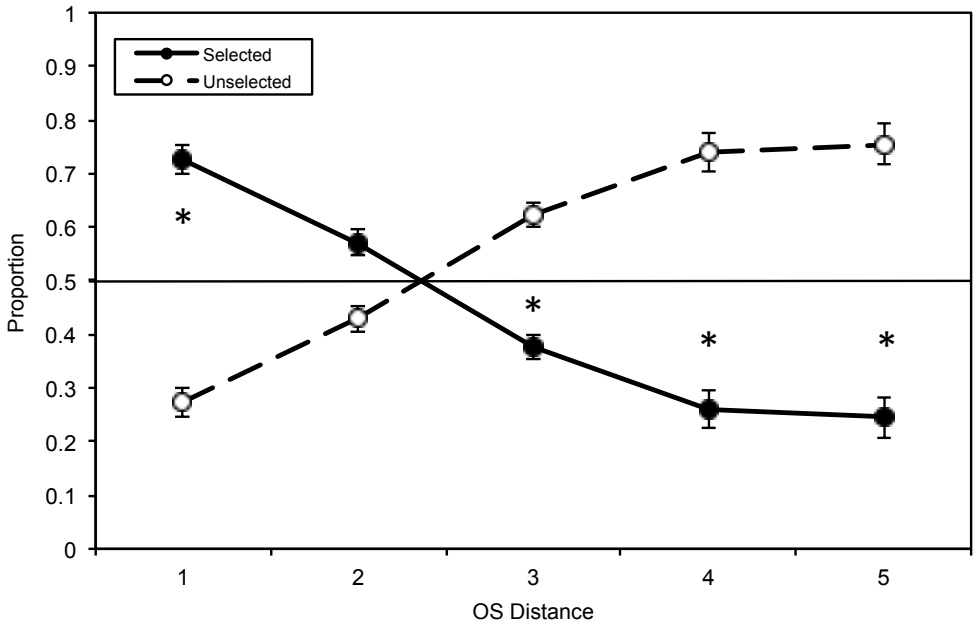

Figure 2.3: The proportion of selected and unselected trials as a function of OS category. Error bars represent standard error (SE). *Significant deviations from chance (.5) using a paired-samples *t*-test with Bonferroni multiplicity adjusted $p < .05$.

For every OS distance, the proportion of selected trials was compared against chance (.5) using a paired-samples *t*-test. A test stimulus with an OS distance of 1 was chosen significantly above chance, $t(9) = 7.97$, $p < 0.001$, $d = 2.52$. Conversely, test stimuli with an OS distance ≥ 3 were selected below chance: OS distance 3, $t(9) = -5.26$, $p = 0.003$, $d = 1.66$; OS distance 4, $t(9) = -6.73$, $p < 0.001$, $d = 2.13$; and OS distance 5, $t(9) = -6.48$, $p < 0.001$, $d = 2.05$. A test stimulus with an OS distance of 2 was selected at chance level, $t(9) = 3.02$, $p = 0.073$, $d = 0.95$.

2.3.2.2 RT as a function of OS distance

Response times (RT) were analyzed as a function of OS distance using a repeated-measure ANOVA to examine potential mean differences and a linear regression analysis to examine a potential linear relationship. These analyses provided insufficient evidence for mean

differences between OS distances, $F(3,27) = 1.48$, $p = 0.238$, $\eta_p^2 = 0.14$; and insufficient evidence for a linear relationship between RT and OS distance, $F < 1$.

2.3.2.3 Accuracy as a function of OS distance

We calculated the proportion of trials on which the test stimulus that is objectively most and least similar to the target was selected for each OS distances. At an OS distance of 0, the OSs between the target and both test stimuli were equal. Therefore, the most and least similar test stimulus selection frequencies were replaced with the left and right test stimulus selection frequencies. This condition serves as a baseline.

For every OS distance, we subtracted the proportion of trials on which the least similar test stimulus was selected from the proportion of trials on which the most similar test stimulus was selected and referred to this metric as perceptual similarity (PS). We then analyzed PS as a function of OS distance (see Figure 4). A Friedman test provided evidence that there was a significant mean difference between OS distances, $\chi^2(3) = 19.73$, $p < 0.001$. Subsequent post-hoc analyses examined potential mean differences between all sequential OS distances and found no significant difference between OS distance 0 and 1, $Z = -1.58$, $p = 0.341$. However, there were significant differences between OS distances 1 and 2, $Z = -2.70$, $p = 0.021$; and between OS distances 2 and 3, $Z = -2.50$, $p = 0.037$. This post hoc analysis suggested a linear distribution of OS distance means, which was then confirmed by a linear regression $F(1,2) = 90.05$, $p = 0.011$, $R^2 = 0.98$.

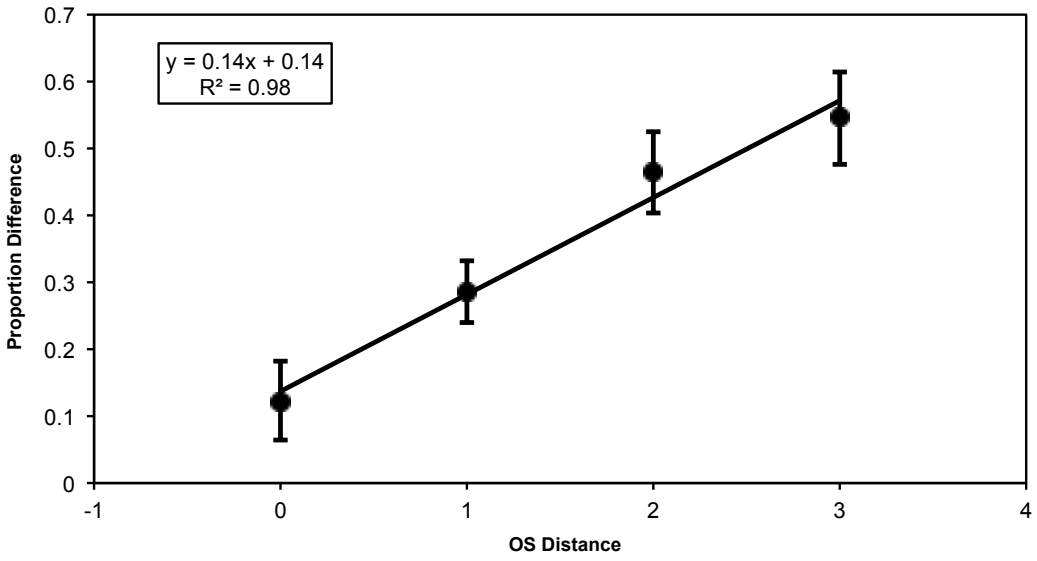

Figure 2.4: Perceptual similarities. Differences between the proportion of trials on which the least similar test stimulus was selected and the proportion of trials on which the most similar test stimulus was selected as a function of OS distance. Error bars represent SE.

2.3.2.4 Transformations of OS distance to perceptual distances

Differences between the proportion of trials on which the least similar test stimulus was selected and the proportion of trials on which the most similar test stimulus was selected (PS) was used to generate estimates of perceptual distance (see Figure 5). First, we fit a Gaussian cumulative distribution function (CDF) to the mean PS as a function of OS distance data (μ = 2.47, σ = 2.46, R^2 = .96). Second, we estimated the point of perceptual certainty (i.e., the OS distance at which PS theoretically equals 1) by calculating the tangent of the mean Gaussian CDF and extrapolated this line to PS = 1. Third, we fit a linear function between the point of perceptual certainty (PS = 1) and the point of perceptual chance (PS = 0). Finally, perceptual distances were computed by linearly transforming each OS distance to the linear function in step 3 using the corresponding PS for each OS distance. These transformations provided our estimate

of perceptual distances between the target and test stimuli.

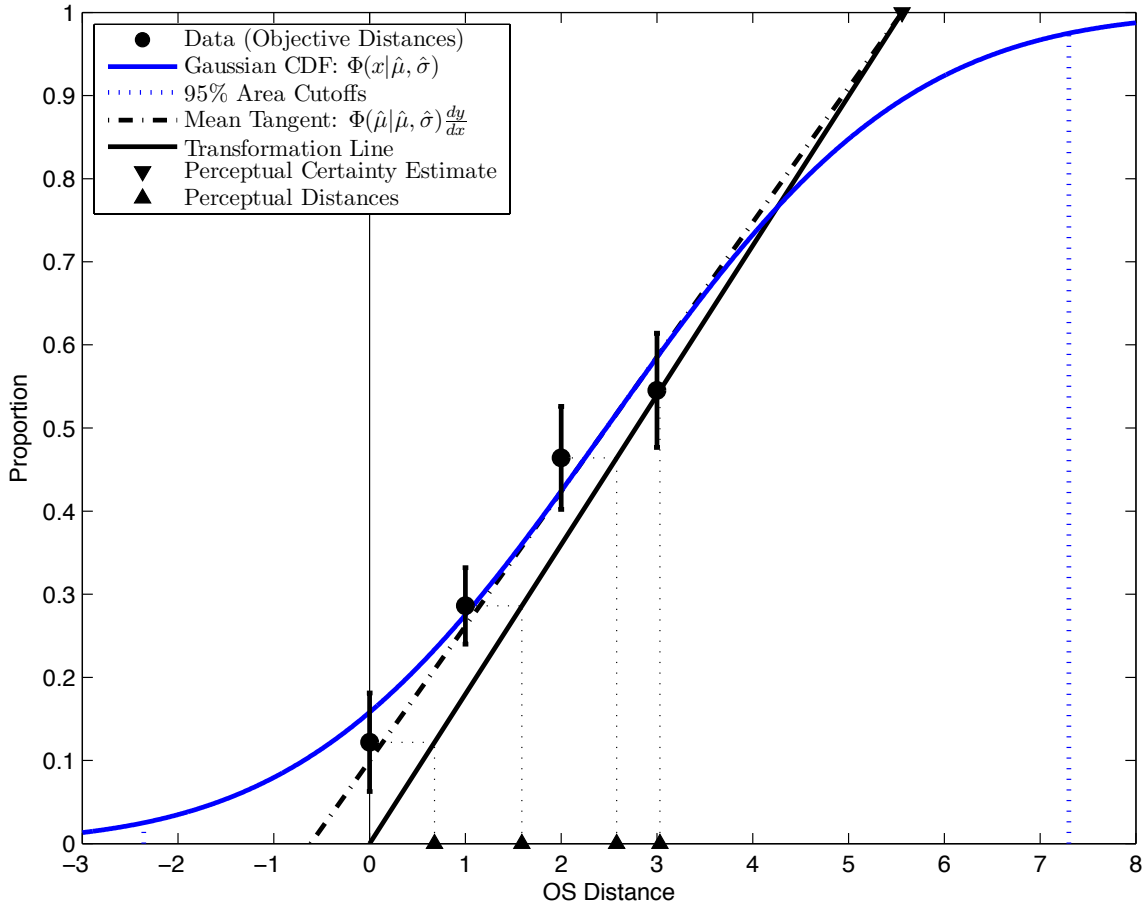

Figure 2.5: Perceptual distance estimates. Upright triangles denote the perceptual distance estimates superimposed on the OS distance number line used in the current experiment. The downward triangle denotes the point of perceptual certainty estimate. The solid black line was utilized for the linear transformation of the OS distances. The broken black line is the tangent of the mean Gaussian CDF. The solid blue line is the fitted Gaussian CDF. The black circles are the mean PS as a function of OS distance. Error bars denote SE.

2.3.3 Discussion

The current results provide compelling evidence that systematically varying the number of line subunits shared between our character stimuli modulates the perceptual similarity

between them. First, by treating OS distances as continuous, we observed that the distance between the target and the selected stimulus was reliably shorter than the distance between the target and the unselected stimulus. This result suggests that participants were systematically selecting the test stimulus that was closer in similarity space to the target. Second, by treating the OS distances as categorical, we observed that when one of the two test stimuli had the shortest possible OS distance to the target (i.e., OS distance = 1), it was selected more than is predicted by chance alone. Similarly, when one of the two test stimuli had a longer OS distance to the target (i.e., OS distance ≥ 3), this test stimulus was chosen less often than is predicted by chance alone. Third, we observed that the proportion of trials on which the test stimulus that is objectively most similar to the target was selected increased linearly as a function of OS distance, where OS distance indicates how much more similar this test stimulus was to the target than the objectively least similar stimulus. Taken together, these results validate our approach to manipulating perceptual similarity.

One possible explanation for these results is that participants sequentially compared each individual line segment in the test stimuli to the line segments in the target and counted the number of differences between each test stimulus and the target. This account predicts that RT should increase linearly as a function of OS distance. However, there was no such relationship between RT and OS distance or any mean differences in RT between OS distances. Thus, the effects of objective similarity on perceptual similarity cannot be attributed to a sequential comparison process and instead likely reflect perceptual judgments based on holistic visual/structural representations of perceived similarity (Palmer, 1977; Tanaka & Farah, 1993).

We performed a linear transformation on the perceptual reporting for each OS distance to convert the OS distances into perceptual distances. This distribution of perceptual distances had

three significant characteristics: (1) The distribution of perceptual distances had an approximately linear range (OS distances between 0 and 2). (2) However, the perceptual distances in the linear range were all rightward shifted (i.e., similarity repulsion). This indicates that perceptual distances, and thus the perceived similarity between these character stimuli, were less than is predicted by their objective distances. (3) Critically, the perceptual distances of 2 and 3 were clustered around the OS distance of 3, which suggests that this is the saturation point in perceptual similarity space for these stimuli. As stimuli exceed this point in OS distance, the perceptual similarity remained constant. As with our neurological predictions, this may be the saturation point for neuronal firing rates for this stimulus set, which will be discussed further in the General Discussion.

Experiment 1 supports our prediction that perceptual distances will saturate after a certain point in OS space. Furthermore, we offer a neurological explanation for this observation whereby a neuron encodes the target and the firing rates of this neuron monotonically increase as a test stimulus placed in its receptive field moves away from the target in feature space, however, the firing rates for this neuron will saturate after a certain range of objective similarity. Interestingly, a converging piece of evidence for this explanation would be to elicit saturation in the opposite direction of perceptual similarity space. If a stimulus set with objects that are highly similar is utilized for this task, then a certain point in OS space will likely need be crossed before perceptual similarity distances even begin to linearly increase. We examined this prediction in Experiment 2.

3.4 Experiment 2: Wagon Wheel Stimuli

We constructed a secondary stimulus set for use in Experiment 2 using the same 6 or 7 individual line orientations, but instead we embedded them along a medial axis of a 2° circle and

situated them between the middle and circumference of the circle. We enclosed the circle with a line of equal width. As such, we refer to these stimuli as wagon wheels given their shape: The line subunits are the "spokes" and the encircling line is the "felloe". These stimuli were utilized because they are likely much more perceptually similar to one another and therefore may elicit a saturation at short distances in OS space. Previous research examining perceptual similarity by Palmer (1977) demonstrated that figures very similar to those utilized in Experiment 1 could be segmented into "good cuts" and "bad cuts" that are determined by Gestalt principles like connectedness and overall contours, suggesting that object subparts may give additional similarity cues to observers. Similarly, Palmer (1978) demonstrated that perceptual similarity judgments between a target and test stimulus with one individual line subunit difference between them can systematically increase if the feature difference preserves the overall contour of the object. The overall contours of our stimulus sets were not well controlled by the objective similarity manipulations utilized in Experiment 1, which could be decreasing the similarity between stimuli. By alternatively utilizing these wagon wheel stimuli, we can reduce/eliminate the impact of subparts, overall contour, and closedness as the line subunits are uniformly encircled. This will therefore ensure that the overall contour is identical between stimuli. Furthermore, orientation differences between wagon wheel "axles" can be made very small and will therefore be much more difficult to parse from the overall object than the orthogonal orientations used for the character stimuli in Experiment 1. Therefore, by utilizing these wagon wheel stimuli, we hypothesize that perceptual distances saturate at short OS distances.

3.4.1 Methods

3.4.1.1 Participants

10 York University undergraduate students (19-29 years old, 2 male) participated in the

experiment for course credit. Participants had normal or corrected-to-normal vision and were naïve to the purpose and design of the experiment. Informed consent was obtained prior to participation. All research was approved by York University's Human Participants Review Committee.

3.4.1.2 Stimuli

2 sets of wagon wheel stimuli were constructed offline using custom algorithms in MATLAB (MathWorks, Natick, MA). Stimuli were constructed by connecting 6 or 7 axial lines (1°× 0.08°) from the center of a circle (diameter = 2°, thickness = 0.08°) through a medial axis to its circumference at 1 of 12 possible angles that were evenly spaced (interval = (1/12) × 2 × pi rad ≈ 0.52 rad) about the circle and included the cardinal axes (see Figure. 6). All other stimulus parameters were identical to the character stimuli in Experiment 1.

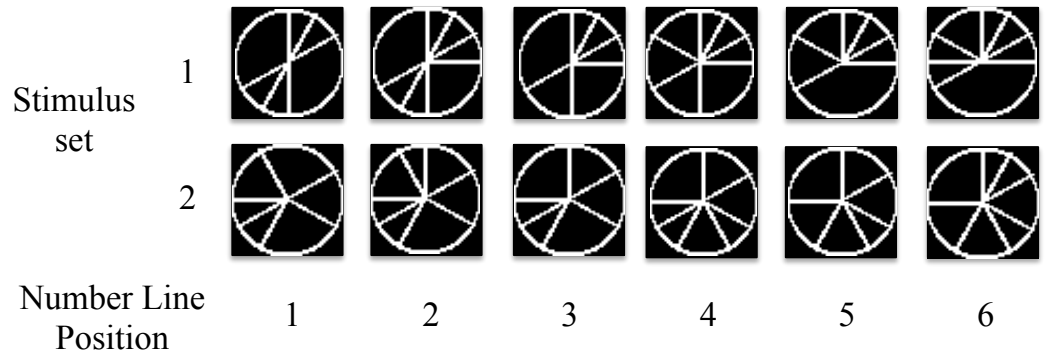

Figure 2.6. Stimulus sets utilized in the experiment 2. Stimuli are placed on a conceptual number line on which the absolute difference between number line positions corresponds to the number of line segment dissimilarities (distance).

3.4.1.3 Apparatus and measurement

The apparatus and measurement was identical to Experiment 1.

3.4.1.4 Task procedure

The task procedure was identical to Experiment 1.

2.4.2 Results

Identical statistical procedures as those utilized in Experiment 1 were utilized for analyzing the data from Experiment 2.

2.4.2.1 OS distances between target and selected and unselected test stimuli

First, OS distance was treated as a continuous variable. As such, a paired-samples *t*-test between selected and unselected test stimulus OS distances to the target demonstrated that the OS of the selected stimulus ($M = 2.26$) was reliably lower than the OS of the unselected stimulus ($M = 2.68$), $t(9) = -4.93$, $p < .001$, $d = 1.56$.

Second, OS distance was treated as a categorical variable. As with Experiment 1, we removed trials with equal OS distances between the target and both test stimuli (OS distance = 0), and then calculated the observed and expected frequencies for every categorical selected and unselected OS distance (min = 1, max = 5) (see Figure 7). Observed frequencies were calculated as the proportion of selected and unselected trials in each OS distance category. Expected frequencies were calculated by dividing the total number of trials in each OS distance category by 2 as participants were forced to choose one stimulus on every trial. A *Chi*-squared analysis demonstrated that the observed frequencies were not randomly distributed across OS distance, $\chi^2(4, N = 3840) = 103.41$, $p < 0.001$, Cramer's $\varphi = 0.08$.

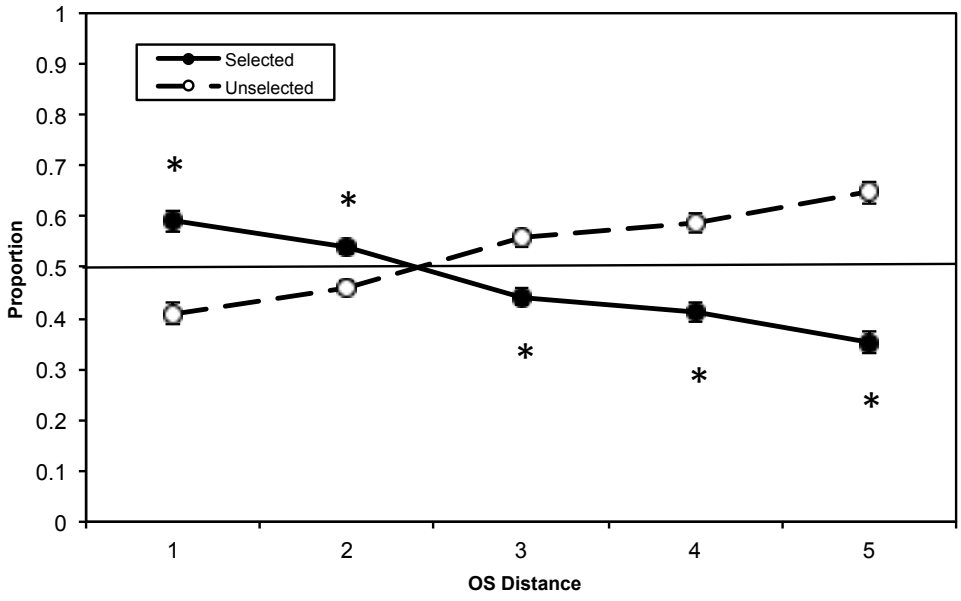

Figure 2.7: The proportion of selected and unselected trials as a function of OS category. Error bars represent SE. *Significant deviations from chance (.5) using a paired-samples *t*-test with Bonferroni multiplicity adjusted $p < .05$.

For every OS distance, the proportion of selected trials was compared against chance (.5) using a paired-samples *t*-test. The selection of test stimuli was not predicted by chance across all 5 OS distances. A test stimulus with an OS distance ≤ 2 was chosen significantly above chance: OS distance 1, $t(9) = 4.31$, $p = 0.009$, $d = 1.36$; OS distance 2, $t(9) = 3.33$, $p = 0.044$, $d = 1.05$. Conversely, test stimuli with an OS distance ≥ 3 were selected below chance: OS distance 3, $t(9) = -3.29$, $p = 0.047$, $d = 1.04$; OS distance 4, $t(9) = -4.29$, $p = 0.010$, $d = 1.36$; and OS distance 5, $t(9) = -6.52$, $p < 0.001$, $d = 2.06$.

2.4.2.2 RT as a function of OS distance

Response times (RT) were analyzed as a function of OS distance using a repeated-measure ANOVA to examine potential mean differences and a linear regression analysis to

examine a potential linear relationship. These analyses demonstrated a marginal, but unreliable mean difference between OS distances, $F(1.38,12.44) = 3.85$, $p = 0.062$, $\eta_p^2 = 0.30$; and insufficient evidence for a linear relationship between RT and OS distance, $F < 1$.

2.4.2.3 Accuracy as a function of OS distance

As in Experiment 1, we calculated the proportion of trials on which the test stimulus that is objectively most and least similar to the target was selected for each OS distances. (At an OS distance of 0, the OSs between the target and both test stimuli were equal. Therefore, the most and least similar test stimulus selection frequencies were replaced with the left and right test stimulus selection frequencies. This condition serves as a baseline.)

We calculated perceptual similarity (PS) in an identical manner as in Experiment 1 and analyzed PS as a function of OS distance (see Figure 8). A repeated-measures ANOVA provided evidence for a significant mean difference between OS distances with a significant linear component, $F(1,9) = 10.04$, $p = 0.011$, $\eta_p^2 = 0.53$. This linear trend was further investigated with a linear regression, which provided evidence for a significant linear relationship between OS distance and perceptual similarity, $F(1,2) = 47.58$, $p = 0.020$, $R^2 = 0.96$.

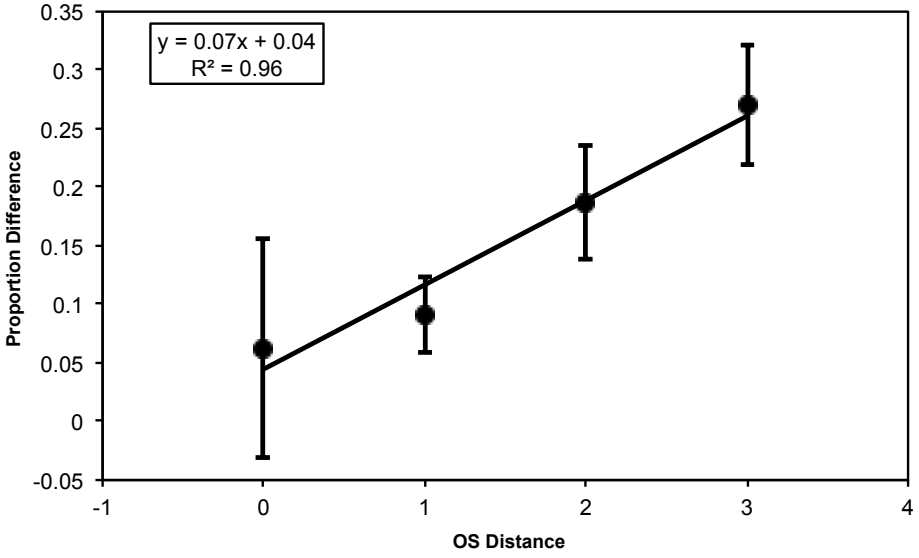

Figure 2.8: Perceptual distances. Differences between the proportion of trials on which the least similar test stimulus was selected and the proportion of trials on which the most similar test stimulus was selected as a function of OS distance. Error bars represent SE. Also depicted is the line of best fit, linear regression equation, and coefficient of determination.

2.4.2.4 Transformations of OS distance to perceptual distances

Estimates of perceptual distances for the wagon wheel stimuli were generated in an identical manner as was used in Experiment 1 (see Figure 9). The Gaussian CDF was fit with μ = 4.68, σ = 2.84, and R^2 = .98.

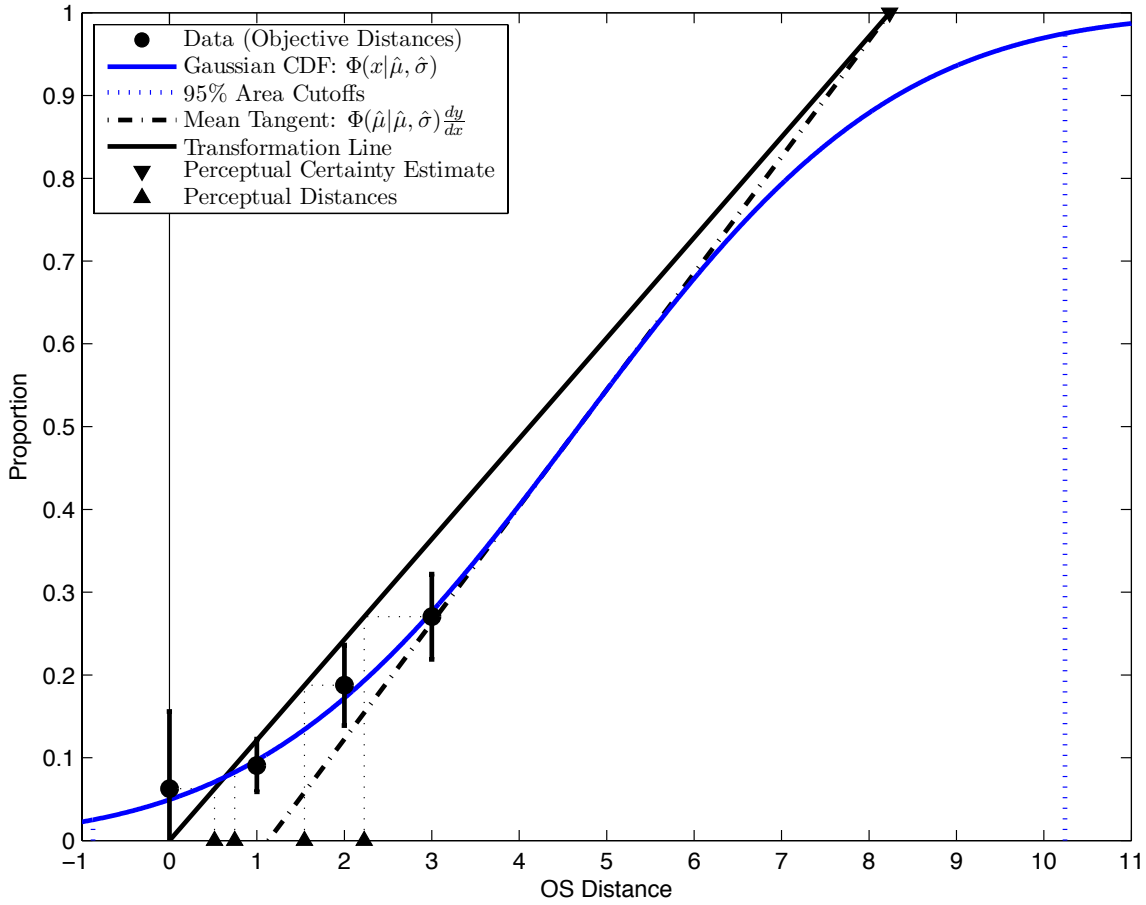

Figure 2.9: Experiment 2 perceptual distance estimates. Upright triangles denote the perceptual distance estimates superimposed on the OS distance number line used in the current experiment. The downward triangle denotes the point of perceptual certainty estimate. The solid black line was utilized for the linear transformation of the OS distances. The broken black line is the tangent of the mean Gaussian CDF. The solid blue line is the fitted Gaussian CDF. The black circles are the mean PS as a function of OS distance. Error bars denote SE.

2.4.3 Discussion

Consistent with the results from Experiment 1, manipulating the number of line subunits shared between stimuli modulates the perceived similarity between them. This result has therefore been replicated using two classes of objects with perceptually significant

visual/structural differences. However, although the pattern of results between Experiment 1 and 2 are qualitatively similar, there are notable quantitative differences that suggest that the wagon wheel stimuli were inherently more perceptually similar to one another than were the character stimuli: (1) When OS distance was analyzed as a continuous variable, the mean difference in OS distance between the target and the selected and unselected test stimuli were greater in Experiment 1 than in Experiment 2 (M_{D1} = .94, M_{D2} = .42; respectively), as were the effect sizes (d_1 = 2.42, d_2 = 1.56; respectively). (2) Conversely, OS distance was analyzed categorically as we calculated the distribution of trials across OS distance categories for the selected and unselected test stimuli (see Figure 3 and Figure 7). The data demonstrated that this distribution deviated further from chance for the character stimuli than for the wagon wheel stimuli, as demonstrated by the effect sizes for a goodness-of-fit analysis (Cramer's φ_1 = 0.19, Cramer's φ_2 = 0.08; respectively, where $N_1 = N_2$). (3) The slope of the linear best fit of perceptual similarity as a function of OS distance (see Figure 4 and Figure 8) is twice as steep for the Experiment 1 data than the Experiment 2 data ($slope_1$ = .14, $slope_2$ = .07; respectively). (4) The mean of the Gaussian CDF fit to the perceptual similarity as a function of OS distance data (see Figure 5 and Figure 9) was less for Experiment 1 than Experiment 2 (μ_1 = 2.47, μ_2 = 4.68; respectively) despite having similar standard deviations (σ_1 = 2.46, σ_2 = 2.84; respectively). The inherent differences in perceptual similarity between the character and wagon wheel stimuli can be explained psychologically by differences in how well the overall contour and closedness is preserved across OS distance (Palmer, 1978), which would likely then also minimize or eliminate the influence of perceptual subparts (Palmer, 1977), and by the discriminability of the individual constituent features of the objects.

As in Experiment 1, the current results cannot be attributed to observers utilizing a simple

comparative process whereby each individual line subunit in the test stimulus are compared to each line subunit in the target as there were no reliable mean RT differences between OS distance and no functional relationship between mean RT and OS distance.

Critically, the results from the current experiment provide converging evidence that perceptual distances saturate outside of a specific range in objective similarity space. As in Experiment 1, there was a linear range of perceptual distances (OS distances 1, 2, 3) and outside of this range the perceptual distances saturated. However, unlike in Experiment 1, the point of saturation actually occurred at early objective similarity distances: the saturation point was approximately a perceptual distance of 1 as the perceptual distances of 0 and 1 were clustered together. This observation coincides with our efforts to make the wagon wheel stimuli more inherently perceptually similar to each other and is consistent with neuronal encoding of similarity as is discussed in the next section.

2.5 General Discussion

We investigated whether the perceptual distances between complex, novel, and meaningless objects would saturate at a certain objective similarity distance as this provides insight into the link between perceptual experience and the neural mechanisms that subserve our perceptions (Parker & Newsome, 1998). Our elementary assumption was that objectively manipulating the number of line subunits shared between our stimuli would modulate the perceived similarity between them and we have reported the results of multiple analyses that have confirmed this assumption. As such, these results are consistent with highly influential structural description theories of visual perception (Biederman, 1987; Biederman & Cooper, 1991; Marr & Nishihara, 1978) and therefore relate the current observations to foundational work in the field. Furthermore, contrasting these results between Experiment 1 and 2 (see

Experiment 2 discussion) also confirms that the inherent similarity between the wagon wheel stimuli was higher than for the character stimuli. As such, there were notable differences in the distribution of perceptual distances between these stimuli, which has implications for the visual encoding of these stimuli discussed below.

In Experiment 1, there were three significant observations pertaining to the distribution of perceptual distances between stimuli that merit discussion: (1) There was an approximately linear range of perceptual distances for stimuli with an OS distance between 0 and 2. (2) This linear range was succeeded by a nonlinear range of perceptual distances for stimuli with an OS distance of 2 and 3. (3) The stimuli in the linear range were all rightward shifted along the similarity dimension (similarity repulsion).

A linear and subsequent nonlinear range of perceptual similarities has important implications as this is a common characteristic for neuronal tuning curves, which encode the physical parameters of visual objects. These nonlinear tuning curves have been observed for simple visual features like orientation (Hubel & Wiesel, 1968) and contrast (Albrecht & Geisler, 1991; Albrecht & Hamilton, 1982), and at the population level, for complex objects such as faces (Loffler et al., 2006) and geometric shapes (Brincat & Connor, 2004, 2006; Fujita et al., 1992; Logothetis et al., 1995; Panis et al., 2008). The neuronal response function for a sensory stimulus is often correlated with or similar in shape to psychometric discrimination functions for that stimulus (reviewed by Parker & Newsome, 1998). Given the evidence for nonlinear neuronal response functions for complex objects reviewed above, the data from Experiment 1 suggests that the perceptual similarity between the character stimuli is determined by an underlying neuronal response function tuned in multi-dimensional feature space for complex objects, which we will therefore refer to herein as “object space”.

If a perceptual similarity psychometric function reflects neuronal tuning in object space, then the nonlinearity in the perceptual distances would suggest saturation in the neuronal tuning function at the corresponding OS distance (approximately 3). This is admittedly speculative because of the limited observations in OS distance. At this tentative point of saturation, perceptual similarity was approximately .5, which corresponds to 75% responding for the objectively most similar stimulus. It could be the case that the psychometric function would reach 1 at a sufficient OS distance, and thus an OS distance of 3 does not reflect the true saturation point. However, it could also be the case that this is the true saturation point and thus perceptual responding would therefore never surpass 75% responding for the objectively most similar stimulus if we measured more perceptual similarities at even greater OS distances. This account predicts that if we added a scaling parameter to the ogival psychometric function so that it reached a maximum height of approximately .5 (as it would if the true saturation point was .5), and recalculated the point of perceptual certainty extrapolated to the height of this scaling parameter, then the resulting distribution of perceptual distances should be the same. We conducted this analysis so to test this assumption and found that the distribution of perceptual distances was qualitatively the same (i.e., rightward shifted, linear range between 0 and 2 with a nonlinearity at 3), but demonstrated one quantitative exception: the saturated distance was at an OS distance of approximately 2.5 as supposed to 3 without this parameter. Given the consistency between these results, it appears that the saturation point in perceptual space corresponds to an OS distance between approximately 2.5 and 3.

Our behavioral paradigm involved comparing two spatially balanced test stimuli to a target (referent stimulus). Interestingly, we observed perceptual repulsion in the data from Experiment 1 as the character stimuli in the linear range were all rightward shifted along the

similarity dimensions. This result is similar to perceptual repulsion effects observed when humans are required to make perceptual judgments for simple features such as orientation (Blakemore, Carpenter, & Georgeson, 1970) or motion direction (Marshak & Sekuler, 1979) in the presence of a secondary orientation or motion field. Such perceptual repulsion effects are thought to reflect an inhibitory interaction between neurons encoding these visual features, where mutual (lateral) inhibition expands the perceived difference between the stimulus orientations (Blakemore et al., 1970) or directions (Marshak & Sekuler, 1979). There is substantial evidence that the location in object space for complex geometric shapes (Brincat & Connor, 2004, 2006; Fujita et al., 1992; Kayaert et al., 2005; Kobatake & Tanaka, 1994) and face space (Freiwald et al., 2009; Leopold et al., 2006) are neurologically encoded as with simple visual features in 1-dimensional feature space like orientation (Hubel & Wiesel, 1968) and contrast (Albrecht & Geisler, 1991; Albrecht & Hamilton, 1982). As such, these complex object representations elicit similar, robust psychophysical effects as simple visual features like affereffects (Leopold et al., 2001; Anderson & Wilson, 2005). However, our data is the first to show perceptual repulsion for a complex class of objects.

In contrast to Experiment 1, the results of Experiment 2 were qualitatively different: (1) the saturation of perceptual distances occurred at the shortest OS distances and (2) there was no repulsion of perceptual distances as perceptual distances were actually compressed. The saturation point at short perceptual distances (an OS distance of approximately 1) suggests that there is an OS distance threshold for observers to perceive dissimilarities between the wagon wheel stimuli that was not observed between the character stimuli. This threshold can account for the lack of perceptual repulsion observed for the wagon wheel stimuli: if the differences between stimuli are below threshold, then repulsion should not occur.

Our results clearly demonstrated that the wagon wheel stimuli were inherently more similar than the character stimuli. One source of these inherent differences is likely the fact that the overall contours of the wagon wheels were always preserved since all orientations were symmetrically encircled by the "felloe", and preserving the overall contour between objects increases the perceived similarity between them (Palmer, 1978). Furthermore, this may have also reduced the influence of additional perceptual cues afforded by perceptual subparts (Palmer, 1977). However, a more fundamental explanation for these results is that as discriminability of the constituent line subunits decreases, the overall discriminability of the objects also decreases. This is consistent with neurophysiological research that has demonstrated that a nonlinear tuning curve for a complex, geometric object is an emergent property from the interactions between multiple linear tuning curves for the underlying constituent features of the object (Brincat & Connor, 2004, 2006). As such, in Experiment 1, stimuli were constructed using just two orthogonal orientations (i.e., horizontal/vertical) that were always intersected at right angles, and orthogonal orientations should maximize an observer's discrimination sensitivity (Campbell, Kulikowski, & Levinson, 1966). Conversely, we used 6 orientations in Experiment 2 (object subunits could be 1 of 12 line orientations evenly spaced by 30°), which should therefore decrease observer sensitivity to the orientations. Furthermore, this also introduced orientations on the oblique axes, which are inherently more difficult to discriminate (Appelle, 1972). If complex object representations are subjected to a similar comparative process across object classes, but the discriminability between objects is an emergent property of the discriminability of the constituent features of the object, this would predict that the psychometric discrimination functions should be the same shape between object classes, but should shift along the axis in similarity space. We observed this phenomenon in the current data: the ogival psychometric

functions had a similar shape between object classes, but were shifted along the OS distance axis (reviewed in Experiment 2 Discussion). These results suggest that a common neural circuit is utilized for similarity computations across object classes.

A possible explanation for the current perceptual reporting results is that observers sequentially compared all line subunits between the test stimuli and the target. However, this account predicts that RT should increase linearly as a function of OS distance since the number of line subunit differences linearly increase as a function of OS distance and since sequential processing temporally increases as a function of task set size (Neisser, 1967). The data from both experiments did not suppose this linear increase in RT as a function of OS distance, nor were there mean differences between OS distances. Furthermore, a serial comparison of the test stimuli to the target stimulus would have also been very unlikely as the current task parameters impose several cognitive limitations on observers. First, we displayed the target stimulus for 500 ms and then displayed the two test stimuli afterwards. Therefore, an effective comparative strategy would require parsing the target stimulus into its constituent line orientations and maintaining each one in visual short-term memory (VSTM). However, the number of individual line segments that the target stimulus is comprised of (6 or 7) exceeds the human capacity for storing line orientations in VSTM, which is estimated to be 4 (Luck & Vogel, 1997). Second, observers were likely unable to rely on a precategorical, iconic memory representation of the target for this comparison because iconic memory rapidly decays after only a few hundred milliseconds (Sperling, 1960) and observers would therefore rapidly lose access to an exact sensory copy of the target stimulus. In fact, for both experiments, mean RTs were always over 500 ms, at which point iconic memory information available can decay by 50% (Sperling, 1960). Third, observers were also likely unable to rely on a precategorical, iconic memory

representation of the target for this comparison because the test stimuli were placed outside of the fovea (eccentricity = 7.5°) and comparing the similarity of a test stimulus to a referent with an iconic memory representation is less effective if the stimuli appear at different locations (Phillips, 1974).

The current experiments provide insight into the perceptual encoding of complex novel objects representations. Our data suggest that complex objects are encoded in *N*-dimensional feature space where each dimension corresponds to a constituent feature for a particular object and the perceptual similarity between two objects corresponds to the inverse of the distance between these objects. This conceptualization of feature space is well supported for both simple features and faces. In the current study, we extend this conceptualization to complex, novel objects elucidating that this is an underlying tenet of object representation in the visual system. As such, we refer to *N*-dimensional feature space for complex objects as "object space". Consistent with perceptual representations in object space, we observed two robust perceptual phenomena for our complex objects that occur for simple visual feature representations: nonlinear perceptual encoding (saturation) at long distances in object space and repulsive perceptual encoding at short distances in object space. Finally, we show that saturation and repulsion of perceived similarity largely depends on the discriminability of the constituent visual features of the objects.

Chapter 3: Visual Similarity between Complex, Novel Objects Functionally Modulates Saccade Curvatures (Manuscript 2)

This manuscript has been submitted to ***The European Journal of Neuroscience***. The co-authors of this manuscript are Selvi Aybulut and Dr. Mazyar Fallah. Devin Heinze Kehoe and Dr. Mazyar Fallah designed the experiment. Devin Heinze Kehoe implemented the experiment and analyzed the data. Devin Heinze Kehoe and Selvi Aybulut collected the data. Devin Heinze Kehoe wrote the manuscript with feedback from Dr. Fallah.

Keywords

saccade curvature, superior colliculus, target selection, weighted-vector average, visual similarity, visual search

3.1 Summary

Oculomotor target selection allows us to select a particular saccade goal at the expense of others. The intermediate layers of the superior colliculus (SCi) are a critical neural substrate for target selection and saccade curvatures are often utilized as a non-invasive behavioral means to study the factors that influence oculomotor target selection. Here, we utilized a visual search saccade task in human participants and measured the curvature of saccades made to a target bilaterally flanked by equidistant distractors, while systematically varying the relative visual similarity between the two distractors and the target. Our results demonstrate that saccades systematically curved away from the distractor that is most similar to the target and that there is a linear relationship between the magnitude of these saccade curvatures and how similar this distractor was to the target. Furthermore, an analysis of saccade curvature as a function of saccade amplitude percentage demonstrated that saccades were only curved in the first 60-80% of the movement. This corresponded to the first 23-31 ms of the movement and thus is consistent with the temporal interval between SCi perisaccadic bursts for parallel-programmed saccades (Port and Wurtz, 2003). As the SCi is insufficient to fully process visual similarity in the current context given the task and stimulus parameters, we propose instead that similarity is computed cortically and mapped onto SCi via top-down inhibition. We elaborate on a model of saccade planning and execution that integrates the current results with previous work on oculomotor competition.

3.2 Significance Statement

We provide new insights into how information in the oculomotor and visual systems is integrated in order to select certain targets for fixation at the expense of others and how the priority for these potential targets are represented along a continuous dimension. Our research

suggests that the oculomotor system, largely subserved by a deep midbrain structure, has a passive role in oculomotor target selection, whereas the visual system, widely distributed across the cortex, has a more active role, contrary to certain influential views. Furthermore, we applied an analytic technique to examine oculomotor data, which yielded insights into the temporal factors that influence oculomotor planning and provided converging evidence with neurophysiological investigations of the temporal principles that guide the oculomotor system.

3.3 Introduction

Saccade deviations elicited in the remote distractor paradigm are commonly examined to determine the visual cognitive factors that influence oculomotor planning. Behavioral experiments have demonstrated that saccades deviate away from task irrelevant distractors (Dolye & Walker, 2001; McSorley et al., 2004, 2006, 2009) and that these saccade deviations are greater if the task relevance of the distractor increases such as with color contingency (Ludwig & Gilchrist, 2003; Mulckhuyse et al., 2009). These results are often attributed to oculomotor competition between parallel planned saccades whereby the competition is modulated by higher cognitive factors (see Findlay & Walker, 1999). A critical site of oculomotor competition is in the intermediate layers of the superior colliculus (SCi) as it is directly involved in saccadic target selection (Horwitz & Newsome, 1999; McPeek & Keller, 2002, 2004; Carello & Krauzlis, 2004; Li & Basso, 2005; Shen & Paré, 2007, 2012, 2014). The seminal work of Robinson (1972) demonstrated that SCi contains a retinotopic motor map on which a particular SCi locus encodes an amplitude and direction specific saccade vector to a corresponding location in contralateral space. Critically, when there is activity at two SCi loci, a saccade is elicited with a weighted vector-average (WVA) of the two loci. More recent neurophysiological investigations have demonstrated that SCi weighted-vector averaging causes saccade curvatures directly via

excitation (McPeek et al., 2003; Port & Wurtz, 2003) or inhibition (Aizawa & Wurtz, 1998; White et al., 2012) at the distractor locus, whereby saccades curve towards or away from distractors respectively. Since task relevance or *priority* is represented on the SCi oculomotor map through connections with various cortical areas (Fecteau & Munoz, 2006), the WVA account predicts that there should be a functional relationship between the behavioral relevance of distractors and the magnitude of saccade curvatures.

Neurophysiological studies have also suggested that temporal factors play a critical role in eliciting saccade curvature. Port & Wurtz (2003) observed that simultaneous peak activity in SCi neurons encoding saccade vectors to two potential targets elicited a straight WVA saccade landing between targets, whereas sequential activity offset by ~20 ms elicited saccades that landed near one target but were curved towards the other (see also McPeek et al., 2003). Critically, the relative timing of peak activity determined the timing of saccade curvatures: saccades began to curve when neurons encoding the first target reached their peak level of activity and stopped curving when neurons encoding the second target reached their peak level of activity ~20 ms later. Similarly, there is evidence that inhibition occurring in this critical epoch ~20 ms prior to saccade initiation causes saccades to curve away from distractors, but is considered more contentious (White et al., 2012). However, this interpretation would be strengthened if a similar spatio-temporal profile observed by Port and Wurtz (2003) occurs in saccades curved away from distractors (i.e., if saccades are curved away from distractors in only the first ~20 ms of their duration).

The aforementioned neurophysiological results suggest that saccade curvatures result from outstanding competitive processing between SCi neurons involved in target selection. SCi target selection can be explained by two possible neural mechanisms: (1) SCi neurons encode

movement vectors to spatially defined objects and the vector weights are modulated from cortical sources or (2) SCi neurons encode object representations with associated features and thus dynamically develop feature selectivity over time. Here, we examined these possibilities by utilizing a visual search saccade task that required participants to discriminate the target from distractors using complex, novel object representations and not simple spatial coordinates. Critically, we systematically varied the task relevance of distractors by manipulating the visual similarity between targets and distractors (see Palmer, 1978). We reason that the cortical visual system was required to compute the visual similarity between our stimuli given their complicated and novel visual characteristics. Therefore, the observation of saccade curvatures in this context suggested that cortical object representations are projected onto the SCi oculomotor map.

3.4 Methods

3.4.1 Participants

25 York University undergraduate students (18-37 years old, 8 male) participated in the experiment for course credit. Participants had normal or corrected-to-normal vision and were naïve to the purpose and design of the experiment. Informed consent was obtained prior to participation. All research was approved by York University's Human Participants Review Committee.

3.4.2 Stimuli

Stimuli were constructed offline using MATLAB (MathWorks, Natick, MA) by intersecting 6 or 7 vertical and horizontal line segments (1°× 0.08°) together at right angles in a configuration that did not resemble meaningful alphanumerical characters to an English speaker (see Figure 1*A*). Individual line segments occupied 1 of 12 possible locations that were embedded in an imaginary box (2°× 2°). Adding and/or removing one line segment at a time

ensured that stimuli were linearly related in objective similarity (OS). We created 2 such sets of 6 stimuli for the experiment. The stimuli were white (x = 119.90, y = 126.02) and were displayed against a black background (x = 0.23, y = 0.20) on a 21-inch CRT monitor (60 Hz, 1024 × 768). Participants viewed stimuli in a dimly lit room from a viewing distance of 57 cm with a headrest stabilizing their head position.

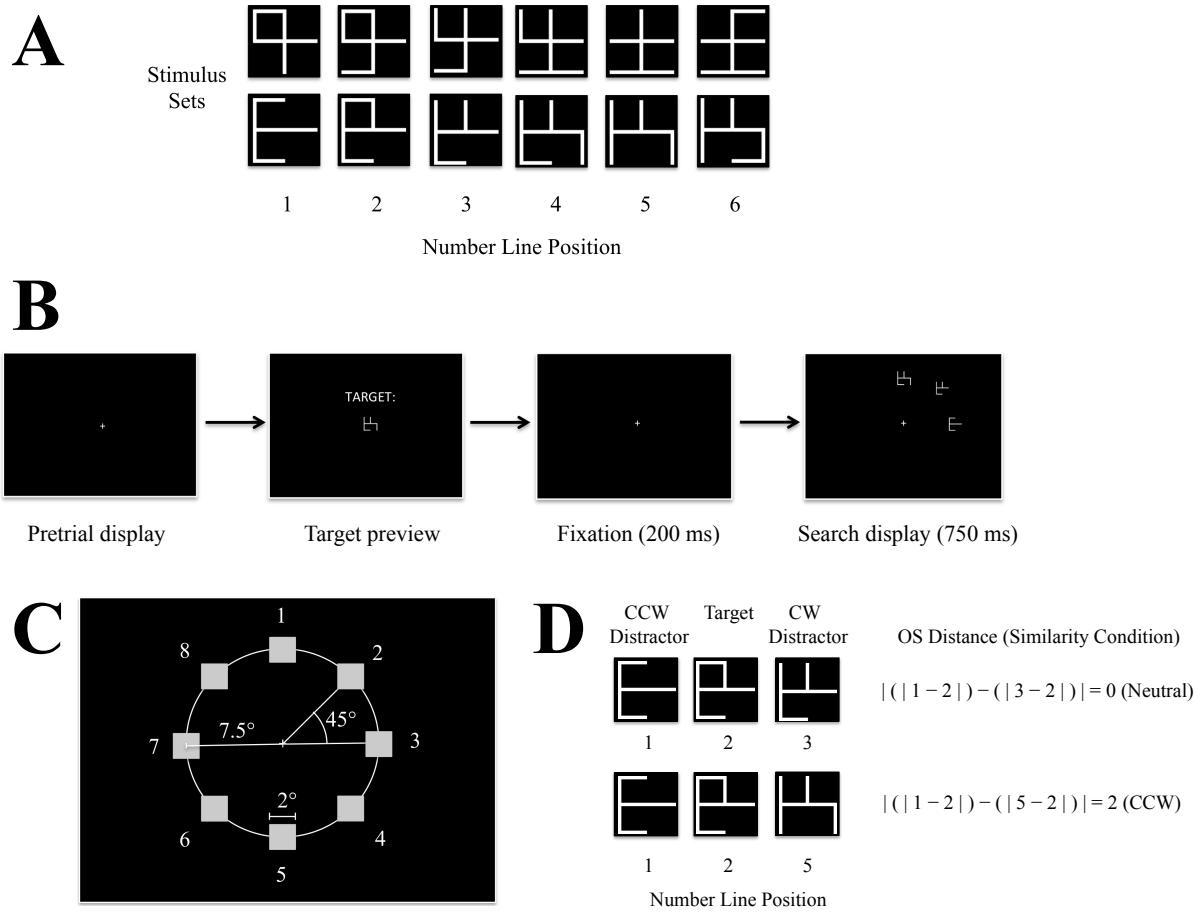

Figure 3.1: Visual search saccade task stimuli and displays. ***A*:** Stimulus sets used in the current experiment. Stimulus sets have been placed on an objective similarity (OS) number line in which the absolute difference between number line positions corresponds to the number of line segment differences. ***B:*** Trial structure. Participants press a button to preview the target stimulus until they are familiar with it. Participants then press the button again to initiate the

search trial. After maintaining fixation for 200 ms, the search display is presented for 750 ms or until a saccade to one of the stimuli is detected. ***C:*** 8 stimulus array locations utilized in the current experiment. Stimulus arrays were centered to 1 of 8 locations along the circumference of an imaginary circle with 45° of angular separation between them and aligned to the cardinal and diagonal axes. ***D:*** Similarity conditions in the current experiment determined by relative OS. Top: OS_{CCW} and OS_{CW} are equal, therefore the OS distance condition is 0 and the similarity condition is neutral. Bottom: OS_{CCW} is less than OS_{CW} by a factor of 2, therefore the OS distance condition is 2 and the similarity condition is CCW.

3.4.3 Apparatus and Measurement

Stimulus presentation was controlled using a computer running Presentation software (www.neurobs.com) and a serial response box (Cedrus, San Pedro, CA). Eye position was recorded using infrared eye tracking (500 Hz, EyeLink II, SR Research, Ontario, Canada). The eye tracker was calibrated at the beginning and halfway point of each experimental session, and as needed.

3.4.4 Task Procedure

Trials were initiated by pressing the center button on the response box (see Figure 1*B*). The target appeared as a preview until they pressed the button a second time. A white, central fixation cross (0.4°× 0.4°) appeared and after participants fixated it (1.89° square window) for 200 ms, the target and distractors appeared at 1 of 8 contiguous locations (7.5°eccentricity, see Figure 1*C*).

The relative OS of the search array was randomly selected on every trial (see Figure 1*D*). Participants were instructed to maintain fixation when the stimuli appeared, use their peripheral vision to determine which stimulus was the target, and then make a saccade to it. The trial ended

when a saccade was made to the target (correct) or distractor (incorrect) or 750 ms had elapsed (time-out). An error tone and message were used to signify incorrect and time-out trials. Time-out trials were randomly replaced back into the block. Participants received accuracy feedback at the end of each block.

Participants completed 1 session with 8 blocks of 49 trials for a total of 392 trials. On each trial, the target location and the distractor positions relative to the target were randomly selected. 3 distractors arrangements were utilized: (1) both distractors flanked the target on the counterclockwise (CCW) side, (2) the clockwise (CW) side, (3) or bilaterally flanked the target. Additionally, baseline trials in which no distractors were embedded in the display were randomly interleaved into the blocks. The proportion of each trial type was randomized on every block.

3.4.5 Saccade Detection and Analysis

Saccades were detected, visualized, filtered and analyzed offline using customized MATLAB algorithms. Trials that contained blinks, endpoint deviations > 3° from the center of the target, or a fixation drift > 0.5° during the presaccadic latency period were excluded from further analysis. Saccades were defined as a velocity exceeding 20 deg/s for at least 8 ms and a peak velocity exceeding 50 deg/s. Saccades were excluded from further analysis if they were less than 100 ms in latency or required corrective-saccades to reach the target (a second saccade >1° in amplitude was detected).

To analyze saccade curvatures, saccade start-points were translated back to the origin and then trigonometrically rotated so that the endpoint was aligned to the positive *y*-axis. Thus, positive deviations correspond to CW deviations, while negative deviations correspond to CCW deviations. The following 3 metrics were used to quantify global saccade curvatures: (1) *sum deviation*, the sum of all *x* deviations along the length of the saccade; (2) *max deviation*, the

maximum *x* deviation along the length of the saccade; (3) *max theta*, the maximum *x* deviation along the length of the saccade in angular degrees. To examine the time course of saccade curvatures, saccades were binned into amplitude quintiles and these same three metrics were used to quantify partial saccade curvature between each consecutive quintile (i.e., between $n-1$ and n quintiles). To differentiate between the global and partial saccade metrics, the partial metrics are referred to as the *partial sum*, *partial max*, and *partial theta*. Two additional metrics were used to quantify saccade curvature at each discrete interval: (1) *deviation*, the *x* deviation at each quintile; and (2) *deviation theta*, the *x* deviation in angular degrees at each quintile. Finally, the following 2 metrics were used to quantify deviations in the overall saccade vector: (1) *endpoint deviation*, the distance of the saccade endpoint away from the center of the target location in degrees; and (2) *endpoint deviation theta*, the angular deviation of the saccade endpoint away from the center of the target location. Saccadic reaction time (SRT) was defined as the time between target onset and saccade initiation. All subsequent statistical analyses reported were conducted in SPSS (IBM SPSS Statistics; IBM, Armonk, NY).

3.5 Results

The data from 3 participants was removed as *Chi*-squared goodness-of-fit tests determined that they did not discriminate the target above chance (ps > .05). As we were interested in examining whether saccade trajectories are functionally related to the relative OS between bilateral distractors and the target independent of spatial factors, correct trials with bilateral distractors were analyzed. All analyses were collapsed across target location on the display. Shapiro-Wilks tests provided insufficient evidence for normally distributed data for various analyses (ps < .05). Therefore, non-parametric Friedman tests and Wilcoxon Signed-Rank tests were used to analyze all repeated-measures mean differences. Bonferroni α

corrections were utilized for all multiple comparisons.

3.5.1 Quantifying Similarity

The objective similarity (OS) between targets and distractors was manipulated by varying the number of line segments shared between targets and distractors (seeure 1*A*). To examine the effect of OS on saccade curvatures, the relative similarity between the bilateral distractors and the target (OS_R) was calculated by subtracting the absolute counterclockwise (CCW) distractor-to-target OS (OS_{CCW}) by the clockwise (CW) distractor-to-target OS (OS_{CW}) such that $OS_R = | OS_{CCW} | - | OS_{CW} |$ with a range of −3 to +3.

First, to examine whether differential OS between the target and each bilateral distractor modulates saccade deviations categorically, trials were categorized based on whether the CCW distractor was more similar to the target than the CW distractor ($OS_{CCW} < OS_{CW}$; $OS_R < 0$), the CW distractor was more similar to the target than the CCW distractor ($OS_{CCW} > OS_{CW}$; $OS_R > 0$), or the CCW and CW distractors were equally similar to the target ($OS_{CCW} = OS_{CW}$; $OS_R = 0$). This categorization is herein referred to as similarity condition with levels CCW, CW, and neutral respectively (see Figure 1*D*).

Second, to examine whether saccade curvatures are functionally related to visual similarity, the absolute mean saccade curvature was averaged for every positive and corresponding negative value of OS_R (e.g., −1 and +1) (see Figure 1*D*). Since each positive and negative value of OS_R is perceptually matched, this grouping eliminated any potential curvature bias in either the CCW or CW direction and provides the average magnitude of saccade curvatures as a function of how disproportionately similar one distractor is to the target as compared to the other. To further reduce bias, baseline saccade curvatures for each subject and in each target location were subtracted from the data. This variable is herein referred to as OS

distance with levels 0, 1, 2, and 3. We examined any potential relationship between saccade curvatures and visual similarity by fitting first-order polynomials to the data using the least-squares method. The decision to use a linear function was due to limited degrees of freedom and since we did not make any assumptions about the shape of this potential functional relationship.

3.5.2 Behavioral Measures

3.5.2.1 Errors

Overall task performance was 54.26%. To determine if our sample performed above chance (33.33%), a paired-samples Student's *t*-test compared the proportion of correct trials for each participant against chance. Participants did discriminate the target significantly above chance, $t(24) = 8.96$, $p < 0.001$.

The distribution of errors across similarity and OS distance conditions were analyzed with *Chi*-squared goodness-of-fit tests to determine if they were randomly distributed. Interestingly, errors were not randomly distributed across the similarity conditions, $\chi^2(2, N = 2704) = 18.35$, $p < 0.001$; or OS distance conditions, $\chi^2(3, N = 2704) = 19.43$, $p < 0.001$. However, an examination of the model residuals suggested that these effects are likely being driven by a high rate of errors in the neutral (similarity) or 0 (OS distance) conditions. Therefore, the analyses were repeated with these conditions removed. Our prediction was confirmed as both analyses demonstrated that errors were randomly distributed across the similarity conditions, $\chi^2(1, N = 2240) = 0.03$, $p = 0.866$; and OS distance conditions, $\chi^2(2, N = 2240) = 1.29$, $p = 0.525$. Furthermore, task performance increased to 62.11%. These results suggest that the task was more difficult on trials when the distractors are equally similar to the target as compared to when one distractor was more similar to the target. However, the difficulty of the task was otherwise equal across similarity and OS distance conditions.

3.5.2.2 Bias

Error trials were categorized according to whether the CCW or CW distractor was selected by participants in order to determine if there was a directionality bias. A *Chi*-squared goodness-of-fit test revealed that there was no overall directionality bias, $\chi^2(1, N = 2704) = 0.02$, $p = 0.878$. Interestingly, when this analysis was repeated for each similarity condition, it demonstrated that there is no bias when the distractors are equally similar to the target (neutral condition), $\chi^2(1, N = 464) = 0.08$, $p = 1$. However, participants did show a selection bias for the distractor most similar to the target in the CCW similarity condition, $\chi^2(1, N = 1124) = 32.80$, $p < 0.001$; and the CW similarity condition, $\chi^2(1, N = 1116) = 28.39$, $p < 0.001$.

Next we investigated whether this selection bias for the distractor most similar to the target varies with OS by calculating the proportion of trials on which the objectively most and least similar distractors were selected for each OS distance (see Figure 2). Since stimuli were equally similar to the target in the 0 condition, most/least similar distractor selection were replaced with CCW/CW selection and this condition was not analyzed as it was identical to the neutral condition analyzed above. There was an unreliable bias in the 1 condition, $\chi^2(1, N = 764) = 4.10$, $p = 0.128$, Cramer's $\varphi = 0.07$. However, there was a reliable bias in the 2 condition, $\chi^2(1, N = 722) = 32.85$, $p < 0.001$, Cramer's $\varphi = 0.21$; and the 3 condition, $\chi^2(1, N = 754) = 33.95$, $p < 0.001$, Cramer's $\varphi = 0.21$. Based on the increasing effect sizes and differences in the proportion of error trials on which the most and least similar distractor was selected across OS distance conditions, it appears that the selection bias for the distractor most similar to the target is modulated by OS distance whereby the more similar the distractor is to the target, the higher the bias.

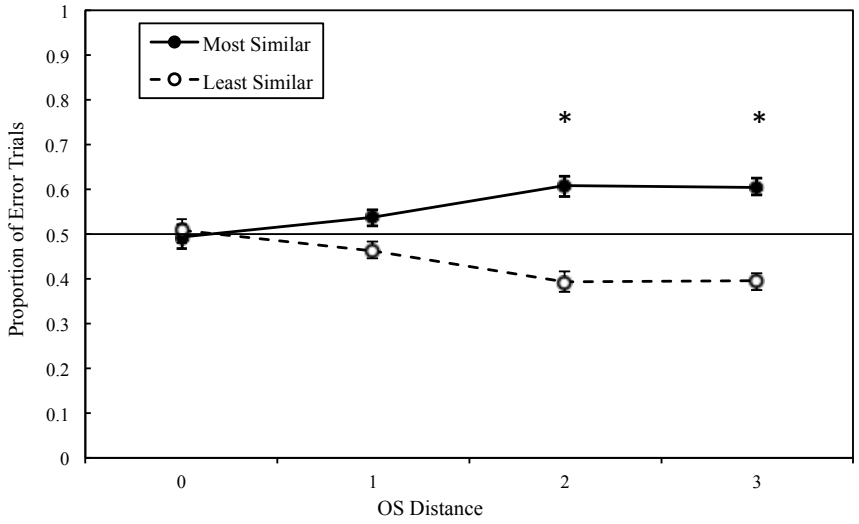

Figure 3.2: The proportion of total error trials. Error proportions are plotted separately for trials on which the distractor that is most similar to the target was selected (filled circles, solid line) and the distractor that is least similar to the target was selected (open circles, broken line) as a function of OS distance. *$p < .001$.

3.5.2.3 SRT

There was no difference in SRT between the CCW and CW similarity conditions, $z = -0.04$, $p = 1$. Furthermore, pooling SRTs from the CCW and CW similarity conditions and comparing them to the neutral similarity group revealed that there was also no difference in SRT when the distractors were equally similar to the target than when they were differentially similar to the target, $z = -1.14$, $p = 0.506$.

Finally, an omnibus Friedman test revealed that there were no mean SRT differences between OS distance conditions, $\chi^2(3) = 3.38$, $p = 0.336$; and a linear regression found no evidence of a functional relationship between SRT and OS distance, $F(1,2) = 1.71$, $p = 0.321$, $R^2 = 0.46$.

3.5.3 Saccade Curvature Metrics

3.5.3.1 Categorical analysis

We analyzed whether saccades were significantly curved in each similarity condition relative to baseline, and critically, whether saccades curved in opposite directions between the CCW and CW conditions (see Figure 3).

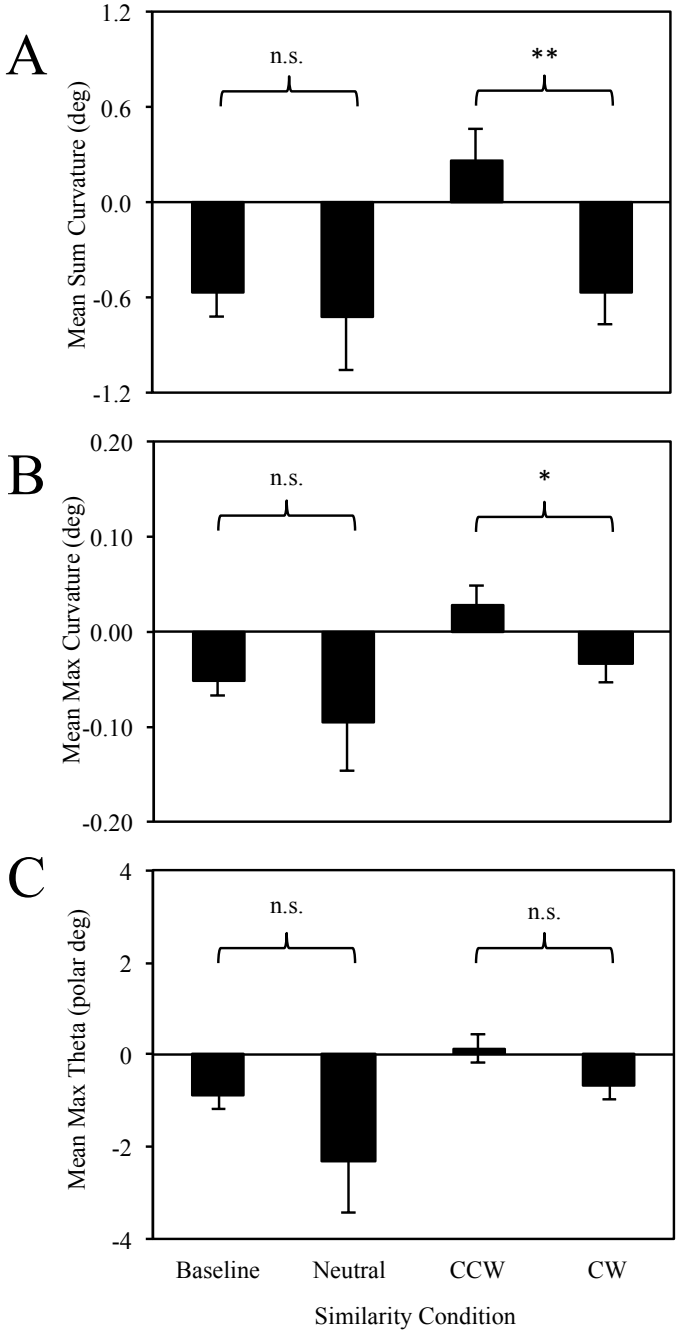

Figure 3.3: Mean saccade curvature as a function of similarity condition. Error bars represent standard error of the mean. ***A*:** Mean sum curvature in degrees of visual angle. ***B*:** Mean max curvature in degrees of visual angle. ***C*:** Mean sum curvature in degrees of angular separation from fixation. * $p < 0.05$, ** $p < 0.01$.

When the distractors were equally similar to the target (neutral condition), saccade curvatures did not differ from saccade curvatures in the baseline condition across all global metrics: sum curvature, $z_{sum} = -0.26$, $p = 1$; max curvature, $z_{max} = -0.15$, $p = 1$; and max theta, $z_{theta} = -0.74$, $p = 1$. Critically, by analyzing the mean difference between the CCW and CW condition, we observed that when one distractor was more similar to the target, saccades curved away from this distractor for the sum curvature, $z_{sum} = -3.11$, $p = 0.008$; and max curvature metrics, $z_{max} = -2.65$, $p = 0.032$; but not for max theta, $z_{theta} = -2.06$, $p = 0.158$. When the CCW distractor was more similar to the target (CCW condition), saccade curvatures were greater than baseline: sum curvature, $z_{sum} = -3.05$, $p = 0.009$; max curvature, $z_{max} = -3.08$, $p = 0.008$; and max theta, $z_{theta} = -3.00$, $p = 0.011$. However, when the CW distractor was more similar to the target (CW condition), saccade curvatures were not greater than baseline: sum curvature, $z_{sum} = -0.20$, $p = 1$; max curvature, $z_{max} = -0.74$, $p = 1$; and max theta, $z_{theta} = -0.55$, $p = 1$. Given that the CCW and CW conditions are perceptually matched within subjects, it seems unlikely that saccades would curve away from the most similar CCW distractor, but not from the corresponding CW distractor especially since saccades curved in opposite directions across these conditions and the difference between them was statistically significant (see Figure 3). Therefore, a subsequent analysis was conducted to examine whether this abnormality can be explained by a saccade curvature bias.

Paired-samples Student's *t*-tests compared baseline saccade curvatures to 0 to examine

whether there was a directional bias for this sample. This analysis demonstrated a strong CCW bias across saccade curvature metrics: sum curvature, $t_{sum}(24) = -3.63$, $p = 0.001$; max curvature, $t_{max}(24) = -3.52$, $p = 0.002$; and max theta, $t_{theta}(24) = -3.37$, $p = 0.003$. This result suggests that curvatures in the CW similarity condition, which curved CCW, may not be reliably different from baseline due to a strong CCW curvature bias in the baseline condition. Saccade curvatures in the similarity conditions will only be hereafter discussed in terms of differences between the CCW and CW conditions.

As our stimuli were constructed from either 6 or 7 line segments, they varied in luminance. However, since we always alternately added and then removed one unique line segment to create our stimuli (see Figure 1*A*), when both distractors were evenly or oddly spaced in OS away from the target, they both contained the same number of line segments. Therefore, in the OS distance 0 and OS distance 2 conditions, the distractors both contained the same number of line segments. As mentioned above, there were no significant saccade curvatures in the OS distance 0 condition, which had balanced distractor OS (see Quantifying Similarity section) and balanced distractor luminance. If there are significant saccade curvatures in the OS distance 2 condition, which has unbalanced distractor OS but balanced distractor luminance, then the effects of saccade curvatures must be attributed to variations in OS. Saccade curvatures were significantly different from the absolute baseline curvatures in the OS distance 2 condition across metrics, $z_{sum} = -3.03$, $p = 0.002$; $z_{max} = -3.09$, $p = 0.002$; $z_{theta} = -2.57$, $p = 0.010$. Therefore, our effects are due to the distractor OS and cannot be attributed to distractor luminance.

3.5.3.2 Functional analysis

The relationship between saccade curvatures and visual similarity was first explored by calculating a Pearson's correlation between OS_R and each global saccade curvature metric using

the raw data. There was a significant correlation for sum curvature, $r_{sum}(1230) = -0.08$, $p = 0.005$; max curvature, $r_{max}(1230) = -0.06$, $p = 0.044$; but not for max theta, $r_{theta}(1230) = -0.04$, $p = 0.198$.

Coinciding with these correlations, regression analyses with OS distance as the independent variable and sum deviation, max deviation, and max theta as the dependent variables found a significant linear relationship for sum curvature, $F_{sum}(1,2) = 32.64$, $p = 0.029$, $R^2 = 0.94$; and for max curvature, $F_{max}(1,2) = 44.92$, $p = 0.022$, $R^2 = 0.96$; but provided insufficient evidence for a linear relationship for max theta ($F < 1$, $R^2 < .01$) (see Figure 4).

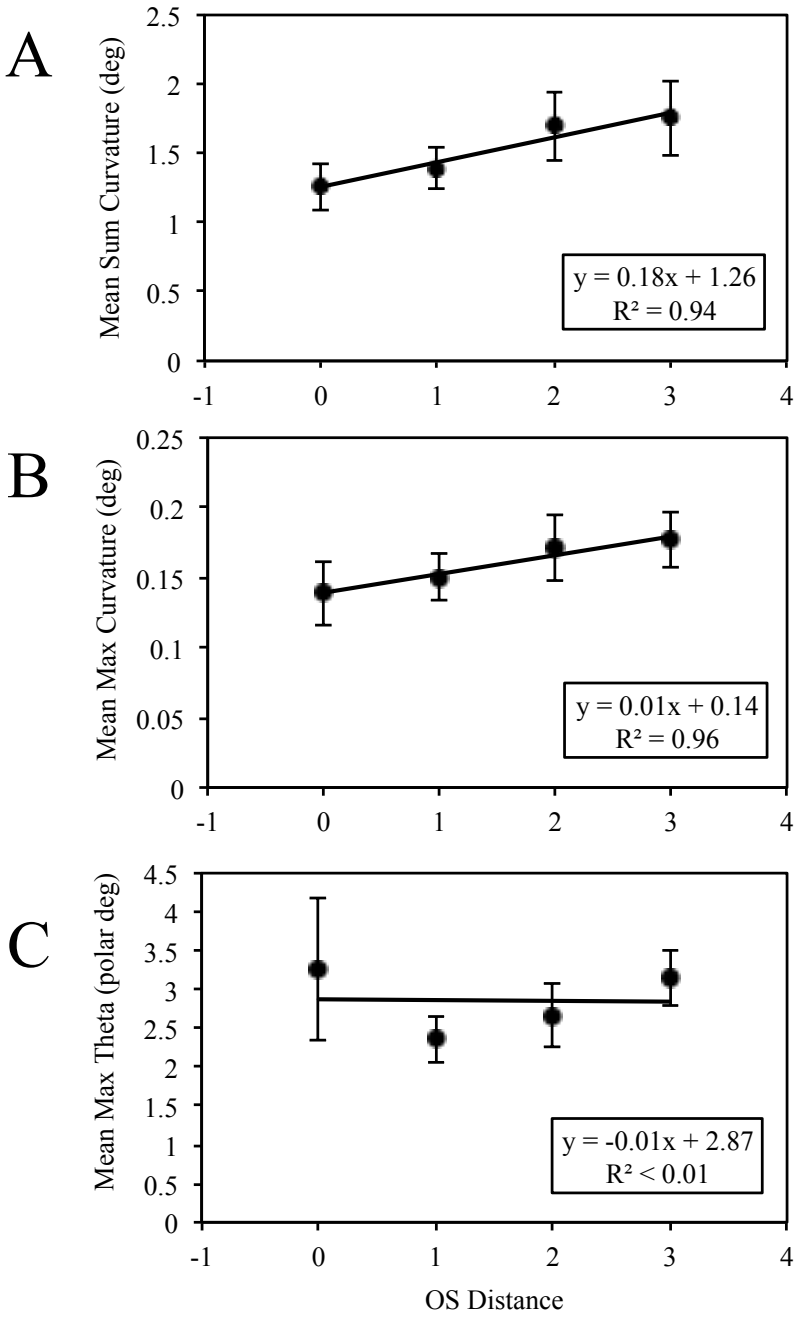

Figure 3.4: Mean global saccade curvatures as a function of OS distance. Error bars represent standard error. ***A*:** Mean sum deviation as a function of OS distance. ***B*:** Mean max deviation as a function of OS distance. ***C*:** Mean max theta as a function of OS distance.

Another possible explanation for the current results to be ruled out is that saccades actually curved towards the least similar distractor. We find this account extremely unlikely for the following reasons: (1) We observed relatively long SRTs in the experiment (M = 322.52 ms), which reflects the difficulty of the task. Previous research has found that saccades begin to curve away from distractors after sufficient distractor processing time (~200 ms), which likely reflects an accumulation of inhibition at the distractor locus on the SCi motor map (McSorley et al., 2006, 2009). (2) The bias for selecting the most similar distractor on error trials (see Figure 1) may suggest an influence of visuospatial attention deployed at the most similar distractor location and previous behavioral research has demonstrated that saccades typically curve away from the locus of attention (Sheliga et al., 1994, 1995). (3) If saccades curved towards the most similar distractor, the functional relationship between saccade curvatures and OS distance would suggest that activity at a particular distractor locus increased as the similarity of the distractor to the target decreased. Although we cannot rule out this possibility, neurophysiological data collected from frontal eye field (FEF) visuo-movement neurons during visual search has demonstrated that neuronal firing rates increase as the feature-based similarity between a stimulus in their receptive field and a target increases during target selection (Bichot et al., 1996; Bichot and Schall, 1999; Sato et al., 2003).

3.5.3.3 Time course

Saccades were binned by amplitude into quintiles and potential mean differences between the similarity groups (CCW vs. CW) were examined for each amplitude quintile bin (referred to herein as amplitude bin 1, 2, 3, 4, and 5). The deviation metric indicates the deviation along the axis perpendicular to a straight line passing through the saccade start- and endpoint in degrees at each 20% interval along the length of the saccade (Figure 5*A*), while the deviation theta metric is

equal to the deviation metric converted into polar degrees (Figure 5*B*), and thus indicates the saccade vector at each 20% interval along the length of the saccade. The partial sum (Figure 5*C*), partial max (Figure 5*D*), and partial theta (Figure 5*E*) metrics correspond to the sum of all *x* deviations in degrees, the maximum *x* deviation, and the maximum *x* deviation converted to polar degrees respectively, and were calculated for each amplitude bin using all the eye samples between bins $n-1$ and n.

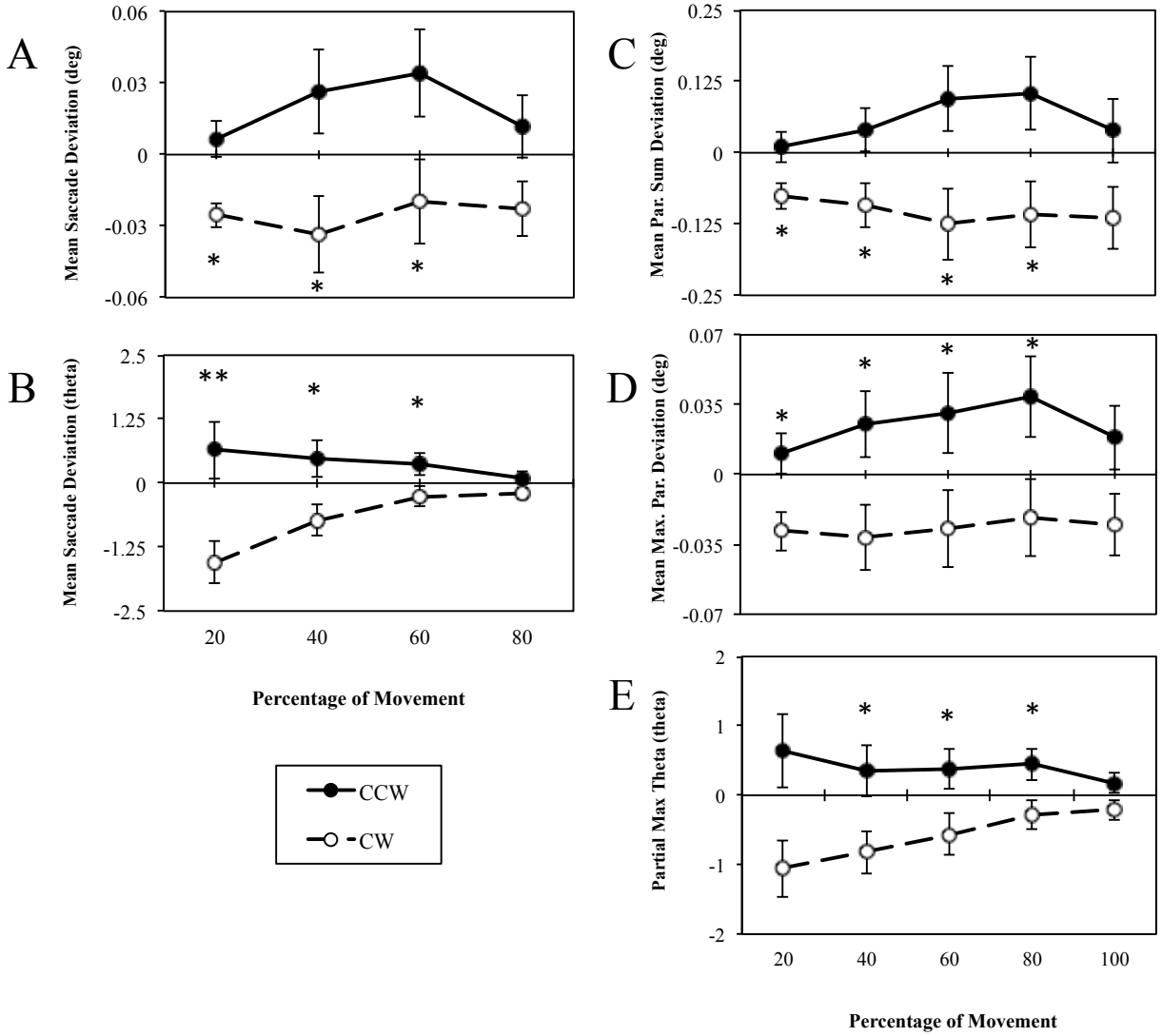

Figure 3.5: Mean saccade curvatures as a function of saccade amplitude bin. Saccade time points correspond to saccade amplitude quintiles. Mean saccade deviations in the CCW condition are plotted with filled circles and solid lines. Mean saccade deviations in the CW

condition are plotted with open circles and broken lines. Error bars represent standard error. ***A*:** Mean deviation as a function of amplitude bin. ***B*:** Mean theta deviation as a function of amplitude bin. ***C*:** Mean partial sum as a function of amplitude bin. ***D*:** Mean partial max as a function of amplitude bin. ***E*:** Mean partial theta as a function of amplitude bin. * $p < 0.05$, ** $p < 0.01$.

The means in Figure 4 quantify the overall (global) saccade curvature, whereas the means in Figure 5 quantify the saccade deviation at various points along the length of the saccade and thus provide an approximation to the overall saccade trajectory. These metrics were used to examine if distractors differentially affect the early and late portions of saccade trajectories as has been observed in monkeys (Port and Wurtz, 2003) and to determine whether movement vector averaging occurs early in the movement, but a winner emerges later in the movement as with pursuit (Recanzone and Wurtz, 1999, 2000).

For the deviation and deviation theta metrics, saccade amplitude bin 5 was not analyzed since this bin corresponds to the saccade endpoint, which equals zero given the rotational method used to calculate saccade deviations.

Interestingly, there was a significant saccade curvature away from the most similar distractor across metrics in all amplitude bins except amplitude bin 4 (80% of movement) for the deviation and deviation theta metrics, amplitude 5 bin (between 80-100% of movement) for all of the partial curvature metrics (see Figure 5), and amplitude bin 1 for the partial theta metric. These results are summarized in Table 1.

Metric	Saccade Amplitude Bin				
	1	2	3	4	5
Deviation					
CCW Curvature	0.01	0.03	0.03	0.01	-
CW Curvature	-0.03	-0.03	-0.02	-0.02	-
z	-3.00	-2.95	-2.87	-2.46	-
p	*0.011	*0.013	*0.017	0.055	-
Deviation Theta					
CCW Curvature	0.64	0.47	0.36	0.10	-
CW Curvature	-1.56	-0.72	-0.27	-0.21	-
z	-3.27	-2.95	-2.73	-2.27	-
p	**0.004	*0.013	*0.025	0.092	-
Partial Sum					
CCW Curvature	0.01	0.04	0.10	0.10	0.04
CW Curvature	-0.08	-0.09	-0.12	-0.11	-0.11
z	-2.65	-2.68	-2.81	-2.89	-2.22
p	*0.040	*0.037	*0.025	*0.019	0.132
Partial Max					
CCW Curvature	0.01	0.03	0.03	0.04	0.02
CW Curvature	-0.03	-0.03	-0.03	-0.02	-0.03
z	-3.03	-3.03	-2.70	-2.84	-2.57
p	*0.012	*0.012	*0.034	*0.023	0.051
Partial Theta					
CCW Curvature	0.64	0.35	0.38	0.45	0.17
CW Curvature	-1.05	-0.82	-0.56	-0.28	-0.22
z	-2.58	-2.63	-2.63	-2.98	-2.43
p	0.050	*0.043	*0.043	*0.014	0.076

Table 3.1: Mean partial saccade curvatures in the CCW and CW conditions with *z* and *p* values for each CCW and CW mean difference. These statistics are repeated for each partial saccade curvature metric, and across saccade amplitude bins. * $p < 0.05$, ** $p < 0.01$

3.5.4 Endpoint Deviation

The endpoint deviations and endpoint deviation thetas were analyzed as a function of OS distance and similarity condition to determine if the distractor similarity modulated the overall saccade vectors as supposed to saccade vector shifts at some point along the length of the saccade.

Comparing baseline endpoint deviations to zero demonstrated a strong CCW bias for endpoint deviations, $t_{deg}(24) = -4.27$, $p = 0.001$; and endpoint deviations theta, $t_{theta}(24) = -4.06$, $p = 0.001$. There was no difference between the baseline and the neutral conditions for endpoint deviation, $z_{deg} = -0.36$, $p = 1$; or endpoint deviation theta, $z_{theta} = -0.202$, $p = 1$. There were also no differences between the baseline and CCW conditions for endpoint deviation, $z_{deg} = -0.85$, $p = 1$; or endpoint deviation theta, $z_{theta} = -0.12$, $p = 1$. There was, however, a difference between the baseline and the CW conditions for endpoint deviation, $z_{deg} = -3.13$, $p = 0.007$; and endpoint deviation theta, $z_{theta} = -3.70$, $p < 0.001$). Saccade endpoints in the CW condition deviated slightly CW as indicated by the mean endpoint deviation theta, however mean endpoint deviation was still CCW, but to a lesser extent than baseline. Similarly, the difference between the CCW and CW conditions was unreliable for endpoint deviation ($z_{deg} = -2.11$, $p = 0.139$), but was marginally reliable for endpoint deviation theta ($z_{theta} = -2.38$, $p = 0.069$). This analysis suggests that overall saccades vectors were marginally shifted in the direction of the most similar distractor.

There was no evidence of a linear relationship between OS distance and endpoint deviation, $F_{deg} < 1$, $R^2 = .01$; or endpoint deviation theta, $F_{theta} < 1$, $R^2 = .05$; and no evidence of mean differences between OS distance conditions for endpoint deviation, $\chi^2(3) = 3.45$, $p = 0.290$; or for endpoint deviation theta, $\chi^2(3) = 3.00$, $p = 0.392$.

3.6 Discussion

This experiment demonstrated that the task relevance of objects encoded by the oculomotor system is represented along a continuous dimension. Our sum curvature and max curvature metrics demonstrated that when one of the bilateral distractors was more similar to the target, saccades curved away from it. Saccades curved in opposite directions in the CCW and

CW conditions, which contained visually identical distractor pairs and differed only insofar as the bilateral distractor placement about the target was reversed. This is consistent with previous research suggesting that task relevance modulates saccade curvatures (Ludwig and Gilchrist, 2003; Mulckhuyse et al., 2009). Furthermore, saccade curvatures were not different between the baseline and neutral conditions. This result is consistent with McSorley et al. (2004) who found that saccades returned to baseline when bilaterally flanked by identical distractors.

The opposite pattern of results was observed for the endpoint deviation theta metric. Similar to saccade curvatures, there was no difference in endpoint deviation theta between the neutral and baseline condition. However, the overall endpoint deviation theta was marginally different between the CCW and CW conditions: overall saccade vectors were marginally shifted towards the most similar distractor. This may be a marginal reflectance of the global effect (Coren and Hoenig, 1972), which can be biased by top-down factors such as target probability (He and Kowler, 1989).

The factors that modulate saccade curvature are typically investigated categorically. We have expanded on this paradigm by investigating whether task relevance functionally modulates saccade curvatures and observed a significant linear relationship between the sum curvature and max curvature metrics and OS distance. Since our stimuli were spatially balanced, this analysis provides direct behavioral evidence that the spatial average of competing saccades vectors computed by the oculomotor system is cognitively weighted. Here, these cognitive weights were determined by the task relevance of stimuli, but since many visual cognitive factors modulate saccade curvatures, it is reasonable to assume that systematically varying these factors may yield similar results, which is an area for future research.

Finally, in our time course analysis, we examined saccade deviations as a function of saccade amplitude percentage to examine whether target-distracter similarity affected the early and late portions of saccades differentially. Our deviation and deviation theta metrics indicated that saccades were curved at 20%, 40%, and 60% of the movement, but not at 80%. Similarly, our partial metrics (i.e., partial sum, partial max, and partial max theta) demonstrated that saccades were curved between 0-80% of their amplitudes, with the exception of partial max theta, which did not indicate any curvature until after the first 20% of the saccade. Across partial metrics, there was no evidence of saccade curvature in the last 20% of the saccade. Clearly, there was a high degree of consistency between our 5 different amplitude metrics, which demonstrated that saccades began to curve between 0-20% of the movement and stopped curving between 60-80% of the movement. This result is consistent with neurophysiological and behavioral data collected from monkeys during target selection (Port and Wurtz, 2003).

Given that saccade curvatures arise due to neuronal interactions on the SCi motor map whereby the level of activation (McPeek et al., 2003; Port and Wurtz, 2003) or inhibition (White et al., 2012) at the distractor locus is proportional to the magnitude of saccade curvatures, and that behavioral relevance is represented in SCi (Fecteau and Munoz, 2006), our results suggest that visual similarity modulates the representational strength of stimuli on the SCi motor map whereby increasing the visual similarity of a distractor to the target increases inhibition at the distractor locus in SCi. This conclusion is consistent with the target selection behavior of SCi neurons in which targets and distractors initially elicit onsets bursts with equal intensity, but over time, distractor activity decreases while target activity either increases or stays consistent (Horwitz and Newsome, 1999; McPeek and Keller, 2002; Kim and Basso, 2008; Shen and Paré, 2007, 2012, 2014). Since SCi inhibition prevents saccades (Quaia et al., 1998) and therefore

plays a pivotal role in target selection by preventing saccades to erroneous stimuli (McPeek and Keller, 2004), the current results suggests that the oculomotor system inhibited both distractor loci to prevent erroneous saccades to distractors. Critically, however, when one distractor was objectively more similar to the target than the other, there was greater inhibition at this locus and thus saccades curved away from the most similar distractor. Furthermore, the functional relationship between saccade curvature and OS distance suggests that SCi inhibition at a distractor locus was proportional to its similarity to the target: inhibition increased as it became more similar to the target and decreased as it became less similar to the target.

A question that arises is whether similarity is computed locally in SCi or whether similarity information is received from outside cortical sources. Since we utilized a visual search task with randomized stimulus locations and identities trial-to-trial, targets were not simply spatially defined, but were defined by their visual features. Furthermore, distractors were always task relevant and had to be distinguished from the target by analyzing these features. There is evidence for sensitivity in SCi neurons for luminance (Bell et al., 2006; Li and Basso, 2008) and isoluminant color (White et al., 2009), but variations in luminance or color cannot account for our effects of visual similarity since our stimuli were defined by complex conjunctions of line orientations. Since there is no evidence for orientation tuning in SCi neurons, this suggests that SCi is insufficient to discriminate the target in the current context. Finally, given that stimulus identities were randomly selected trial-to-trial from a large set of complicated and novel stimuli (see Figure 1*A*), it is unlikely that SCi neurons developed sensitivity for a particular stimulus as being a target or distractor from repeated consecutive appearances. Therefore, we argue that oculomotor target selection in the current context involved two stages: (1) The cortical visual system integrates visual and cognitive information to encode object representations with

associated features and behavioral relevance. (2) The subcortical oculomotor system spatially encodes potential saccade vectors and these vectors are continuously weighted by cortical input.

A thoroughly examined source of SCi inhibition that integrates visual and cognitive signals from a diverse set of cortical areas—such as FEF, lateral intraparietal area, and dorsal lateral prefrontal cortex—is the substantia nigra pars recticulata, (SNr) (reviewed by Hikosaka et al., 2000). SNr inhibits the initiation of saccades by projecting a tonic GABAnergic blanket of activity over SCi (Hikosaka et al., 2000). Conversely, SNr can initiate saccades through spatially selective disinhibition of SCi (Hikosaka and Wurtz, 1983, 1985). SNr is the most likely source of SCi inhibition to explain the current results because (1) saccades curved away from a distractor, which suggests inhibition; and (2) although there is evidence for a local source of inhibition in SCi (McPeek and Keller, 2002; Munoz and Istvan, 1998), the saccade curvatures in the current experiment suggest that the distractors were not equally inhibited and the computations required to differentiate these distractors likely was not computed in SCi.

A rapid burst of excitation in the critical epoch between −30 and 0 ms prior to the initiation of a saccade has been causally demonstrated to elicit saccades curved towards distractors (McPeek et al., 2003). A recent study has found evidence that a burst of inhibition in this critical epoch may also cause saccades to curve away from distractors (White et al., 2012). In the case of excitation, this critical epoch is also behaviorally evident: saccade curvatures begin and end within ~20 ms (Port and Wurtz, 2003). The current results from our temporal analysis suggests that saccade curvature modulation by visual similarity occurred in the first approximately 20-30 ms. Since our observed curvatures were likely due to inhibition, this strengthens the interpretation that the same spatio-temporal profile of SCi activity elicits saccades curved towards and away from distractors.

We found evidence that the visual similarity between two bilateral, equidistant distractors and a target modulates saccade curvatures during a visual search task, consistent with previous behavioral experiments (Ludwig and Gilchrist, 2003; Mulckhuyse et al., 2009). Critically, we also discovered a continuous linear relationship between the magnitude of saccade curvatures and visual similarity between targets and distractors, which demonstrates that the oculomotor system computes a weighted-vector average of possible saccade goals and that high-order cognitive factors can mediate the values assigned to these weights. Conversely, when these bilateral distractors were equally similar to the target, the oculomotor system spatially averaged distractor vectors with equal weights and saccade trajectories returned to baseline, as with identical bilateral distractors (McSorley et al., 2004). By analyzing saccade curvature as a function of saccade amplitude percentage, we demonstrated that saccades were only curved in the first 20-30 ms of the movement, which is consistent with neurophysiological observations (Port and Wurtz, 2003). Finally, our task parameters likely preclude SCi as sufficient to compute visual similarity in the current context, which suggests a downstream role of SCi in target selection.

Chapter 4: A Rapid Accumulation of Inhibition Can Account for Saccades Curved Away from Distractors (Manuscript 3)

This manuscript will be submitted to ***The Journal of Neurophysiology***. The co-author of this manuscript is Dr. Mazyar Fallah. Devin Heinze Kehoe and Dr. Mazyar Fallah designed the experiment. Devin Heinze Kehoe implemented the experiment and analyzed the data. Devin Heinze Kehoe and Selvi Aybulut collected the data. Devin Heinze Kehoe wrote the manuscript with feedback from Dr. Fallah.

Keywords

superior colliculus, target selection, saccade curvature, inhibition, modeling

4.1 Summary

Saccades curved towards a distractor are accompanied by a perisaccadic burst at the distractor locus in the intermediate layers of the superior colliculus (SCi) ~20-30 ms prior to the initiation of a saccade (McPeek et al., 2003; Port and Wurtz, 2003). Although saccades curve away from inhibited SCi loci (Aizawa et al., 1998), whether inhibition is restricted to a similar critical epoch for saccades curved away from a distractor remains unclear (White et al., 2012). We examined this possibility by modeling human saccade curvature as a function of the duration of visual input from an irrelevant luminance- or color-modulated distractor prior to an impending saccade, referred to as saccade distractor onset asynchrony (SDOA). Our results demonstrated that 70 ms of luminance-modulated distractor processing or 90 ms of color-modulated distractor processing is required to modulate the trajectory of a saccade curved towards the distractor. As these behavioral results mirror the very robust transient visual onset latencies observed from SCi visuo-movement (VM) neurons for luminance- (Boehnke and Munoz, 2008) and color-modulated (White et al., 2009) stimuli, this method seems to provides an accurate non-invasive means to estimate the timing of peak firing rates of populations of VM neurons in SCi. We modeled SDOA functions separately for saccades curved towards and away from distractors and observed that a similar temporal process determined the magnitude of saccade curvatures in both contexts suggesting that saccades deviate away from a distractor due to a rapid accumulation of inhibition in the critical epoch prior to saccade initiation.

4.2 New and Noteworthy

In this research article, we propose a novel, non-invasive approach to behaviorally model the time course of competitive oculomotor processing. Our results highly resembled those from previously published neurophysiological experiments utilizing similar oculomotor processing

contexts, thus validating our approach. Furthermore, this methodology provided new insights into the underlying neural mechanism subserving oculomotor processing as we applied it to a context with which the neural mechanism is more contentious and the results clearly favored one view.

4.3 Introduction

Interest in using saccade curvatures to examine competitive oculomotor processing of potential saccade goals has increased in the last several decades. This interest is likely due in part to the striking correlation between the neurophysiology and behavioral output of the oculomotor system: potential oculomotor movement goals are represented in the intermediate layers of the superior colliculus (SCi), a midbrain structure with a highly ordered movement map (Wurtz and Goldberg, 1972; Robinson, 1972) that projects directly to the brainstem saccade pulse generators (Moschovakis et al., 1988) and contributes to target selection for both pursuit (Basso et al., 2000; Carello and Krauzlis, 2004; Krauzlis and Dill, 2002; Krauzlis, 2003, 2005) and saccadic eye movements (Basso and Wurtz, 1997, 1998; Horwitz and Newsome, 2001; McPeek and Keller 2002, 2004). Activity on the motor map is spatially averaged whereby saccade vectors curve towards an area with excitation (McPeek et al., 2003; Port and Wurtz, 2003) or curve away from an area with inhibition (Aizawa and Wurtz, 1998). In addition to spatial factors, saccade curvatures are also affected by robust temporal factors.

McPeek et al. (2003) reported that saccades that landed near a target but curved towards a distractor were accompanied by a perisaccadic burst at the SCi locus encoding the distractor, which occurred approximately 30 ms before the perisaccadic burst at the SCi locus encoding the target. This was then causally demonstrated whereby subthreshold microstimulation administered to the distractor locus with the same spatiotemporal profile elicited a saccade

curved towards the distractor. A subsequent study reported that these curved saccade trajectories conform to a vector average model weighted by the activity levels of the neuronal populations encoding vectors to the target and distractor (Port & Wurtz, 2003). The spatiotemporal factors that relate SCi excitation to saccades curved towards distractors are well understood. However, these factors are more controversial for linking SCi inhibition to saccades curved away from distractors.

The sources of excitation in SCi are transient visual onset bursts that immediately follow the onset of a stimulus (reviewed by Boehnke & Munoz, 2008) and perisaccadic bursts that immediately precede the initiation of an eye movement (Wurtz & Goldberg, 1972). The sources of SCi inhibition are local lateral inhibitory circuits (McPeek & Keller, 2002; Munoz & Istvan, 1998) or top-down cortical inhibition indirectly projected to SCi through the substantia nigra pars reticulata (SNr) nucleus of the basal ganglia (Hikosaka & Wurtz, 1983). This top-down inhibitory input imposes spatially selective tonic GABAergic activity on populations of SCi neurons encoding specific saccade vectors (Hikosaka & Wurtz, 1985). As such, SCi inhibition predictably modulates saccade vectors: inhibitory SCi injections elicit saccades with endpoints shifted away from the injection site (Lee et al., 1988) or that curve away from the injection site (Aizawa et al., 1998), therefore demonstrating the same spatial averaging principle as SCi excitation (Robinson, 1972; van Gisbergen et al., 1987). However, the temporal principle relating to SCi inhibition to saccade curvatures is more contentious.

Neurophysiological experiments have demonstrated that inhibition of potential saccade goals (e.g., a distractor stimulus) slowly accumulates over time (McPeek & Keller, 2002). This is also reflected in behavioral studies as saccade curvatures are generally curved towards a distractor at early saccade reaction times (SRTs), but begin to curve away from the distractor

after approximately 200 ms (McSorley et al., 2006, 2009; Walker et al., 2006). Interested in examining the temporal factors that cause saccades to curve away from distractors, White et al. (2012) examined the activity of SCi neurons encoding the distractor vector during a saccade task specifically on trials with saccades curved away from the distractor. They observed that the magnitude of these saccade curvatures only correlated with distractor-related neuronal activity in the epoch between −22 and 0 ms before saccade initiation and argued that this was too brief to reflect a slow accumulation of top-down inhibition. However, this critical epoch in which SCi inhibition correlates with the magnitude of saccades curved away from distractors is entirely consistent with the epoch in which distractor-related excitation correlates with the magnitude of saccades curved towards distractors (McPeek et al., 2003; Port & Wurtz, 2003). Given that SNr inhibition is tonically projected onto SCi at a quick temporal frequency of 50-100 Hz (Hikosaka et al., 2000), then as acknowledged by White et al. (2012), it is possible that saccades curve away from a distractor when inhibition rapidly accumulates at the distractor locus in SCi in this critical epoch.

Here, we examined this possibility by examining the time course of competitive distractor processing by noninvasively measuring saccade curvatures while human participants completed a simple saccade task and by modeling this process as a function of how long the oculomotor system has had access to the distractor. To manipulate how long the oculomotor system has had access to a distractor we utilized various distractor-target onset asynchronies (DTOAs) and subtracted from them saccade response times (SRTs), which provided a metric we refer to as saccade-distractor onset asynchrony (SDOA). As we observed in a pilot study that SRTs cluster around 200 ms for this saccade task, we utilized DTOAs of 50, 100, 150, 200, and 250 ms so to probe a wide range of the SRT distribution and consequently capture a wide SDOA

range. We modeled saccade curvature as a function of SDOA for saccades curved towards and away from the distractor and found that saccades curvatures varied as a function of SDOA with a nearly identical temporal profile for saccades curved towards and away from distractors, suggesting that a rapid accumulation of excitation and inhibition can account for saccades curved towards or away from distractors respectively.

4.4 Methods

4.4.1 Participants

22 York University undergraduate students (18-28 years old, 11 male) participated in the experiment for course credit. Participants had normal or corrected-to-normal visual acuity, had normal red-green color vision as assessed by Ishihara color plates (Ishihara, 2006), and were naïve to the purpose and design of the experiment. Informed consent was obtained prior to participation. All research was approved by York University's Human Participants Review Committee.

4.4.2 Stimuli

The saccade target was a white ($x = 117.30$, $y = 122.70$) square that subtended 0.6° × 0.6° and was located 12° above or below central fixation. We replicated the Gabor patches utilized by Burr and Morrone (1993) as our distractors, which were created offline using MATLAB (MathWorks, Natick, MA) by superimposing equiluminant red (peak intensity: $x = 14.50$, $y = 7.58$) and green (peak intensity: $x = 3.78$, $y = 7.57$) sinusoidal waves with a spatial frequency of 1°/cycle and a phase shift of either 1 (luminance-modulation) or .5 (color-modulation) convolved with a 2D Gaussian filter ($\sigma = 1.5°$). Stimuli were imbedded in a grey ($x = 7.21$, $y = 7.51$) background. Distractors faded to grey by weighting the blue color channel with the inverse of the 2D Gaussian filter. The stimuli were displayed on a 21-inch CRT monitor (85 Hz, 1024 × 768).

Participants viewed stimuli in a dimly lit room from a viewing distance of 57 cm with a headrest stabilizing their head position.

4.4.3 Apparatus and Measurement

Stimulus presentation was controlled using a computer running Presentation software (www.neurobs.com). Eye position was recorded using infrared eye tracking (500 Hz, EyeLink II, SR Research, Ontario, Canada). The eye tracker was calibrated at the beginning and halfway point of each experimental session, and as needed.

4.4.4 Task Procedure

Trials were initiated by maintaining fixation (1.89° square window) to a white, central fixation cross (0.4°× 0.4°) for 200 ms, after which the fixation cross offset and the target onset 12° above or below fixation (see Figure 1). Participants were instructed to fixate the target as soon as it appeared. After an interval of 50, 100, 150, 200, or 250 ms, the luminance- or color-modulated distractor onset to the left or right of the target at an eccentricity of 12° with an angular separation of 45° to the target. This interval is subsequently referred to as the distractor-target onset asynchrony (DTOA). The trial ended when a saccade was made to the target or 500 ms had elapsed (time-out). Time-out trials were randomly replaced back into the block and were signified with an error tone and message. Trials were separated by a 1000 ms intertrial interval (ITI) with a blank, grey display.

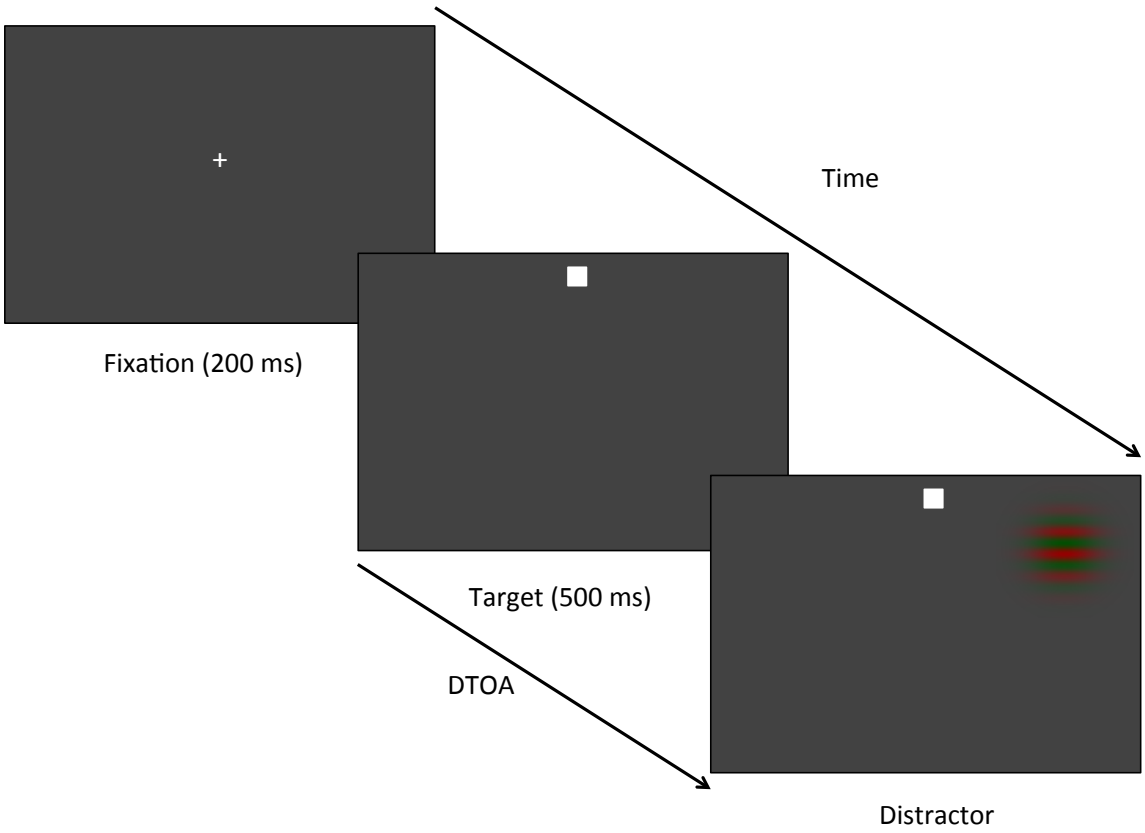

Figure 4.1: Example trial sequence. After viewing fixation for 200 ms, the target onset above or below fixation until it was fixated or the trial timed out (500 ms). The luminance- or color-modulated distractor appeared to the left or right of the target 50, 100, 150, 200, or 250 ms after target onset (DTOA).

Participants completed 1 session with 10 blocks of 78 trials for a total of 780 trials. For half of the participants (determined by the order in which they appeared in the lab), we utilized DTOAs of 50, 100, and 150 ms. For the remaining half, we utilized DTOAs of 150, 200, and 250 ms. On each trial, the target location, distractor location, distractor feature, and DTOA were randomized. This design contained a total of 24 (2×2×2×3) experimental conditions. Baseline trials with targets at both target locations and no distractors were randomly interleaved into the blocks and increased the number of conditions to 26. There were an equal proportion of trials from all 26 conditions on every block.

4.4.5 Saccade Detection and Analysis

Saccades were detected, visualized, filtered and analyzed offline using customized MATLAB algorithms. Trials that contained blinks, endpoint deviations > 3° from the center of the target, or a fixation drift > 0.5° during the pre-saccadic latency period were excluded from further analysis. Saccades were defined as a velocity exceeding 20 deg/s for at least 8 ms and a peak velocity exceeding 50 deg/s. Saccades were excluded from further analysis if they had a latency less than 100 ms. The data from 2 participants was not analyzed as over 50% of trials were removed.

To analyze saccade curvatures, saccade start-points were translated back to the origin and then trigonometrically rotated so that the endpoint was aligned to the positive *y*-axis. The following metrics were then used to quantify saccade curvatures: (1) *sum deviation*, the sum of all *x* deviations along the length of the saccade; and (2) *max deviation*, the maximum *x* deviation along the length of the saccade. Baseline saccade curvatures for each participant at each target location were subtracted from the data to reduce inherent, idiosyncratic curvature. The curvature metrics were then recoded so that positive deviations correspond to deviations towards a distractor, while negative deviations correspond to deviations away from a distractor.

We calculated the saccade distractor onset asynchrony (SDOA) by subtracting SRTs from DTOA such that, SDOA = DTOA − SRT. Thus, this metric indicates how much time the distractor has been displayed for relative to saccade initiation, where a negative value indicates how long *before* saccade initiation the distractor onset. SDOA values greater than zero were not analyzed as this indicates that the distractor appeared after the initiation of the saccade. We binned the SDOA data such that each bin contained data from a 20 ms SDOA interval aligned to an SDOA of zero. We herein refer to each individual bin by its center (e.g., bin −10 contains the

SDOA data between −20 and 0 ms). We performed a regression analysis on the average sum curvature and max curvature as a function of bin center for every bin that contained ≥ 20 trials. Since there was an uneven SDOA distribution across subjects, we averaged saccade curvatures across subjects in each bin. Using a customized MATLAB implementation of the maximum likelihood estimation (MLE) method, the mean saccade curvature as a function of SDOA bin center was fit to the following two functions:

(1) Gaussian:

$$f_G(x) = (\alpha - \delta) \bullet e^{-\frac{(x-\mu)^2}{2\sigma^2}} + \delta$$

where α is the height of the function, μ is the midpoint of function, σ is the slope of the function, and δ is the floor of the function and

(2) logistic:

$$f_L(x) = \frac{L - \delta}{1 + e^{k(x-x_0)}} + \delta$$

where L is the height of the function, x_0 is the midpoint of the function, k is the slope of the function, and δ is the floor of the function.

4.5 Results

Trials were removed if the sum curvature was 3 standard deviations (SD) above or below the mean in each SDOA bin. Trials were categorized as having curved towards or away from the distractor. Saccades that could not be classified according to this dichotomy (i.e., so-called "cubic" saccades, Ludwig & Gilchrist, 2002) were also omitted from subsequent analyses. As we were interested in determining how much distractor processing time is sufficient for saccade vector modulation by the distractor, we calculated the unsigned magnitude of saccade curvatures

in each SDOA bin (regressed using bin centers) by averaging the absolute mean saccade curvature for each subject. Furthermore, to determine when saccade curvatures had significantly deviated from baseline, we compared the absolute subject means in each SDOA bin to the fitted floor parameter (δ) from the regression analysis using a two-tailed, paired-samples *t*-test and a Bonferroni multiplicity adjustment. We assessed whether each function accounted for a significant proportion of the variance using an *F*-test regression analysis. If both models significantly fit the data, we assessed whether the Gaussian or logistic model provided a statistically better fit to the data using an *F*-test performed on the ratio of the sum-of-squared model residuals with $N - k$ degrees of freedom. Similarly, the goodness-of-fit of each function to the data was evaluated by calculating the coefficient of determination (R^2).

4.5.1 Overall SDOA Functions

The overall sum curvature data was significantly fit by the Gaussian, $F(3,7) = 21.34$, $p < .001$, $R^2 = .90$ (see Figure 2*A*); and logistic models, $F(3,7) = 11.35$, $p = .004$, $R^2 = .84$ (see Figure 2*B*). Neither model provided a statistically better fit of the data, $F < 1$. However, a comparison of the R^2 values and a visual inspection of the fit suggested that the Gaussian model provides a better mathematical description of the distractor integration process. As such, the Gaussian model demonstrated that sum curvatures significantly deviated from baseline in SDOA bins ≤ -70 ms, suggesting that approximately 70 ms of distractor processing time is required for saccade vector modulation.

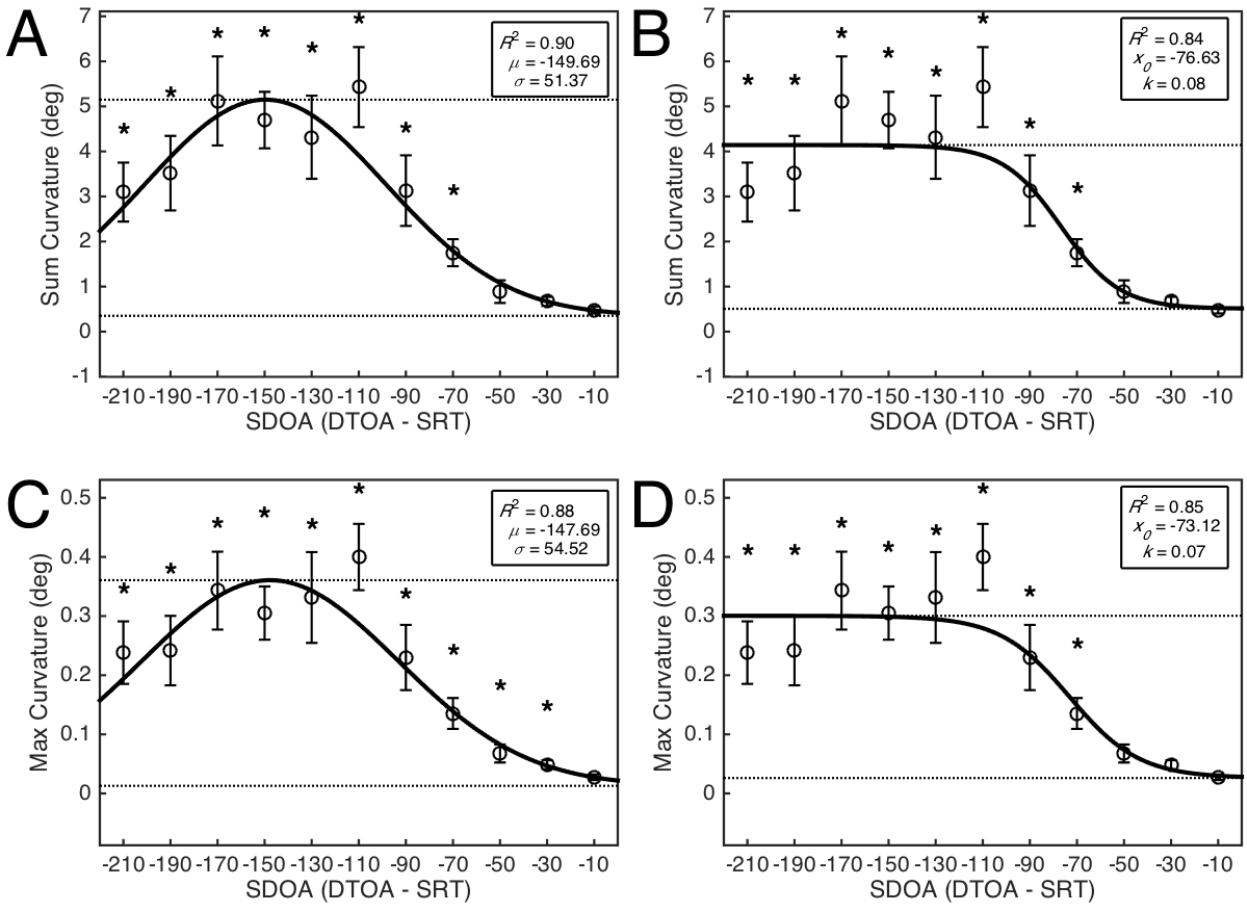

Figure 4.2: Function fits for overall SDOA data. Gaussian and logistic models fitted to the overall mean sum and max curvatures as a function of SDOA bin center. Datapoints (open, black circles) represent mean saccade curvature. Error bars represent standard error. Broken lines depict fitted floor and ceiling parameters Asterisks denote significant curvature deviations from baseline. ***A*:** Gaussian model fitted to the overall sum curvature data. ***B*:** Logistic model fitted to the overall sum curvature data. ***C*:** Gaussian model fitted to the overall max curvature data. ***D*:** Logistic model fitted to the overall max curvature data.

The overall max curvature data was also significantly fit by the Gaussian, $F(3,7) = 17.63$, $p = .001$, $R^2 = .88$ (see Figure 2*C*); and logistic models, $F(3,7) = 11.85$, $p = .004$, $R^2 = .85$ (see Figure 2*D*). Neither model provided a statistically better fit of the data, $F < 1$. A similar inspection as before suggests that the Gaussian model provides a better mathematical description

of the distractor integration process. According to the Gaussian model, max curvatures significantly deviated from baseline in SDOA bin ≤ −30 ms. This result conflicts with the estimate from the sum curvature data for the minimum distractor processing time required for saccade vector modulation. However, given that the mean and SD of the fitted Gaussian models for the sum and max curvature data are quite similar (μ_{sum} = −149.69, σ_{sum} = 51.37; μ_{max} = −147.69, σ_{max} = 54.52 respectively), the sum and max curvature appear to reflect the same process. Furthermore, the logistic model demonstrated that max curvatures significantly deviated from baseline in SDOA bins ≤ −70 ms (see Figure 2*D*), consistent with the sum curvatures. Taken together, these results suggest that the max curvature −50 ms and −30 ms bins likely significantly deviated above baseline due to extremely low variability in these bins and a small fitted floor parameter by the Gaussian model. We maintain that our data show that approximately 70 ms of distractor processing time is required for saccade vector modulation.

4.5.2 Color Differences

To examine potential feature differences in the sum and max saccade curvatures, we split the data into trials with a luminance-modulated distractor and a color-modulated distractor (see Figure 3). The Gaussian model significantly fit the sum curvature data from luminance trials, $F(3,7) = 13.61$, $p = .003$, $R^2 = .86$; and color trials, $F(3,7) = 12.16$, $p = .004$, $R^2 = .79$ (see Figure 3*A*). The logistic model also significantly fit the data from luminance trials, $F(3,7) = 8.74$, $p = .009$, $R^2 = .80$; and color trials, $F(3,7) = 34.60$, $p < .001$, $R^2 = .85$ (see Figure 3*B*). Neither model was a statistically better fit to the luminance data, $F < 1$. However, the logistic model provided a marginally better fit to the color data, $F(7,7) = 3.25$, $p = .072$, $\eta^2 = .76$. Based on a comparison of the R^2 and a subjective evaluation, it appears as though the Gaussian model provided a better description of luminance-modulated distractor processing, whereas the logistic model provided a

better description of color-modulated distractor processing with marginal, yet unreliable, statistical evidence for this conclusion. The Gaussian model indicated that the sum curvatures measured on trials with luminance-modulated distractors deviated from baseline in SDOA bins ≤ −70 ms as with the overall data. However, the logistic model indicated that the sum curvatures measured on trials with color-modulated distractors deviated from baseline in SDOA bins ≤ −90 ms.

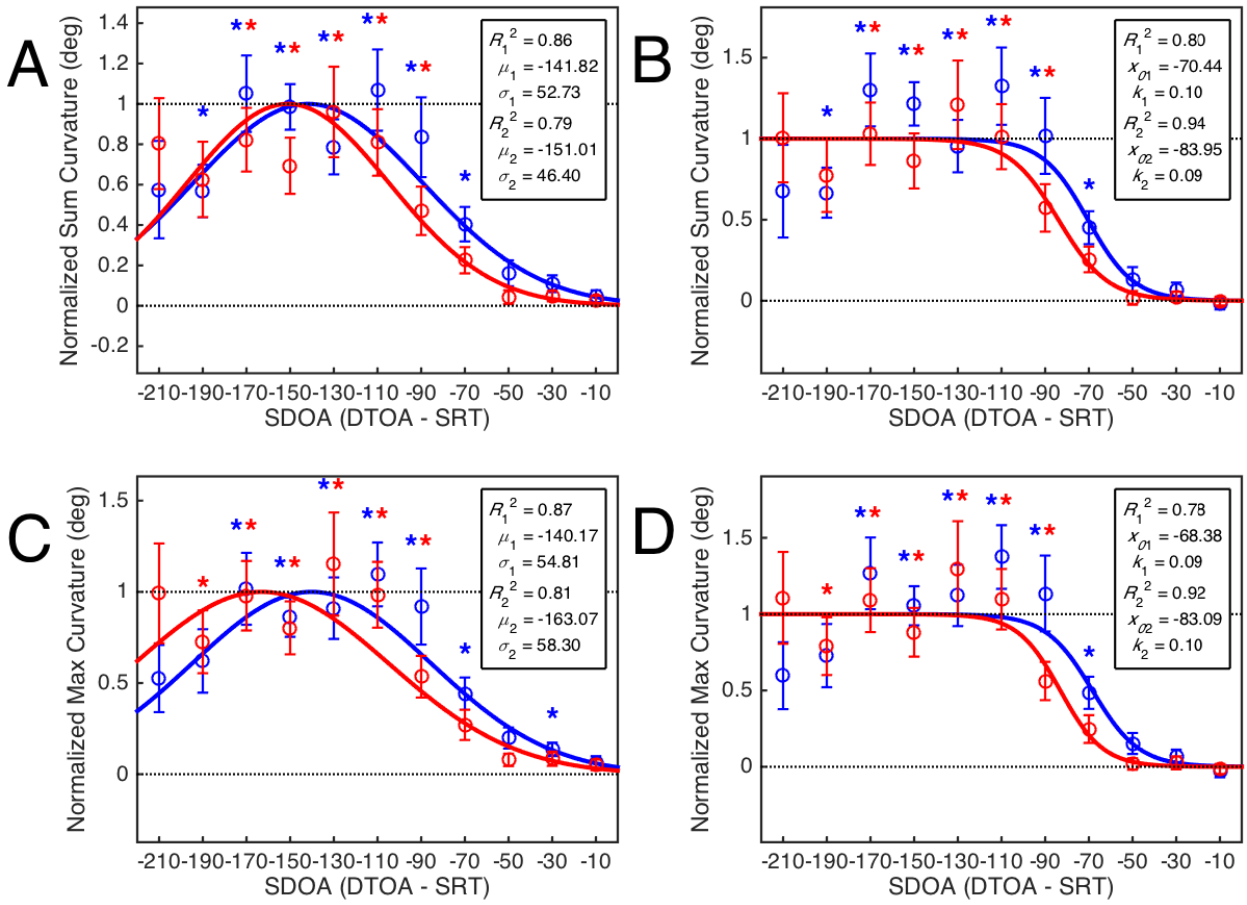

Figure 4.3: Function fits for color differences. Gaussian and logistic models fitted to mean sum and max curvatures as a function of SDOA bin centers split into trials with a luminance-modulated distractor (blue) and color-modulated distractors (red). Datapoints (open, colored circles) represent mean saccade curvature. Error bars represent standard error. Broken lines depict fitted floor and ceiling parameters. Asterisks denote significant curvature deviations from

baseline. ***A*:** Gaussian model fitted to the sum curvature data. ***B*:** Logistic model fitted to the sum curvature data. ***C*:** Gaussian model fitted to the max curvature. ***D*:** Logistic model fitted to max curvature data.

We repeated the above analyses for the max curvature metric, which provided consistent results (see Figure 3). The Gaussian model significantly fit the max curvature data for luminance trials, $F(3,7) = 14.56$, $p = .002$, $R^2 = .87$; and color trials, $F(3,7) = 9.59$, $p = .007$, $R^2 = .81$ (see Figure 3*C*). The logistic model also significantly fit the data on luminance trials, $F(3,7) = 7.78$, $p = .012$, $R^2 = .78$; and color trials, $F(3,7) = 23.32$, $p < .001$, $R^2 = .92$ (see Figure 3*D*). Consistent with the sum curvature data, neither model was a statistically better fit to the luminance data, $F < 1$. Furthermore, the logistic model was not a statistically better fit of the color data, $F(7,7) = 2.29$, $p = .148$, $\eta^2 = .70$. However, based on a comparison of the R^2 and a subjective evaluation, it appears as though the Gaussian model provided a better description of luminance-modulated distractor processing, whereas the logistic model provided a better description of color-modulated distractor processing. Consistent with the sum curvature data, the Gaussian model indicated that the max curvatures measured on trials with luminance-modulated distractors deviated from baseline in SDOA bins ≤ −70 ms, whereas the logistic model indicated that the max curvatures measured on trials with color-modulated distractors deviated from baseline in SDOA bins ≤ −90 ms. These results clearly demonstrate that color information elicits an onset transient burst in SCi neurons between 20-40 ms (i.e., the minimum and maximum bin width respectively) later than luminance information.

4.5.3 Directional Differences

As we were interested in examining potential differences in saccade curvature as a function of SDOA when saccades curved towards or away from the distractor, we split the data

into trials on which saccades curved towards the distractor and trials on which saccades curved away from the distractor (see Figure 4). For the sum curvature data, the Gaussian model significantly fit the data for trials with saccades curved towards distractors, $F(3,7) = 10.97$, $p = .005$, $R^2 = .77$; and away from distractors, $F(3,7) = 13.63$, $p = .003$, $R^2 = .84$ (see Figure 4*A*). Conversely, the logistic model did not provide a significant fit to the data for trials with saccades curved towards distractors, $F(3,7) = 1.93$, $p = .213$, $R^2 = .474$; and a unreliable, yet marginal, fit for trials with saccades curved away from distractors, $F(3,7) = 3.93$, $p = .062$, $R^2 = .64$. The fitted Gaussian model demonstrated that sum curvatures towards distractors deviated from baseline in the −110 ms SDOA bin, while the sum curvatures away from distractors deviated from baseline in the −170 and −150 ms SDOA bins.

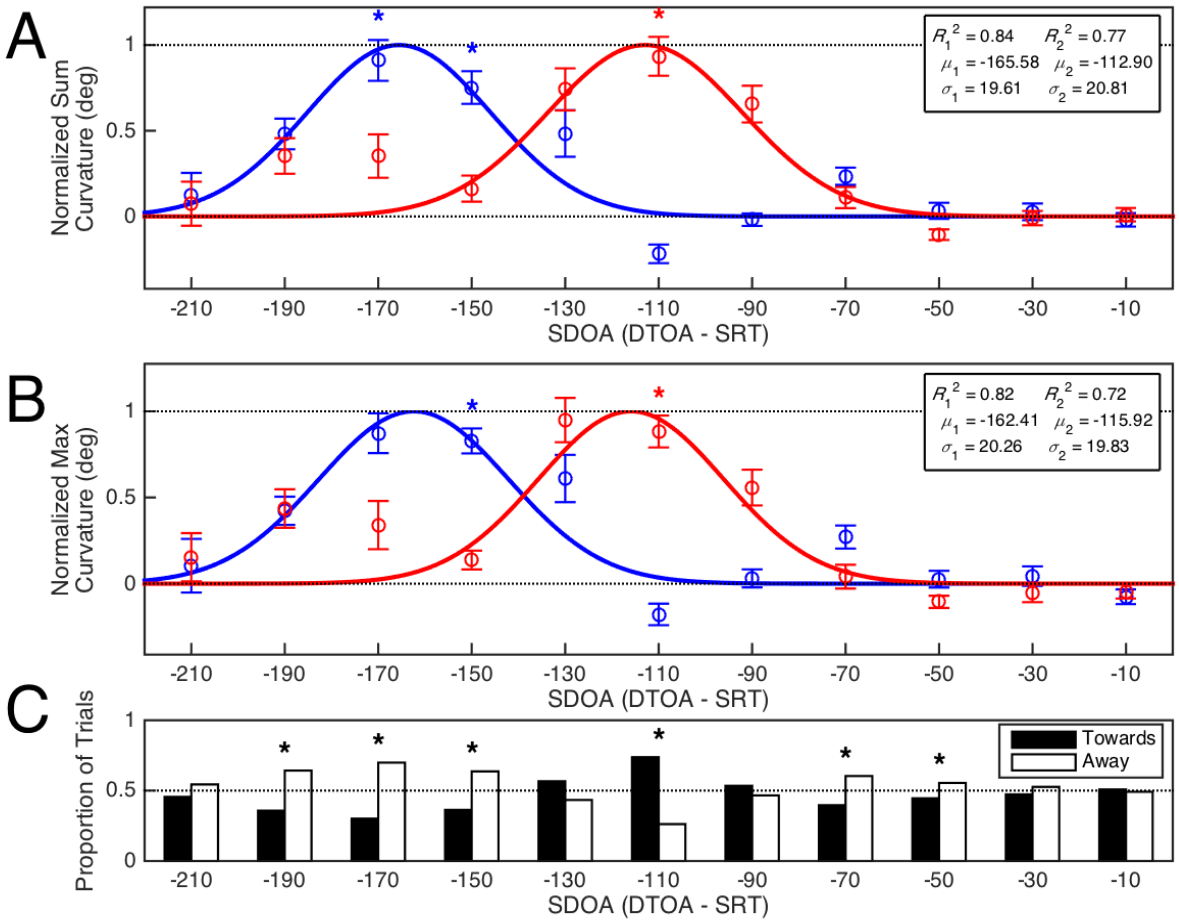

Figure 4.4: Function fits for directional differences. Gaussian model fitted to sum and max

curvatures as a function of SDOA bin split into trials with a saccade curved away from the distractor (blue) and towards the distractor (red). Datapoints (open, colored circles) represent mean saccade curvature, error bars represent standard error, broken lines depict fitted floor and ceiling parameters, and asterisks denote significant curvature deviations from baseline (*A*, *B*). ***A*:** Gaussian models fitted to the sum curvature data. ***B*:** Gaussian models fitted to the max curvature data. ***C*:** Proportion of trials with a saccade curved towards (black bars) or away (white bars) from a distractor in each SDOA bin. Asterisks denote deviations from a random distribution of trials with saccades curved towards or away from distractors.

For the max curvature data, the Gaussian model significantly fit the data for trials with a saccade curved towards distractors, $F(3,7) = 7.49$, $p = .014$, $R^2 = .72$; and away from distractors, $F(3,7) = 11.74$, $p = .004$, $R^2 = .82$. (see Figure 4*B*) The logistic model did not significantly fit the data for trials with a saccade curved towards distractors, $F(3,7) = 2.37$, $p = .156$, $R^2 = .53$; but did fit the data for trials with a saccade curved away from distractors, $F(3,7) = 4.43$, $p = .048$, $R^2 = .61$; and neither model was statistically better fit to the data, $F < 1$. However, a comparison of the R^2 and a subjective evaluation suggested that the Gaussian model provided a better description of inhibitory influences on distractor processing. Consistent with the sum curvature data, the fitted Gaussian model demonstrated that sum curvatures towards distractors deviated from baseline in the −110 ms SDOA bin and marginally in the −130 bin ($p = .067$), while the sum curvatures away from distractors deviated from baseline in the −150 ms SDOA bin and marginally in the −170 bin ($p = .093$). Taken together, these results suggest that oculomotor inhibition responsible for saccades curved away from the distractor is processed slower than the excitation responsible for saccades curved towards the distractor, although these excitatory and inhibitory influences accumulate at the same rate since the slope parameters were nearly identical.

A *Chi*-squared goodness-of-fit analysis demonstrated that there was a higher probability of saccades curved away from distractors than saccades curved towards distractors, $\chi^2(1, N = 6792) = 12.04$, $p < .001$. Similarly, a subsequent *Chi*-squared test-of-independence analysis demonstrated that the frequency distribution of saccades across SDOA bins was related to the directionality of saccades, $\chi^2(10, N = 6792) = 241.33$, $p < .001$. As such, we analyzed the proportion of saccades that curved towards and away from distractors in each SDOA bin using *Chi*-squared goodness-of-fit analyses weighted using the Bonferroni multiplicity adjustment (see Figure 5*C*). This analysis demonstrated that the SDOA time point of peak saccade curvature towards a distractor corresponded to a higher probability of saccades curved towards distractors. Similarly, the SDOA time point of peak saccade curvature away from a distractor corresponded to a higher probability of saccades curved away from distractors.

4.6 Discussion

We examined the time course of competitive oculomotor processing by analyzing saccade curvatures as a function of the duration of time that the oculomotor system has received distractor visual input prior to saccade initiation (SDOA). We performed two analyses to validate this methodological approach to modeling the time course of competitive oculomotor processing. The first analysis linked the current behavioral data to a very robust pattern of neuronal responses observed in SCi VM neurons after a transient visual onset. Second, the current study provides the behavioural sequelae to a recent neurophysiological observation that showed that these visual onset latencies differ between luminance and color onsets. Finally, having validated SDOA modeling, we analyzed SDOA functions separately for saccades curved towards and away from distractors. This analysis provided insights into the time course for the accumulation of oculomotor inhibition, which has been a contentious topic in the study of competitive

oculomotor processing. Here, we discuss the main findings and implications of these three analyses in turn.

4.6.1 Saccade Curvature Timing

Our analysis of the overall sum curvature data as a function of SDOA demonstrated that saccade curvatures significantly deviated from baseline when the oculomotor system received distractor input at least 70 ms prior to the initiation of an impending saccade. Consistent with this result is converging evidence from various other behavioral methodologies suggesting that there is a point of no return for modulating the trajectory of an impending saccade, which is estimated to be between 60 and 80 ms prior to saccadic initiation (Becker and Jürgen, 1979; Findlay and Harris, 1984; Ludwig et al., 2007; Reingold and Stampe, 2002; cf. Buonocore et al., 2016). The time between saccade initiation and the point of no return has been called saccadic dead time (SDT; Ludwig et al., 2007). Critically, this SDT time estimate provided by the overall sum curvature data is consistent with the known neurophysiological correlates of saccade curvature: the latencies of transient onset bursts measured in monkey SCi are usually between 40 and 70 ms after stimulus onset (Boehnke & Munoz, 2008). At an SDOA of −70 ms, this burst of distractor-related activity is occurring well within the critical epoch of 0 to 30 ms prior to saccade initiation, and it has been causally demonstrated that subthreshold distractor activity occurring in this epoch elicits curved saccades (McPeek et al., 2003). Therefore, the behavioral results of the overall sum curvature analysis can be directly linked to SCi neurophysiology.

When we conducted the overall saccade curvature analysis for the max curvature metric, we observed that the SDT estimate generated by the Gaussian function dropped to a minimum of 30 ms prior to the initiation of an impending saccade. Alternatively, the logistic function fit to the max curvature data suggested that 70 ms is the minimum time required for saccade trajectory

modulation. Therefore, the 30 ms SDT estimate is likely due to a small fitted floor parameter and extremely small variability in the −50 and −30 ms bins as the SDOA distribution contained a high number of observations in these bins. This was also corroborated by subsequent logistic fits to the max curvature data for luminance- and color-modulated distractors also suggesting that 70 ms is the minimum time required for saccade trajectory modulation. Furthermore, as previously mentioned, the fastest transient onset burst latencies for SCi visuo-movement (VM) neurons are approximately 40 ms. Given that the −30 SDOA bin includes SDOA observations between −40 and −20 ms, most values fall outside of the critical temporal epoch for eliciting curved saccades. However, the −50 SDOA bin does actually fall better into this range and seems more plausible from a neurophysiological standpoint. A second technique that could be used to estimate the SDT would be to simply use the half-height of the Gaussian or midpoint parameter of the logistic functions. However, in the case of the logistic midpoint parameter, this suggests that approximately 70 ms is indeed the correct SDT estimate for both the sum and max curvature data. Similarly, in the case of the half-height of the Gaussian, the fitted slope and midpoint parameters are nearly identical between the sum and max curvature data suggesting that both estimates should indeed be similar. Clearly, there is strong reason to believe that a minimum of 70 ms exposure time is required for a distractor to interfere with an impending saccade despite the significant deviations from baseline in the −30 and −50 SDOA bins to the contrary.

4.6.2 Color Differences in Saccade Curvature Timing

We also found that luminance- and color-modulated distractors produced different results with regards to the time course of saccade curvatures and these results helped further relate our current behavioral results to SCi neurophysiology. A recent neurophysiological investigation by White et al. (2009) discovered SCi VM neurons with color “sensitivities” (as supposed to

selectivities due to their very broad tuning), contrary to classic studies suggesting an absence of color projections to the colliculus from either the lateral geniculate nucleus (Schiller et al., 1979) or from retinal ganglion cells (Schiller and Malpeli, 1977). An interesting property observed for these color sensitive neurons is that the transient onset burst latencies were 30-35 ms longer for color targets (i.e., equiluminant with the display background, but a different color) than the latencies for luminance targets (i.e., a higher luminance than the background display). The distractors utilized in the current experiment have similar visual properties as the targets utilized by White et al. and should then elicit a similar pattern of onset burst latencies in SCi VM neurons. Consistent with this prediction, our current data demonstrated that the SDT for color-modulated distractors is 20±10 ms longer than for luminance-modulated distractors as saccade curvatures deviated from baseline in the −90 SDOA bin for color-modulated distractors, but deviated from baseline in the −70 SDOA bin for luminance-modulated distractors. This was consistent across sum and max curvature metrics and across fit functions, although the Gaussian fit of the max curvature data did show a significant deviation from baseline in the −30 SDOA bin. However, since there was no deviation in the −50 SDOA bin, this further strengthens our interpretation of the results in −30 and −50 SDOA bins for the overall max curvature Gaussian fit and we similarly find this observation unlikely. Critically, these differences between luminance and color cannot be attributed to practice effects (see Gilbert et al., 2001 for a review), as participants observed an equal number of luminance and color distractors and the presentation of these features were not predictable.

One interesting consideration is whether the latency differences between color and luminance input to SCi are due to the fact that latencies vary inversely with luminance (Bell et al., 2006; Li and Basso, 2008) and since the luminance modulated distractors were more

luminous than the color-modulated distractors. This explanation is unlikely given that the mathematical descriptions of the SDOA functions were different for trials with a luminance (Gaussian) or color (logistic) distractor, therefore alternatively suggesting that luminance and color projections to SCi are processed separately through distinct anatomical channels. This is consistent with this reasoning, White et al. (2009) observed that the visual onset burst latency differences between color and luminance targets did not covary with the magnitude of the neuronal responses.

The analyses of overall curvature and color differences demonstrated that there is a close temporal relationship between the current behavioral results and SCi neurophysiology. These analyses therefore validate the current methodology as a non-invasion, behavioral means to infer the timing of critical neurophysiological events that influence competitive oculomotor processing such as the peak firing rates of populations of VM neurons in response to transient onsets as well as the time course of oculomotor inhibition. As such, we utilized similar regression analyses to investigate the time course of saccades curved towards and away from distractors separately, which yielded several results that merit discussion.

4.6.3 Timing Effects on Saccade Curvature

The analysis of directional differences suggested that the processing responsible for eliciting saccades curved towards a target occurs before the processing responsible for eliciting saccades curved away from distractors as the Gaussian functions were shifted by approximately 50 ms along the SDOA axis relative to one another. This temporal difference between processes is consistent with previous behavioral studies that have examined saccade deviations as a function of SRT on trials with synchronous distractors and target onsets and found that saccades curve towards distractors at short latencies between 150-200 ms, but then begin to curve away

from distractors after latencies of approximately 200 ms (McSorley et al., 2006, 2009; Walker et al., 2006). However, a neurophysiological study examining the time course of SCi target selection suggested that inhibition likely begins to accumulate before 200 ms as SCi VM neurons can discriminate a target from distractor after ~110 ms from visual onset (McPeek and Keller, 2002). Interestingly, the current results are consistent with this estimate of distractor inhibition accumulation beginning ~110 after stimulus onset in two ways: (1) When we modeled the oculomotor processes for excitation (i.e., distribution of curvatures for saccades curved towards distractors) and inhibition (i.e., distribution of curvatures for saccades curved towards distractors), we observed that these processes were offset by 50-55 ms, which is consistent with excitation occurring 55 ms [on average as (70+40)/2 = 55] after stimulus onset (Boehnke and Munoz, 2008) and inhibition occurring 55 ms later (McPeek and Keller, 2002). (2) We observed significant saccade deviations from baseline for saccades curved away from the distractor in the −150 SDOA bin. This means that the critical epoch for distractor activity to elicit saccade curvature began ~120 ms after onset using the 30 ms estimate provided by McPeek et al. (2003). As the −150 SDOA bin includes saccade curvatures away from distractors occurring between an SDOA interval of −140 and −160, this means that the critical epoch can be decreased to 110 ms using the lower bound of the interval. Therefore, if distractor related inhibition occurred ~110 ms after distractor onset, this aligns the inhibitory activity with this critical epoch. Furthermore, the Gaussian shape of the SDOA functions for each saccade direction indicates that the exact timing of distractor inhibition stochastically varies trial-to-trial according to a Gaussian distribution. Our fits would indicate that this variability has a SD of ~40 ms. This variability suggests that there is a certain probability that inhibition accumulates at a time point greater than 110 ms, which can account for the observations of a significant deviation from baseline in the −170 SDOA bin

according to the sum curvature analysis and a higher probability of saccades curved away from a distractor in the −150, −170, and −190 SDOA bins according to the proportion analysis.

This same logic can also be applied to the time course of SCi excitation as the shape of the Gaussian fits were nearly identical between the SDOA functions for saccades curved towards and away from distractors, which was also consistent between the sum and max curvature metrics. There was a significant deviation from baseline in the −110 SDOA bin for saccades curved towards distractors. Taking the lower bound of this bin, and subtracting 30 ms provides a critical epoch estimate for saccades curved towards distractors beginning 60 ms after distractor onset, which also aligns well with latency estimates of 40-70 ms for visual onset bursts (Boehnke & Munoz, 2008). As with the Gaussian SDOA function for saccades curved away from distractors, this critical epoch likely stochastically varies according to a Gaussian distribution and can therefore also elicit saccade curvatures for excitatory bursts with latencies that vary about 60 ms. This model of saccade curvature assumes that the latency of saccade initiation and the latency of inhibitory accumulation are independent processes. McPeek and Keller (2002) observed that the target discrimination time for VM neurons did not covary with SRT therefore convincingly demonstrating such independence.

Neurophysiological investigations have demonstrated that saccades curved towards distractors are caused by excitation at the distractor SCi distractor locus ~20-30 ms prior to the initiation of a saccade (McPeek et al., 2003; Port & Wurtz, 2003). Although a neurophysiological experiment has demonstrated that saccades curved away from distractors are caused by inhibition at the distractor locus in SCi (Aizawa & Wurtz, 1998), the temporal mechanics of these saccades curved away from distractors are disputed (White et al., 2012). Our data clearly show that for a particular SDOA value, there is a corresponding Gaussian distributed probability of eliciting a

curved saccade. For saccades curved towards a distractor, this corresponds to the probability that the onset burst aligns with the critical temporal epoch of 30 ms prior to saccade initiation (McPeek et al., 2003). Similarly for saccades curved away from a distractor, this corresponds to the probability that the accumulation of inhibition aligns with the critical temporal epoch of 30 ms prior to saccade initiation. We reason that the source of this variability is likely attributed to the inherent variability observed in the onset burst latencies of SCi VM neurons (Boehnke and Munoz, 2008) even for saccades curved away from distractors as inhibition will likely only accumulate after excitation has been elicited. As the shape of the Gaussian functions for saccades that are curved towards and away from distractors were nearly identical, this suggests that, like excitation, inhibition must also occur in the critical epoch prior to saccade initiation in order to elicit curved saccades. As such, our data suggests that saccades curved away from distractors are caused by a rapid accumulation of inhibition at the SCi distractor locus.

4.6.4 Conclusion

The current experiment demonstrated that a minimum of 70 ms is required for saccade vector modulation by a distractor. This was consistent with the results from behavioral studies employing various methodologies and analytic techniques (Becker and Jürgen, 1979; Findlay and Harris, 1984; Ludwig et al., 2007; Reingold and Stampe, 2002; cf. Buonocore et al., 2016) in addition to various monkey neurophysiological recordings from SCi, which is a critical neural structure associated with eliciting saccades (reviewed by Boehnke & Munoz, 2008). We also observed that the visual features that characterize the distractor modulated this time course for saccade vector modulation, as color distractors required an additional approximately 20 ms of processing time in order to modulate saccade vectors. The underlying neural mechanism producing this result can also be explained by the neurophysiology of the oculomotor system, as

the response times of SCi VM neurons demonstrate a similar time course discrepancy (White et al., 2009). These results validated our current approach to inferring the time course of competitive oculomotor processing using SDOA modeling. As such, we modeled the SDOA functions for saccades curved towards and away from a distractor separately and observed that these function fits had nearly identical slope parameters. As these functions define the time course of competitive oculomotor processing, these results elucidate similar spatiotemporal profiles of oculomotor processing that elicit saccades curved towards and away from distractors, which likely involves a rapid accumulation of excitation (Port and Wurtz, 2003; McPeek et al., 2003) or inhibition at the SCi distractor locus.

Chapter 5: General Discussion and Conclusions

5.1 Research Questions

The manuscripts presented here have provided answers to the questions originally posed in section 1.4. The first manuscript demonstrated that just as the neurological encoding of objects seems to generalize across all classes of object (i.e., simple vs. complex and familiar vs. unfamiliar) (Brincat & Connor, 2004, 2006; Kayaert et al., 2005; Freiwald et al., 2009), so too does perceptual encoding as we observed a similar perceptual effect for complex, novel stimuli that have hitherto only been observed for simple features: perceptual repulsion (Blakemore et al., 1970; Marshak & Sekuler, 1979). This observation led us to propose a unified account of object perceptual encoding we called "object space" encoding. The second manuscript demonstrated that in certain visual contexts, SCi likely does not functionally contribute to target selection processing as we observed evidence of competitive target selection (i.e., saccade curvatures), but used stimuli for which SCi has no sensitivities. As such, SCi is likely encoding saccade vectors, but not object representations with associated features. If this were true in some contexts, then a parsimonious account of SCi functionality would conclude that this generalizes across visual contexts. These results therefore suggest a limited role of feature processing for SCi during target selection. The third manuscript demonstrated that the time course of competitive oculomotor processing for saccades curved towards and away from a distractor is the same. The temporal neural correlates of saccades that are curved towards a distractor have been described in great detail (see Port & Wurtz, 2003; McPeek et al., 2003). However, whether the same temporal neural mechanism is responsible for saccades curved away from distractors has been disputed (White et al., 2012). As such, the data from this manuscript suggests that saccades curved away from a distractor are attributable to a rapid accumulation of inhibition at the distractor locus in

SCi. Perhaps more interesting than the individual contributions of each research manuscript in isolation is the combined contribution of these research manuscripts, which is the topic of discussion in the next section.

5.2 General Discussion

The complex stimuli utilized in the experiments from Chapter 2 and 3 were most likely processed in the ventral stream, as there is neurophysiological evidence for the processing of complex novel objects in IT (Brincat & Connoer, 2004, 2006; Desimone et al., 1984; Fujita et al., 1992; Kayaert et al., 2009; Kobatake & Tanaka, 1994) and the perceptual similarity functions in Chapter 2 were similar to the population-level neuronal response functions for similarity between other complex objects (Loffler et al., 2005; Panis et al., 2008). This reasoning has implications for the results from Chapter 3: (1) If the SCi does not functionally contribute to visually processing object representations with associated features, the similarity computations were performed in cortex and vector weights were mapped on to SCi vector representations. If SCi does functionally contribute to visual processing object representations with associated features, there are two remaining possibilities: (2) These similarity computations were performed in cortex for Chapter 2 experiments as it did not contain any oculomotor component. Conversely, these computations were performed in the SCi for the Chapter 3 experiment, which would therefore be a redundant neural circuit. (3) These similarity computations were performed in SCi across the experiments in Chapter 2 and 3. As there is no evidence to support the feature sensitivities necessary for such computations in SCi, the third possibility is unlikely. Furthermore, as it very unlikely for the nervous system to contain a duplicated, redundant circuit, the second possibility is unlikely. Therefore, the results from Chapter 2 and 3 strengthen the conclusions about the nature of SCi target selection processing.

For the character stimuli from Chapter 2, perceptual saturation was observed at the longest objective similarity distances. However, conversely, for the wagon wheel stimuli, perceptual saturation was observed at the shortest objective similarity distances. Furthermore, the perceptual similarity response function shifted rightward for the wagon wheel stimuli suggesting that the wagon wheel stimuli had to be more objectively dissimilar to achieve the same perceptual dissimilarity as character stimuli. We concluded that the inherent similarity between the wagon wheels was greater than between the character stimuli and discussed this observation in terms of the inherent discriminability between the constituent visual features for both classes of objects. Therefore, if the results from this similarity computation are projected into the oculomotor system and are responsible for the effects of objective similarity distance in Chapter 3, then if this experiment were repeated using the wagon wheel stimuli, the effects should be either diminished or eliminated. Furthermore, these results would likely also generalize to other perceptual tasks such as change detection (Richards et al., 2004; Smilek et al., 2000).

The results from Chapter 3 and 4 are consistent with data reported from several neurophysiological experiments examining the temporal interactions that elicit saccade curvatures towards or away from distractors. Port and Wurtz (2003) measured SCi neuronal activity during a saccade task in which two potential targets onset in quick temporal succession and monkeys were rewarded for saccading to the target that onset first. They observed that simultaneous peak activity in the SCi neurons encoding saccade vectors to the two potential targets elicited a straight vector-averaged saccade with an endpoint between targets, which replicates the behaviour observed when two locations in SCi were simultaneously microstimulated (Robinson, 1972). Conversely, sequential activity in these neurons elicited curved saccades: when the neurons encoding the first target reached their peak level of activity,

the saccade was initiated and was directed towards the first target or to an intermediate location between targets. When the neurons encoding the second target reached their peak level of activity approximately 20 ms later, the saccade was then redirected towards the second target and landed near this target. Therefore, the timing of peak neuronal activity was predictive of saccade curvature: the first burst of activity corresponded to the time when saccades began to curve, while the second burst corresponded to the time when saccades stopped curving. Similarly, McPeek et al. (2003) observed that on trials in which saccades curved towards a distractor during a visual search task, there was a perisaccadic burst from visuo-movement (VM) neurons in SCi encoding the distractor location, which occurred approximately 30 milliseconds prior to saccade initiation. Conversely, no such burst was observed on trials in which saccades trajectories were straight and landed near the target. The results from both of these experiments are consistent with Robinson (1972) who double-stimulated two loci on the SCi motor map encoding saccade vectors in orthogonal directions within 30 ms of each other and observed that the second saccade mechanically interfered with the initial saccade by partially or completely replacing it. Furthermore, a similar phenomenon, redirected saccades, has been observed behaviourally (Godijn & Theeuwes, 2002; McPeek & Keller, 2001; McPeek et al., 2000). These results were replicated in Chapter 3 as saccades were curved in approximately the first 30 ms of the movement, but then stopped curving, and also in Chapter 4 as significant saccade deviations towards the distractor occurred if the distractor onset ~110 ms prior to the initiation of the saccade. This meant the critical epoch prior to saccade initiation was ~80 after saccade onset, which is equal to a distractor onset latency of 60 ms sustained for 20 ms. Interestingly, this temporal profile of saccade curvature timing in Chapters 3 was consistent with neurophysiological data (Port & Wurtz, 2003) and occurred for saccades curved away from

distractors. Furthermore, in Chapter 4, significant saccade deviations occurred for saccades away from distractors if they onset 150 ms prior to saccade initiation. The critical epoch for a saccade with a latency of 150 ms would be 120 ms. As saccade inhibition emerges ~110 ms after stimulus onset (McPeek & Keller, 2002), this is consistent with the lower bound of the critical epoch measured in the data from Chapter 4. Therefore, the results from Chapter 3 and 4 provide converging evidence that (1) an identical spatiotemporal profile of SCi neuronal activity elicits saccades curved towards and away from distractors, contrary arguments from other researchers (White et al., 2012); (2) there is a remarkable temporal correlation between the neural processing and behavioural output of the oculomotor system and therefore the current results validate using the time course and SDOA analyses to infer the timing of major SCi neural events involved in target selection. Interestingly, it appears that the SDOA methodology is a non-invasive approximation to the effects of double stimulation paradigm in SCi (Robinson, 1972), which could have applications in diagnosing neurodegenerative diseases such as progressive supranuclear palsy.

Another important implication elucidated by contrasting the results from Chapter 3 and 4, is that top-down cortical inhibition may exclusively be the source of inhibition during target selection. Many previous studies that have examined the factors that influence human saccade curvatures utilized a saccade task in which the target was spatially defined and the distractor was completely irrelevant to the task (Dolye & Walker, 2001; Godijn & Theeuwes, 2002; McSorley et al., 2004, 2006, 2009; Van der Stigchel & Theeuwes, 2005; Van der Stigchel et al., 2007; Walker et al., 2006). There are two known sources of inhibition for the SCi motormap: local inhibitory circuits (Munoz & Istvan, 1998) and top-down cortical input likely via SNr (Hikosaka & Wurtz, 1983, 1985; Hikosaka et al., 2000). Since these tasks did not have a top-down

component, some authors have speculated that SCi lateral inhibition (Munoz & Istvan, 1998) may be sufficient to account for saccade deviations away from the distractor (Wang, Kruijne, & Theeuwes, 2012). Although many authors still consider the influence of top-down cortical inhibition (Doyle & Walker, 2001; Godijn & Theeuwes, 2002; McSorley et al., 2004, 2006; 2009; Van der Stigchel et al., 2007; Walker et al., 2006). However, lateral inhibition is insufficient to explain the results from Chapters 3 and 4. In Chapter 3, we argued that local inhibition in SCi is an unlikely explanation given that the SCi does not possess the featural selectivities necessary for the similarity computations that elicited the saccade curvatures. In Chapter 4, we demonstrate that the time scales are inconsistent with local inhibition given that local inhibition circuits in SCi inhibit neighbouring populations of neurons on extremely short times scales of about 5 ms. However, our SDOA analysis demonstrated that inhibition did not accumulate until ~120 ms after stimulus onset, which is also consistent with neurophysiological observations (i.e., ~110 ms, McPeek & Keller, 2002).

Another interesting aspect of the fact that it was likely top-down inhibition that elicited saccades curved away from distractors in Chapters 3 and 4, is that in Chapter 4, the task was devoid of any top-down component: the target and distractors never occupied the same location and were visually quite dissimilar. In reference back to the discussion on the visual processing capabilities of SCi, this observation would suggest that SCi visual processing is nearly absent in the context of even the simplest visual tasks.

5.3 Conclusions

The research projects in Chapters 2, 3, and 4 have all met their objectives and provided answers to the questions asked at the beginning of this thesis. By utilizing a variety of methodologies and analytic techniques, these experiments have provided insight into how the

visual system processes information, and then feeds this information into the oculomotor system with certain temporal constraints, so to enhancing processing a specific object. This thesis contributes to our understanding of human visual cognitive neuroscience as it shows that the visual system plays a much more central role in oculomotor target selection processing than is acknowledged by some influential investigators. Furthermore, it appears that the language the visual system uses to communicate with the oculomotor system is inhibition and, rather than being smooth and gradual, these inhibitory signals can be rapid and transient.

Chapter 6: References

Afifi, A. K. & Bergman, R. A. (2005). *Functional neuroanatomy: Text and atlas* (2nd ed.). New York: McGraw-Hill.

Aizawa, H., & Wurtz, R. H. (1998). Reversible inactivation of monkey superior colliculus. I. Curvature of saccadic trajectory. *Journal of Neurophysiology*, *79*(4), 2082–2096.

Albrecht, D.G. & Geisler, W.S. (1991). Motion selectivity and the contrast-response function of simple cells in the visual cortex. *Visual Neuroscience*, *7*(6), 531–546.

Albrecht, D.G. & Hamilton, D.B. (1982). Striate cortex of monkey and cat: Contrast response functions. *Journal of Neurophysiology*, *48*(1), 217–237.

Anderson, N.D. & Wilson, H.R. (2005). The nature of synthetic face adaptation. *Vision Research*, *45*(14), 1815–1828.

Appelle, S. (1972). Perception and discrimination as a function of stimulus orientation: The "oblique effect" in man and animals. *Psychological Bulletin*, *78*(4), 266–278.

Awh, E., Armstrong, K. M., & Moore, T. (2006). Visual and oculomotor selection causes and implications for spatial attention. *Trends in Cognitive Sciences*, *10*(3), 124–130.

Bahill, A. T., & Stark, L. (1975). Neurological control of horizontal and vertical components of oblique saccadic eye movements. *Mathematical Biosciences*, *27*(3), 287–298.

Basso, M. A., & Wurtz, R. H. (1997). Modulation of neuronal activity by target uncertainty. *Nature*, *389*, 66–69.

Basso, M. A., & Wurtz, R. H. (1998). Modulation of neuronal activity in superior colliculus by changes in target probability. *The Journal of Neuroscience*, *18*(18), 7519–7534.

Basso, M. A., Krauzlis, R. J., & Wurtz, R. H. (2000). Activation and inactivation of rostral superior colliculus neurons during smooth-pursuit eye movements in monkeys. *Journal of Neurophysiology*, *84*(2), 892–908.

Baylis, G. C. & Rolls, E. T. (1987). Responses of neurons in the inferior temporal cortex in short term and serial recognition memory tasks. *Experimental Brain Research*, *65*(3), 614–622.

Baylis, G.C., Rolls, E.T., & Leonard, C.M. (1985). Selectivity between faces in the responses of population of neurons in the cortex in the superior temporal sulcus of the monkey. *Brain Research*, *342*(1), 91–102.

Baylis, G.C., Rolls, E.T., & Leonard, C.M. (1987). Functional subdivisions of the temporal lobe neocortex. *The Journal of Neuroscience*, *7*(2), 330–342.

Becker, W. (1989). Metrics. In R. H. Wurtz & M. E. Goldberg (Eds.), *The neurobiology of saccadic eye movements* (Vol. 3). Amsterdam: Elsevier.

Bell, A. H., Meredith, M. A., Van Opstal, A. J., & Munoz, D. (2006). Stimulus intensity modifies saccadic reaction time and visual response latency in the superior colliculus. *Experimental Brain Research*, *174*(1), 53–59.

Belopolsky, A. V., & Van der Stigchel, S. (2013). Saccades curve away from previously inhibited locations: evidence for the role of priming in oculomotor competition. *Journal of Neurophysiology*, *110*(10), 2370–2377.

Bichot, N. P., & Schall, J. D. (1999). Effects of similarity and history on neural mechanisms of visual selection. *Nature Neuroscience*, *2*(6), 549–554.

Bichot, N. P., Schall, J. D., & Thompson, K. G. (1996). Visual feature selectivity in frontal eye fields. *Nature*, *381*, 697–699.

Biederman, I. (1987). Recognition-by-components: A theory of human image understanding.

Psychological Review, *94*(2), 115–147.

Biederman, I. & Cooper, E.E. (1991). Priming contour-deleted images: Evidence for intermediate representations in visual object recognition. *Cognitive Psychology*, *23*(3), 393–419.

Biederman, I. & Ju, G. (1988). Surface versus edge-based determinants of visual recognition. *Cognitive Psychology*, *20*(1), 38–64.

Bisley, J. W. (2011). The neural basis of visual attention. *Journal of Physiology*, *589*(1), 49–57.

Blakemore, C., Carpenter, R.H.S., & Georgeson, M.A. (1970). Lateral inhibition between orientation detectors in the human visual system. *Nature*, *228*, 37–39.

Boehnke, S. E., & Munoz, D. P. (2008). On the importance of the transient visual response in the superior colliculus. *Current Opinion in Neurobiology*, *18*(6), 544–551.

Brincat, S .L. & Connor, C. E. (2004). Underlying principles of visual shape selectivity in posterior inferotemporal cortex. *Nature Neuroscience*, *7*(8), 880–886.

Brincat, S. L. & Connor, C. E. (2006). Dynamic shape synthesis in posterior inferotemporal cortex. *Neuron*, *49*(1), 17–24.

Bruce, C. J., & Goldberg, M. E. (1984). Physiology of the frontal eye fields. *Trends in Neurosciences*, *7*(11), 436–441.

Bruce, C. J., & Goldberg, M. E. (1985). Primate frontal eye fields. I. Single neurons discharging before saccades. *Journal of Neurophysiology*, *53*(3), 603–635.

Bruce, C. J., Goldberg, M. E., Bushnell, M. C., & Stanton, G. (1985). Primate frontal eye fields. II. Physiological and anatomical correlates of electrically evoked eye movements. *Journal of Neurophysiology*, *54*(3), 714–734.

Bruce, V, Doyle, T., Dench, N., & Burton, M. (1991). Remembering facial configurations.

Cognition, *38*(2), 109–144.

Bruce, V., Burton, M.A., & Dench, N. (1994). What's distinctive about a distinctive face? *The Quarterly Journal of Experimental Psychology Section A*, *47*(1), 119–141.

Buonocore, A., McIntosh, R. D., & Melcher, D. (2016). Beyond the point of no return: Effects of visual distractors on saccade amplitude and velocity. *Journal of Neurophysiology*, *115*(2), 752–762.

Burr, D. C., & Morrone, M. C. (1993). Impulse-response functions for chromatic and achromatic stimuli. *Journal of the Optical Society of America*, *10*(8), 1706–1713.

Campbell, F.W., Kulikowski, J.J., Levinson, J. (1966). The effect of orientation on the visual resolution of gratings. *Journal of Physiology*, *187*(2), 427–436.

Carello, C. D., & Krauzlis, R. J. (2004). Manipulating intent: Evidence for a causal role of the superior colliculus in target selection. *Neuron*, *43*(4), 575–583.

Carrasco, M. (2011). Visual attention: The last 25 years. *Vision Research*, *51*(13), 1484–1525.

Connor, C. E., Gallant, J. L., Preddie, D. C., & Van Essen, D. C. (1996). Responses in area V4 depend on the spatial relationship between stimulus and attention. *Journal of Neurophysiology*, *75*(3), 1306–1308.

Corbetta, M., Akbudak, E., Conturo, T. E., Snyder, A. Z., Ollinger, J. M., Drury, H. A., ... & Shulman, G. L. (1998). A common network of functional areas for attention and eye movements. *Neuron*, *21*(4), 761–773.

Coren, S., & Hoenig, P. (1972). Effect of non-target stimuli upon length of voluntary saccades. *Perceptual and Motor Skills*, *34*(2), 499–508.

Cowey, A., & Perry, V. H. (1980). The projection of the fovea to the superior colliculus in rhesus monkeys. *Neuroscience*, *5*(1), 53–61.

Curcio, C. A., Sloan, K. R., Kalina, R. E., & Hendrickson, A. E. (1990). Human photoreceptor topography. *The Journal of Comparative Neurology*, *292*(4), 497–523.

Cynader, M., & Berman, N. (1972). Receptive-field organization of monkey superior colliculus. *Journal of Neurophysiology*, *35*(2), 187–201.

Dassonville, P., Schlag, J., & Schlag-Rey, M. (1992). The frontal eye field provides the goal of saccadic eye movement. *Experimental Brain Research*, *89*(2), 300–310.

Desimone, R., Albright, T. D., Gross, C. G., & Bruce, C. (1984). Stimulus-selective properties of inferior temporal neurons in the macaque. *The Journal of Neuroscience*, *4*(8), 2051–2062.

Deuble, H., Wolf, W., & Hauske, G. (1984). The evaluation of the oculomotor error signal. *Advances in Psychology*, *22*, 55–62.

DeYoe, E. A., & Van Essen, D. C. (1988). Concurrent processing streams in monkey visual cortex. *Trends in Neurosciences*, *11*(5), 219–226.

Dorris, M. C., Pare, M., & Munoz, D. P. (1997). Neuronal activity in monkey superior colliculus related to the initiation of saccadic eye movements. *The Journal of Neuroscience*, *17*(21), 8566–8579.

Doyle, M., & Walker, R. (2001). Curved saccade trajectories: Voluntary and reflexive saccades curve away from irrelevant distractors. *Experimental Brain Research*, *139*(3), 333–344.

Duffy, C. J., & Wurtz, R. H. (1991a). Sensitivity of MST neurons to optic flow stimuli. I. A continuum of response selectivity to large-field stimuli. *Journal of Neurophysiology*, *65*(6), 1329–1345.

Duffy, C. J., & Wurtz, R. H. (1991b). Sensitivity of MST neurons to optic flow stimuli. II. Mechanisms of response selectivity revealed by small-field stimuli. *Journal of Neurophysiology*, *65*(6), 1346–1359.

Duffy, C. J., & Wurtz, R. H. (1997). Medial superior temporal area neurons respond to speed patterns in optic flow. *The Journal of Neuroscience*, *17*(8), 2839–2851.

Edelman, J. A., & Keller, E. L. (1996). Activity of visuomotor burst neurons in the superior colliculus accompanying express saccades. *Journal of Neurophysiology*, *76*(2), 908–926.

Edwards, S. B. (1980). The deep cell layers of the superior colliculus: Their reticular characteristics and structural organization. In J.A. Hobson & M.A.B. Brazier (Eds.), *The reticular formation revisited* (Vol. 6, pp. 193–209). New York: Raven Press.

Everling, S., & Munoz, D. P. (2000). Neuronal correlates for preparatory set associated with pro-saccades and anti-saccades in the primate frontal eye field. *The Journal of Neuroscience*, *20*(1), 387–400.

Fahy, F. L., Riches, I. P., & Brown, M. W. (1993). Neuronal activity related to visual recognition memory: Long-term memory and the encoding of recency and familiarity information in the primate anterior and medial inferior temporal and rhinal cortex. *Experimental Brain Research*, *96*(3), 457–472.

Fecteau, J. H., & Munoz, D. P. (2006). Salience, relevance, and firing: a priority map for target selection. *Trends in Cognitive Sciences*, *10*(8), 382–390.

Felleman, D. J. & Van Essen, D. C. (1991). Distributed hierarchical processing in the primate cerebral cortex, *Cerebral Cortex*, *1*(1), 1–47.

Findlay, J. M. (1982). Global visual processing for saccadic eye movements. *Vision Research*, *22*(8), 1033–1045.

Findlay, J. M. & Harris, L. R. (1984). Small saccades to double-stepped targets moving in two dimensions. In A. G. Gale & F. Johnson (Eds.), *Theoretical and applied aspects of eye movement research* (pp. 71–78). Amsterdam: North-Holland/Elsevier Science.

Findlay, J. M., & Blythe, H. I. (2009). Saccade target selection: Do distractors affect saccade accuracy? *Vision research*, *49*(10), 1267–1274.

Findlay, J. M., & Kapoula, Z. (1992). Scrutinization, spatial attention, and the spatial programming of saccadic eye movements. *The Quarterly Journal of Experimental Psychology*, *45*(4), 633–647.

Findlay, J. M., & Walker, R. (1999). A model of saccade generation based on parallel processing and competitive inhibition. *Behavioral and Brain Sciences*, *22*(4), 661–674.

Freiwald, W.A., Tsao, D.Y., & Livingstone, M.S. (2009). A face feature space in the macaque temporal lobe. *Nature Neuroscience*, *12*(9), 1–10.

Fujita, I., Tanaka, K., Ito, M., & Cheng, K. (1992). Columns for visual features of objects in monkey inferotemporal cortex. *Nature*, 360 343–346.

Gentner, D. (1983). Structure-mapping: A theoretical framework for analogy. *Cognitive Science*, *7*(2), 155–170.

Gibson, J. J., & Radner, M. (1937). Adaptation, aftereffect and contrast in the perception of tilted lines. I. Quantitative studies. *Journal of Experimental Psychology*, *20*(5), 453–467.

Gilbert, C. D., Sigman, M., & Crist, R. E. (2001). The neural basis of perceptual learning. *Neuron*, *31*(5), 681–697.

Glimcher, P. W., & Sparks, D. L. (1992). Movement selection in advance of action in the superior colliculus. *Nature*, *355*, 542–545.

Glimcher, P. W., & Sparks, D. L. (1993). Representation of averaging saccades in the superior colliculus of the monkey. *Experimental Brain Research*, *95*(3), 429–435.

Godijn, R., & Theeuwes, J. (2002). Programming of endogenous and exogenous saccades: evidence for a competitive integration model. *Journal of Experimental Psychology: Human Perception and Performance*, *28*(5), 1039–1054.

Goldberg, M. E., & Bruce, C. J. (1990). Primate frontal eye fields. III. Maintenance of a spatially accurate saccade signal. *Journal of Neurophysiology*, *64*(2), 489–508.

Goldberg, M. E., & Wurtz, R. H. (1972). Activity of superior colliculus in behaving monkey. I. Visual receptive fields of single neurons. *Journal of Neurophysiology*, *35*(4), 542–559.

Goldman, P. S., & Nauta, W. J. (1976). Autoradiographic demonstration of a projection from prefrontal association cortex to the superior colliculus in the rhesus monkey. *Brain Research*, *116*(1), 145–149.

Goldstone, R.L. (1994). The role of similarity in categorization: Providing a groundwork. *Cognition*, *52*(2), 125–157.

Goldstone, R.L., Medin, D.L., & Gentner, D. (1991). Relational similarity and the nonindependence of features in similarity judgments. *Cognitive Psychology*, *23*(2), 222–262.

Goodale, M. A., & Milner, A. D. (1992). Separate visual pathways for perception and action. *Trends in Neurosciences*, *15*(1), 20-25.

Gross, C. G., Rocha-Miranda, C. E., & Bender, D. B. (1972). Visual properties of neurons in inferotemporal cortex of the macaque, *Journal of Neurophysiology*, *35*(1), 96–111.

Hanes, D. P., & Schall, J. D. (1996). Neural control of voluntary movement initiation. *Science*, *274*(5286), 427–430.

Hanes, D. P., Patterson, W. F., & Schall, J. D. (1998). Role of frontal eye fields in countermanding saccades: Vvisual, movement, and fixation activity. *Journal of Neurophysiology*, *79*(2), 817–834.

Harting, J. K., Casagrande, V. A., & Weber, J. T. (1978). The projection of the primate superior colliculus upon the dorsal lateral geniculate nucleus: Autoradiographic demonstration of interlaminar distribution of tectogeniculate axons. *Brain Research*, *150*(3), 593–599.

Harting, J. K., Updyke, B. V., & van Lieshout, D. P. (1992). Corticotectal projections in the cat: Anterograde transport studies of twenty-five cortical areas. *Journal of Comparative Neurology*, *324*(3), 379–414.

He, P., & Kowler, E. (1989). The role of location probability in the programming of saccades: Implications for "center-of-gravity" tendencies. *Vision Research*, *29*(9), 1165–1181.

Heeman, J., Theeuwes, J., & Van der Stigchel, S. (2014). The time course of top-down control on saccade averaging. *Vision Research*, *100*, 29–37.

Hikosaka, O., & Wurtz, R. H. (1983). Visual and oculomotor functions of monkey substantia nigra pars reticulata. IV. Relation of substantia nigra to superior colliculus. *Journal of Neurophysiology*, *49*(5), 1285–1301.

Hikosaka, O., & Wurtz, R. H. (1985). Modification of saccadic eye movements by GABA-related substances. II. Effects of muscimol in monkey substantia nigra pars reticulata. *Journal of Neurophysiology*, *53*(1), 292–308.

Hikosaka, O., Takikawa, Y., & Kawagoe, R. (2000). Role of the basal ganglia in the control of purposive saccadic eye movements. *Physiological Reviews*, *80*(3), 953–978.

Horwitz, G. D., & Newsome, W. T. (1999). Separate signals for target selection and movement specification in the superior colliculus. *Science*, *284*, 1158–1161.

Horwitz, G. D., & Newsome, W. T. (2001). Target selection for saccadic eye movements: Prelude activity in the superior colliculus during a direction-discrimination task. *Journal of Neurophysiology*, *86*(5), 2543–2558.

Hubel, D. H. & Wiesel, T. N. (1962). Receptive fields, binocular interaction and functional architecture in the cat's visual cortex, *Journal of Physiology*, *160*(1), 106–154.

Hubel, D. H. & Wiesel, T. N. (1968). Receptive fields and functional architecture of monkey striate cortex, *Journal of Physiology*, *195*(1), 215–243.

Hubel, D. H., LeVay, S., & Wiesel, T. N. (1975). Mode of termination of retinotectal fibers in macaque monkey: An autoradiographic study. *Brain Research*, *96*(1), 25–40.

Huerta, M. F., Krubitzer, L. A., & Kaas, J. H. (1986). Frontal eye field as defined by intracortical microstimulation in squirrel monkeys, owl monkeys, and macaque monkeys: I. Subcortical connections. *Journal of Comparative Neurology*, *253*(4), 415–439.

Huerta, M. F., Krubitzer, L. A., & Kaas, J. H. (1987). Frontal eye field as defined by intracortical microstimulation in squirrel monkeys, owl monkeys, and macaque monkeys II. Cortical connections. *Journal of Comparative Neurology*, *265*(3), 332–361.

Hummel, J.E. (2000). Where view-based theories break down: The role of structure in human shape perception. In E. Dietrich & A. Markman (Eds.), *Cognitive dynamics: Conceptual change in humans and machines* (pp. 157–185). Mahwah, NJ: Erlbaum.

Humphreys, G.W., Riddoch, M.J., & Quinlan, P.T. (1988). Cascade processes in picture identification. *Cognitive Neuropsychology*, *5*(1), 67–103.

Isa, T. (2002). Intrinsic processing in the mammalian superior colliculus. *Current Opinion in Neurobiology*, *12*(6), 668–677.

Isa, T., & Saito, Y. (2001). The direct visuo-motor pathway in mammalian superior colliculus; novel perspective on the interlaminar connection. *Neuroscience Research*, *41*(2), 107–113.

Ishihara S. (2006). *The series of plates designed as a test for colour deficiency* (Concise ed.). Tokyo: Kanehara Trading Inc.

Johnston, R.A., Milne, A.B., Williams, C., & Hoise, J. (1997). Do distinctive faces come from outer space? An investigation of the status of a multidimensional face-space. *Visual Cognition*, *4*(1), 59–67.

Kayaert, G., Biederman, I., Op de Beeck, H., & Vogels, R. (2005). Tuning for shape dimensions in macaque inferior temporal cortex. *European Journal of Neuroscience*, *22*(1), 212–224.

Kim, B., & Basso, M. A. (2008). Saccade target selection in the superior colliculus: A signal detection theory approach. *The Journal of Neuroscience*, *28*(12), 2991–3007.

Kobatake, E. & Tanaka, K. (1994). Neuronal selectivities to complex object features in the ventral visual pathway of the macaque cerebral cortex. *The Journal of Neurophysiology*, *71*(3), 856–867.

Kohn, A. (2007). Visual adaptation: Physiology, mechanisms, and functional benefits. *Journal of Neurophysiology*, *97*(5), 3155–3164.

Krauzlis, R. J. (2003). Neuronal activity in the rostral superior colliculus related to the initiation of pursuit and saccadic eye movements. *The Journal of Neuroscience*, *23*(10), 4333–4344.

Krauzlis, R. J. (2005). The control of voluntary eye movements: New perspectives. *The Neuroscientist*, *11*(2), 124–137.

Krauzlis, R. J., & Dill, N. (2002). Neural correlates of target choice for pursuit and saccades in

the primate superior colliculus. *Neuron*, *35*(2), 355–363.

Künzle, H., & Akert, K. (1977). Efferent connections of cortical, area 8 (frontal eye field) in Macaca fascicularis. A reinvestigation using the autoradiographic technique. *Journal of Comparative Neurology*, *173*(1), 147–163.

Künzle, H., Akert, K., & Wurtz, R. H. (1976). Projection of area 8 (frontal eye field) to superior colliculus in the monkey. An autoradiographic study. *Brain Research*, *117*(3), 487–492.

Laidlaw, K. E., Badiudeen, T. A., Zhu, M. J., & Kingstone, A. (2015). A fresh look at saccadic trajectories and task irrelevant stimuli: Social relevance matters. *Vision Research*, *111*, 82–90.

Lamme, V. A. F. & Roelfsema, P. R. (2000). The distinct modes of vision offered by feedforward and recurrent processing, *Trends in Neuroscience*, *23*(11), 571–579.

Laws, K.R. & Gale, T.M. (2002). Category-specific naming and the 'visual' characteristics of line drawn stimuli. *Cortex*, *38*(1), 7–21.

Lee, C., Rohrer, W. H., & Sparks, D. L. (1988). Population coding of saccadic eye movements by neurons in the superior colliculus. *Nature*, *332*, 357–360.

Leopold, D.A., Bondar, I.V., & Giese, M.A. (2006). Norm-based face encoding by single neurons in the monkey inferotemporal cortex. *Nature*, *442*, 572–575.

Leopold, D.A., O'Toole, A.J., Vetter, T., & Blanz, V. (2001). Prototype-referenced shape encoding revealed by high-level aftereffects. *Nature Neuroscience*, *4*(1), 89–94.

Leopold, D.A., Rhodes, G., Müller, K.M., & Jeffery, L. (2005). Dynamics of visual adaptation to faces. *Proceedings of the Royal Society of London B: Biological Science*, *272*, 897–904.

Li, X., & Basso, M. A. (2005). Competitive stimulus interactions within single response fields of superior colliculus neurons. *The Journal of Neuroscience*, *25*(49), 11357–11373.

Li, X., & Basso, M. A. (2008). Preparing to move increases the sensitivity of superior colliculus neurons. *The Journal of Neuroscience*, *28*(17), 4561–4577.

Livingstone, M. & Hubel, D. H. (1988). Segregation of form, color, movement, and depth: Anatomy, physiology, and perception. *Science*, *240*, 740–749.

Loffler, G., Yourganov, G., Wilkinson, F., & Wilson, H.R. (2005). fMRI evidence for the neural representation of faces. *Nature Neuroscience*, *8*(10), 1386–1390.

Logothetis, N.K., Pauls, J., & Poggio, T. (1995). Shape representation in the inferior temporal cortex of monkeys. *Current Biology*, *5*(5), 552–563.

Logothetis, N.K., Pauls, J., Augath, M. Trinath, T., & Oeltermann, A. (2001). Neurophysiological investigation of the fMRI signal. *Nature*, *412*, 150–157.

Luck, S.J. & Vogel, E.K. (1997). The capacity of visual working memory for features and conjunctions. *Nature*, *390*, 279–281.

Ludwig, C. J., & Gilchrist, I. D. (2002). Measuring saccade curvature: a curve-fitting approach. *Behavior Research Methods, Instruments, & Computers*, *34*(4), 618–624.

Ludwig, C. J., & Gilchrist, I. D. (2003). Target similarity affects saccade curvature away from irrelevant onsets. *Experimental Brain Research*, *152*(1), 60–69.

Ludwig, C. J., Mildinhall, J. W., & Gilchrist, I. D. (2007). A population coding account for systematic variation in saccadic dead time. *Journal of Neurophysiology*, *97*(1), 795–805.

Lynch, J. C., & Tian, J. R. (2006). Cortico-cortical networks and cortico-subcortical loops for the higher control of eye movements. *Progress in Brain Research*, *151*, 461–501.

Lynch, J. C., Graybiel, A., & Lobeck, L. J. (1985). The differential projection of two cytoarchitectonic subregions of the inferior parietal lobule of macaque upon the deep layers of the superior colliculus. *Journal of Comparative Neurology*, *235*(2), 241–254.

Lynch, J. C., Hoover, J. E., & Strick, P. L. (1994). Input to the primate frontal eye field from the substantia nigra, superior colliculus, and dentate nucleus demonstrated by transneuronal transport. *Experimental Brain Research*, *100*(1), 181–186.

Marino, R. A., Rodgers, C. K., Levy, R., & Munoz, D. P. (2008). Spatial relationships of visuomotor transformations in the superior colliculus map. *Journal of Neurophysiology*, *100*(5), 2564–2576.

Marr, D. & Nishihara, H.K. (1978). Representation and recognition of the spatial organization of three-dimensional shapes. *Proceedings of the Royal Society of London B: Biological Sciences*, *200*, 269–294.

Marshak, W. & Sekuler, R. (1979). Mutual repulsion between moving visual targets. *Science*, *205*, 1399–1401.

Mays, L. E., & Sparks, D. L. (1980). Dissociation of visual and saccade-related responses in superior colliculus neurons. *Journal of Neurophysiology*, *43*(1), 207–232.

McPeek, R. M. (2006). Incomplete suppression of distractor-related activity in the frontal eye field results in curved saccades. *Journal of Neurophysiology*, *96*(5), 2699–2711.

McPeek, R. M., & Keller, E. L. (2001). Short-term priming, concurrent processing, and saccade curvature during a target selection task in the monkey. *Vision Research*, *41*(6), 785–800.

McPeek, R. M., & Keller, E. L. (2002). Saccade target selection in the superior colliculus during a visual search task. *Journal of Neurophysiology*, *88*(4), 2019–2034.

McPeek, R. M., & Keller, E. L. (2004). Deficits in saccade target selection after inactivation of superior colliculus. *Nature neuroscience*, *7*(7), 757–763.

McPeek, R. M., Han, J. H., & Keller, E. L. (2003). Competition between saccade goals in the superior colliculus produces saccade curvature. *Journal of Neurophysiology*, *89*(5), 2577–2590.

McPeek, R. M., Skavenski, A. A., & Nakayama, K. (2000). Concurrent processing of saccades in visual search. *Vision Research*, *40*(18), 2499–2516.

McSorley, E., Haggard, P., & Walker, R. (2004). Distractor modulation of saccade trajectories: Spatial separation and symmetry effects. *Experimental Brain Research*, *155*(3), 320–333.

McSorley, E., Haggard, P., & Walker, R. (2006). Time course of oculomotor inhibition revealed by saccade trajectory modulation. *Journal of Neurophysiology*, *96*(3), 1420–1424.

McSorley, E., Haggard, P., & Walker, R. (2009). The spatial and temporal shape of oculomotor inhibition. *Vision Research*, *49*(6), 608–614.

Medin, D.L., Goldstone, R.L., & Gentner, D. (1990). Similarity involving attributes and relations: Judgments of similarity and difference are not inverses. *Psychological Science*, *1*(1), 64–69.

Mohler, C. W., Goldberg, M. E., & Wurtz, R. H. (1973). Visual receptive fields of frontal eye field neurons. *Brain Research*, *61*, 385–389.

Moore, T., Armstrong, K. M., & Fallah, M. (2003). Visuomotor origins of covert spatial attention. *Neuron*, *40*(4), 671–683.

Moschovakis, A. K., & Highstein, S. M. (1994). The anatomy and physiology of primate neurons that control rapid eye movements. *Annual Review of Neuroscience*, *17*(1), 465–488.

Moschovakis, A. K., Karabelas, A. B., & Highstein, S. M. (1988). Structure-function relationships in the primate superior colliculus. II. Morphological identity of presaccadic neurons. *Journal of Neurophysiology*, *60*(1), 263–302.

Mulckhuyse, M., Van der Stigchel, S., & Theeuwes, J. (2009). Early and late modulation of saccade deviations by target distractor similarity. *Journal of Neurophysiology*, *102*(3), 1451–1458.

Munoz, D. P., & Istvan, P. J. (1998). Lateral inhibitory interactions in the intermediate layers of the monkey superior colliculus. *Journal of Neurophysiology*, *79*(3), 1193–1209.

Munoz, D. P., & Wurtz, R. H. (1995). Saccade-related activity in monkey superior colliculus. I. Characteristics of burst and buildup cells. *Journal of Neurophysiology*, *73*(6), 2313–2333.

Neisser, U. (1967). *Cognitive Psychology*. New York: Appleton-Centruy-Crofts.

Ottes, F. P., Van Gisbergen, J. A., & Eggermont, J. J. (1986). Visuomotor fields of the superior colliculus: A quantitative model. *Vision research*, *26*(6), 857–873.

Palmer, S. (1977). Hierarchical structure in perceptual representation. *Cognitive Psychology*, *9*(4), 441–474.

Palmer, S. (1978). Structural aspects of visual similarity. *Memory & Cognition*, *6*(2), 91–97.

Panis, S., Vangeneugden, J., Op de Beeck, H., & Wagemans, J. (2008). The representation of subordinate shape similarity in human occipitotemporal cortex. *Journal of Vision*, *8*(10), 1–15.

Parker, A.J. & Newsome, W.T. (1998). Sense and the single neuron: Probing the physiology of perception. *Annual Review of Neuroscience*, *21*, 227–277.

Pasupathy, A., & Connor, C. E. (1999). Responses to contour features in macaque area V4. *Journal of Neurophysiology*, *82*(5), 2490–2502.

Perry, C. J. & Fallah, M. (2014). Feature integration and object representations along the dorsal stream visual hierarchy. *Frontiers in Computational Neuroscience*, *8*, 84.

Perry, V. H., & Cowey, A. (1984). Retinal ganglion cells that project to the superior colliculus and pretectum in the macaque monkey. *Neuroscience*, *12*(4), 1125–1137.

Phillips, W.A. (1974). On the distinction between sensory storage and short-term visual memory. *Perception and Psychophysics*, *16*(2), 283–290.

Polyak, S. L. (1957). *The vertebrate visual system*. Chicago: University of Chicago Press.

Port, N. L., & Wurtz, R. H. (2003). Sequential activity of simultaneously recorded neurons in the superior colliculus during curved saccades. *Journal of Neurophysiology*, *90*(3), 1887–1903.

Posner, M. I & Petersen, S. E. (1990). The attention system of the human brain. *Annual Reviews of Neuroscience*, *13*, 25–42.

Quaia, C., Aizawa, H., Optican, L. M., & Wurtz, R. H. (1998). Reversible inactivation of monkey superior colliculus. II. Maps of saccadic deficits. *Journal of Neurophysiology*, *79*(4), 2097–2110.

Recanzone, G. H., & Wurtz, R. H. (1999). Shift in smooth pursuit initiation and MT and MST neuronal activity under different stimulus conditions. *Journal of Neurophysiology*, *82*(4), 1710–1727.

Recanzone, G. H., & Wurtz, R. H. (2000). Effects of attention on MT and MST neuronal activity during pursuit initiation. *Journal of Neurophysiology*, *83*(2), 777–790.

Reingold, E. M. & Stampe, D. M. (2002). Saccadic inhibition in voluntary and reflexive saccades. *Journal of Cognitive Neuroscience*, *14*(3), 371–388.

Reynolds, J. H. & Chelazzi, L. (2004). Attentional modulation of visual processing, *Annual Reviews of Neuroscience*, *27*, 611–647.

Richards, E., Tombu, M., Stolz, J.A., & Jolicoeur, P. (2004). Features of perception: Exploring

the perception of change in a psychological refractory period paradigm. *Visual Cognition*, *11*(6), 751–780.

Riches, I. P., Wilson, F. A. W., & Brown, M. W. (1987). The effects of visual stimulation and memory on neurons of the hippocampal formation and the neighboring parahippocampal gyrus and inferior temporal cortex of the primate. *The Journal of Neuroscience*, *11*(6), 1763–1779.

Riches, I.P., Wilson, F.A.W., & Brown, M.W. (1987). The effects of visual stimulation and memory on neurons of the hippocampal formation and the neighboring parahippocampal gyrus and inferior temporal cortex of the primate. *The Journal of Neuroscience*, *11*(6), 1763–1779.

Robinson, D. A. (1972). Eye movements evoked by collicular stimulation in the alert monkey. *Vision Research*, *12*(11), 1795–1808.

Robinson, D. A., & Fuchs, A. F. (1969). Eye movements evoked by stimulation of frontal eye fields. *Journal of Neurophysiology*, *32*(5), 637–648.

Rodieck, R. W. (1998). *The first steps in seeing*. Sunderland, MA: Sinauer Associates.

Sato, T. R., & Schall, J. D. (2003). Effects of stimulus-response compatibility on neural selection in frontal eye field. *Neuron*, *38*(4), 637–648.

Sato, T. R., Watanabe, K., Thompson, K. G., & Schall, J. D. (2003). Effect of target-distractor similarity on FEF visual selection in the absence of the target. *Experimental Brain Research*, *151*(3), 356–363.

Schall, J. D. (1991). Neuronal activity related to visually guided saccades in the frontal eye fields of rhesus monkeys: comparison with supplementary eye fields. *Journal of Neurophysiology*, *66*(2), 559–579.

Schall, J. D., Morel, A., King, D. J., & Bullier, J. (1995). Topography of visual cortex connections with frontal eye field in macaque: convergence and segregation of processing streams. *The Journal of Neuroscience*, *15*(6), 4464–4487.

Schein, S. J., & Desimone, R. (1990). Spectral properties of V4 neurons in the macaque. *The Journal of Neuroscience*, *10*(10), 3369–3389.

Schiller, P. H., & Koerner, F. (1971). Discharge characteristics of single units in superior colliculus of the alert rhesus monkey. *Journal of Neurophysiology*, *34*(5), 920–936.

Schiller, P. H., & Malpeli, J. G. (1977). Properties and tectal projections of monkey retinal ganglion cells. *Journal of Neurophysiology*, *40*(2), 428–445.

Schiller, P. H., & Malpeli, J. G. (1977). Properties and tectal projections of monkey retinal ganglion cells. *Journal of Neurophysiology*, *40*(2), 428–445.

Schiller, P. H., Malpeli, J. G., & Schein, S. J. (1979). Composition of geniculostriate input to superior colliculus of the rhesus monkey. *Journal of Neurophysiology*, *42*(4), 1124–1133.

Schiller, P. H., Stryker, M., Cynader, M., & Berman, N. (1974). Response characteristics of single cells in the monkey superior colliculus following ablation or cooling of visual cortex. *Journal of Neurophysiology*, *37*(1), 181–194.

Schlag-Rey, M., Schlag, J., & Dassonville, P. (1992). How the frontal eye field can impose a saccade goal on superior colliculus neurons. *Journal of Neurophysiology*, *67*(4), 1003–1005.

Schmidt, L. J., Belopolsky, A. V., & Theeuwes, J. (2012). The presence of threat affects saccade trajectories. *Visual Cognition*, *20*(3), 284–299.

Segraves, M. A., & Goldberg, M. E. (1987). Functional properties of corticotectal neurons in the monkey's frontal eye field. *Journal of Neurophysiology*, *58*(6), 1387–1419.

Sheliga, B. M., Riggio, L., & Rizzolatti, G. (1994). Orienting of attention and eye movements. *Experimental Brain Research*, *98*(3), 507–522.

Sheliga, B. M., Riggio, L., & Rizzolatti, G. (1995). Spatial attention and eye movements. *Experimental Brain Research*, *105*(2), 261–275.

Shen, K., & Paré, M. (2007). Neuronal activity in superior colliculus signals both stimulus identity and saccade goals during visual conjunction search. *Journal of Vision*, *7*(5), 1–13.

Shen, K., & Paré, M. (2012). Neural basis of feature-based contextual effects on visual search behavior. *Frontiers in Behavioral Neuroscience*, *5*, 91.

Shen, K., & Paré, M. (2014). Predictive saccade target selection in superior colliculus during visual search. *The Journal of Neuroscience*, *34*(16), 5640–5648.

Shepard, R.N. (1962a). The analysis of proximities: Multidimensional scaling with an unknown distance function. I., *Psychometrika*, *27*(2), 125–140.

Shepard, R.N. (1962b). The analysis of proximities: Multidimensional scaling with an unknown distance function. II., *Psychometrika*, *27*(3), 219–246.

Sloutsky, V.M., Lo, T.F., & Fisher, A.V. (2001). How much does a shared name make tings similar? Linguistic labels, similarity, and the development of inductive inference, *Child Development*, *72*(6), 1695–1709.

Smilek, D., Eastwood, J.D., Merikle, P.M. (2000). Does unattended information facilitate change detection? *Journal of Experimental Psychology: Human Perception and Performance*, *26*(2), 480–487.

Smith, L.B. & Heise, D. (1992). Perceptual similarity and conceptual structure. In B. Burns (Ed.), *Percepts, concepts and categories: The representation and processing of*

information. Advances in psychology, *Vol. 93* (pp. 233–272). Amsterdam: North-Holland.

Sommer, M. A., & Wurtz, R. H. (1998). Frontal eye field neurons orthodromically activated from the superior colliculus. *Journal of Neurophysiology*, *80*(6), 3331–3335.

Sommer, M. A., & Wurtz, R. H. (2004). What the brain stem tells the frontal cortex. I. Oculomotor signals sent from superior colliculus to frontal eye field via mediodorsal thalamus. *Journal of Neurophysiology*, *91*(3), 1381–1402.

Sommer, M. A., & Wurtz, R. H. (2004). What the brain stem tells the frontal cortex. II. Role of the SC-MD-FEF pathway in corollary discharge. *Journal of Neurophysiology*, *91*(3), 1403–1423.

Sommer, M. A., & Wurtz, R. H. (2006). Influence of the thalamus on spatial visual processing in frontal cortex. *Nature*, *444*(7117), 374–377.

Sommer, M. A., & Wurtz, R. H. (2008). Brain circuits for the internal monitoring of movements. *Annual Review of Neuroscience*, *31*, 317–338.

Sparks, D., Rohrer, W. H., & Zhang, Y. (2000). The role of the superior colliculus in saccade initiation: A study of express saccades and the gap effect. *Vision Research*, *40*, 2763–2777.

Sperling, G. (1960). The information available in brief visual presentations. *Psychological Monographs: General and Applied*, *74*(11), 1–29.

Stanton, G. B., Bruce, C. J., & Goldberg, M. E. (1995). Topography of projections to posterior cortical areas from the macaque frontal eye fields. *Journal of Comparative Neurology*, *353*(2), 291–305.

Stanton, G. B., Goldberg, M. E., & Bruce, C. J. (1988). Frontal eye field efferents in the macaque monkey: II. Topography of terminal fields in midbrain and pons. *Journal of Comparative Neurology*, *271*(4), 493–506.

Stanton, G. B., Goldberg, M. E., & Bruce, C. J. (1988). Frontal eye field efferents in the macaque monkey: I. Subcortical pathways and topography of striatal and thalamic terminal fields. *Journal of Comparative Neurology*, *271*(4), 473–492.

Thompson, K. G., Hanes, D. P., Bichot, N. P., & Schall, J. D. (1996). Perceptual and motor processing stages identified in the activity of macaque frontal eye field neurons during visual search. *Journal of Neurophysiology*, *76*(6), 4040–4055.

Tian, J. R., & Lynch, J. C. (1997). Subcortical input to the smooth and saccadic eye movement subregions of the frontal eye field in Cebus monkey. *The Journal of Neuroscience*, *17*(23), 9233–9247.

Tononi, G., & Koch, C. (2008). The neural correlates of consciousness. *Annals of the New York Academy of Sciences*, *1124*(1), 239–261.

Treisman, A. (1996). The binding problem, *Current Opinion in Neurobiology*, *6*(2), 171–178.

Treisman, A. & Gelade, G. (1980). A feature-integration theory of attention, *Cognitive Psychology*, *12*(1), 97–136.

Tversky, A. (1977). Features of similarity. *Psychological Review*, *84*(4), 327–352.

Ungerleider, L. G. & Mishkin, M. (1982). Two cortical visual systems. In D.G. Ingle, M.A. Goodale, & R.J.Q. Mansfield (Eds.), *Analysis of visual behaviour*. Cambridge, MA: MIT Press.

Valentine, T. (1991). A unified account of the effects of distinctiveness, inversion, and race in face recognition. *The Quarterly Journal of Psychology*, *43*(2), 161–204.

Van der Stigchel, S., & Nijboer, T. C. W. (2013). How global is the global effect? The spatial characteristics of saccade averaging. *Vision Research*, *84*, 6–15.

Van der Stigchel, S., Meeter, M., & Theeuwes, J. (2007). The spatial coding of the inhibition evoked by distractors. *Vision Research*, *47*(2), 210–218.

Van Essen, D. C. & Maunsell, J. H. (1983). Hierarchical organizations and functional streams in the visual cortex, *Trends in Neuroscience*, *6*, 370–375.

Van Essen, D. C., Anderson, C. H., & Felleman, D. J. (1992). Information processing in the primate visual system: An integrated systems perspective. *Science*, *255*, 419–423.

Van Essen, D. C., Felleman, D. J., DeYoe, E. A., Olavarria J., & Knierim, J. J. (1990). Modular and hierarchical organization of extrastriate visual cortex in the macaque monkey, *Cold Spring Harbor Symposium on Quantitative Biology*, *55*, 679–696

Van Gisbergen, J. A. M., Van Opstal, A. J., & Tax, A. A. M. (1987). Collicular ensemble coding of saccades based on vector summation. *Neuroscience*, *21*(2), 541–555.

Van Opstal, A. J., & Van Gisbergen, J. A. M. (1990). Role of monkey superior colliculus in saccade averaging. *Experimental Brain Research*, *79*(1), 143–149.

van Zoest, W., Donk, M., & Van der Stigchel, S. (2012). Stimulus-salience and the time-course of saccade trajectory deviations. *Journal of Vision*, *12*(8), 16–16.

Walker, R., Deubel, H., Schneider, W. X., & Findlay, J. M. (1997). Effect of remote distractors on saccade programming: evidence for an extended fixation zone. *Journal of Neurophysiology*, *78*(2), 1108–1119.

Walker, R., McSorley, E., & Haggard, P. (2006). The control of saccade trajectories: Direction of curvature depends on prior knowledge of target location and saccade latency. *Perception & Psychophysics*, *68*(1), 129–138.

Weaver, M. D., Lauwereyns, J., & Theeuwes, J. (2011). The effect of semantic information on saccade trajectory deviations. *Vision Research*, *51*(10), 1124–1128.

White, B. J., Boehnke, S. E., Marino, R. A., Itti, L., & Munoz, D. P. (2009). Color-related signals in the primate superior colliculus. *The Journal of Neuroscience*, *29*(39), 12159-12166.

White, B. J., Theeuwes, J., & Munoz, D. P. (2012). Interaction between visual-and goal-related neuronal signals on the trajectories of saccadic eye movements. *Journal of Cognitive Neuroscience*, *24*(3), 707-717.

Wilson, H.R., Loffler, G., & Wilkinson, F. (2005). Synthetic faces, face cubes, and the geometry of face space. *Vision Research*, *42*(27), 2909–2923.

Wurtz, R. H. & Goldberg, M. E. (1971). Superior colliculus cell response related to eye movements in awake monkeys. *Science*, *171*, 82–84.

Wurtz, R. H. & Goldberg, M. E. (1972). Activity of superior colliculus in behaving monkey. III. Cells discharging before eye movements. *Journal of Neurophysiology*, *35*(4), 575–586.

Wurtz, R. H., & Mohler, C. W. (1976). Enhancement of visual responses in monkey striate cortex and frontal eye fields. *Journal of Neurophysiology*, *39*(4), 766–772.

Yau, J. M., Pasupathy, A., Brincat, S. L., & Connor, C. E. (2012). Curvature processing dynamics in macaque area V4. *Cerebral Cortex*, *23*, 198–209.

Zeki, S. (1993). *A vision of the brain*. New York: Wiley.